Atmospheric
Chemistry
and Physics

Supplement of

Spatial distributions of X_{CO_2} seasonal cycle amplitude and phase over northern high-latitude regions

Nicole Jacobs et al.

Correspondence to: William R. Simpson (wrsimpson@alaska.edu)

S1 Seasonal cycle fits

In this section, we report parameters from and show plots of seasonal cycle fits to a skewed sine wave, using the methods of Lindqvist et al. (2015) and further explained in Sect. 2.6 of the manuscript. Designated 5° latitude by 20° longitude zones are mapped in Fig. 1 of the manuscript and labels for zones follow the numbering on that map. Regions are abbreviated in this supplement as follows:

ASB Asian Boreal

ASTem Asian Temperate

ASTun Asian Tundra

EUB European Boreal

EUTem European Temperate

NAB North American Boreal

NATem North American Temperate

NATun North American Tundra.

The names of the five ground sites considered (see descriptions in Sect. 2.1, 2.2, and 3.1 as well as locations in Table S1) are abbreviated as follows:

**BIA** Bialystok, Poland

BRE Bremen, Germany

ETL East Trout Lake, Saskatchewan, Canada

SOD Sodankylä, Finland

UAF Fairbanks, Alaska, U.S.A.

S1.1 Seasonal cycle fits for ground sites and 5° latitude by 10° longitude coincidence regions

Tables and figures in this section show the details of seasonal cycle fits to daily average X_{CO_2} across three scales at five northern high latitude sites (see abbreviations and names of sites, above), the results from which are compared in Sect. 3.1 of the manuscript. The ground sites considered include four TCCON sites and EM27/SUN measurements collected in Fairbanks, Alaska (see details in Sect. 2.2 of the manuscript). Seasonal cycles at the ground sites are obtained by fitting a skewed sine wave function (see methods described in Sect. 2.6) to near noon ground-based (NNG) observations, as well as CAMS and GC-CT2019 model estimates at the model grid-point nearest to the location of each site (see coordinates of sites and corresponding model grid-point in Table 1 and Fig. 1 in the manuscript). Tables S1, S2, S3, and S4 provide the standard errors used in each fit, the seasonal fit parameters, and an estimate of parameter uncertainty for fits to NNG data and model estimates at each site, as well as for OCO-2 data, CAMS, CT2019B, and GC-CT2019 model estimates of X_{CO_2} averaged spatially over the 5° latitude by 10° longitude coincidence regions centered on each site (labeled "5x10"). OCO-2 observations in this analysis have an alternative bias correction (ABC) applied, following methods described by Jacobs et al. (2020b), and Fig. S1 shows that the ABC yields both SCA and HDD with better agreement between OCO-2 data in the coincidence regions and NNG observations than the standard global bias correction for ACOS B9 retrievals (B9 BC). Figures S2, S3 and S4 show the plotted time-series of observational and model-derived daily X_{CO_2} and corresponding fits at the five sites and at all three spatial scales, including single-point information at or nearest the ground site, averaged within the 5° latitude by 10° longitude coincidence region, and averaged within the 5° latitude by 20° longitude zone that encompasses each site (see map in Fig. 1 for the manuscript).
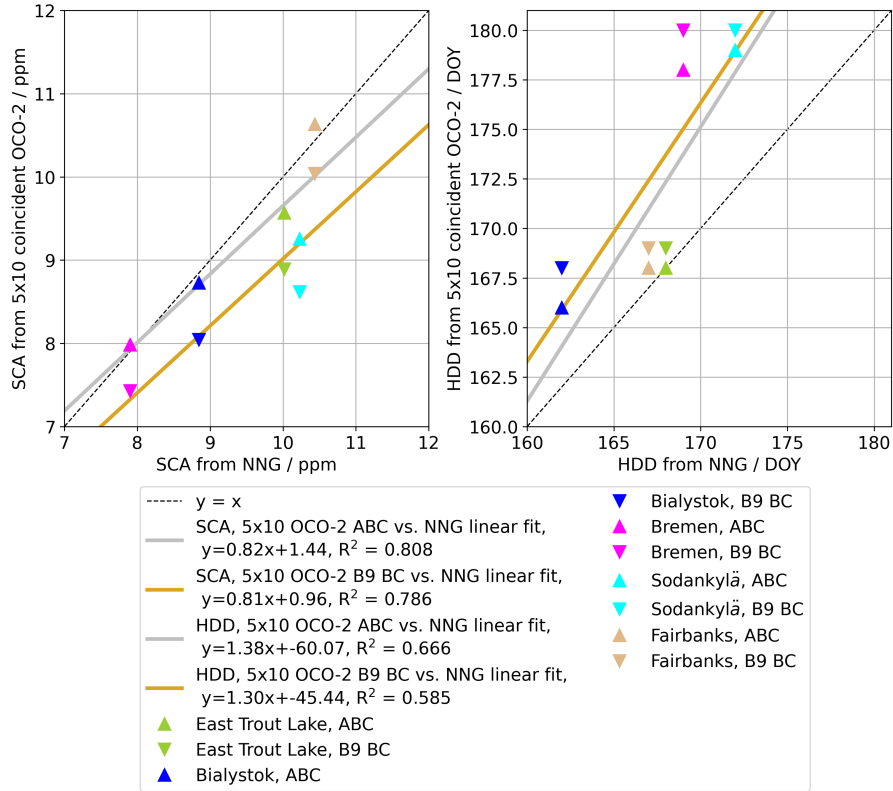
Figure S1. SCA and HDD from NNG observations correlated with those from OCO-2 data in the $5°$ latitude by $10°$ longitude coincidence regions corrected by either the alternative bias correction (ABC), described by Jacobs et al. (2020b), or the standard global bias correction for ACOS B9 retrievals (B9 BC).

Table S1. Seasonal cycle fit parameters, a_i, with uncertainty estimates, σ_{a_i}, for fits of near noon ground-based (NNG) data and OCO-2 data in the 5° latitude by 10° longitude coincidence regions centered at each ground site (review Sect. 2.1, 2.2, and 3.1 of the manuscript for more information) to Eq. 1 in the manuscript, as well as corresponding standard errors, $\bar{\sigma}$, used in fit optimization.

Site	$\bar{\sigma}$ ppm	a_0 ppm	σ_{a_0} ppm	a_1 ppm days^{-1}	σ_{a_1} ppm days^{-1}	a_2 ppm	σ_{a_2} ppm	a_3 days	σ_{a_3} days	a_4	σ_{a_4}	a_5 days	σ_{a_5} days
BIA	0.496	394.732	0.012	7.104e-03	8.3e-09	4.424	3.7e-03	54.427	1.097	-0.500	7.3e-04	-77.628	11.162
BRE	0.500	394.898	0.029	7.146e-03	1.8e-08	3.951	0.012	63.255	3.934	-0.427	2.7e-03	-70.229	71.141
ETL	0.506	395.742	0.039	6.289e-03	1.3e-08	5.009	3.8e-03	65.743	0.438	-0.715	1.9e-04	-90.354	2.445
SOD	0.391	393.799	7.1e-03	7.238e-03	3.3e-09	5.115	2.4e-03	62.481	1.471	-0.660	2.5e-04	-73.322	7.750
UAF	0.368	396.620	0.063	5.946e-03	2.2e-08	5.219	5.5e-03	57.112	3.027	-0.762	4.5e-04	-82.481	9.772
BIA, 5x10	1.291	396.199	0.058	6.650e-03	2.4e-08	4.363	0.014	67.449	7.077	-0.429	2.5e-03	-90.438	112.270
BRE, 5x10	1.272	396.313	0.051	6.657e-03	2.3e-08	3.992	0.012	71.975	8.035	-0.501	3.1e-03	-64.495	80.156
ETL, 5x10	1.190	395.528	0.026	7.051e-03	1.2e-08	4.783	6.5e-03	69.868	2.737	-0.677	6.0e-04	-96.879	16.390
SOD, 5x10	1.380	394.368	0.069	7.063e-03	3.0e-08	4.627	0.015	74.091	48.645	-0.758	3.5e-03	-75.782	129.616
UAF, 5x10	1.430	395.298	0.032	7.052e-03	1.8e-08	5.317	9.5e-03	80.909	11.176	-0.816	1.1e-03	-111.311	26.989

Table S2. Seasonal cycle fit parameters, a_i, with uncertainty estimates, σ_{a_i}, for fits of CAMS estimated X_{CO_2} from the grid-points nearest to the ground sites (see Table 1, in the manuscript, for exact coordinates) and CAMS estimated X_{CO_2} averaged over the 5° latitude by 10° longitude coincidence regions centered at each ground site (using actual coordinate of the ground site as center) to Eq. 1 in the manuscript, as well as corresponding standard errors, $\bar{\sigma}$, used in fit optimization.

Site	$\bar{\sigma}$ ppm	a_0 ppm	σ_{a_0} ppm	a_1 ppm days^{-1}	σ_{a_1} ppm days^{-1}	a_2 ppm	σ_{a_2} ppm	a_3 days	σ_{a_3} days	a_4	σ_{a_4}	a_5 days	σ_{a_5} days
BIA	0.289	395.263	2.2e-03	6.960e-03	1.0e-09	4.455	9.3e-04	54.139	0.197	-0.560	1.2e-04	-69.083	1.885
BRE	0.231	395.287	2.0e-03	6.873e-03	9.3e-10	4.399	9.1e-04	61.253	0.217	-0.646	1.0e-04	-60.591	1.409
ETL	0.212	395.187	1.5e-03	6.753e-03	6.7e-10	4.961	8.3e-04	63.245	0.096	-0.716	3.9e-05	-81.583	0.509
SOD	0.249	394.381	2.5e-03	7.125e-03	1.2e-09	5.482	1.2e-03	57.489	0.188	-0.679	7.7e-05	-64.031	1.056
UAF	0.148	394.688	1.1e-03	6.986e-03	5.1e-10	5.323	6.5e-04	65.471	0.065	-0.741	2.4e-05	-79.559	0.311
BIA, 5x10	0.445	395.360	2.0e-03	6.951e-03	9.0e-10	4.364	8.1e-04	53.409	0.179	-0.539	1.1e-04	-68.342	1.883
BRE, 5x10	0.365	395.417	1.9e-03	6.874e-03	8.8e-10	4.245	8.2e-04	59.290	0.218	-0.615	1.1e-04	-59.068	1.604
ETL, 5x10	0.340	395.189	1.3e-03	6.755e-03	5.9e-10	4.966	7.4e-04	63.262	0.085	-0.717	3.5e-05	-81.476	0.449
SOD, 5x10	0.384	394.430	1.9e-03	7.080e-03	8.8e-10	5.355	9.0e-04	58.974	0.146	-0.678	6.1e-05	-64.223	0.827
UAF, 5x10	0.295	394.673	9.7e-04	7.010e-03	4.4e-10	5.264	5.7e-04	66.506	0.057	-0.744	2.1e-05	-78.977	0.269

Table S3. Seasonal cycle fit parameters, a_i, with uncertainty estimates, σ_{a_i}, for fits of CAMS estimated X_{CO_2} from the grid-points nearest to the ground sites (see Table 1, in the manuscript, for exact coordinates) and CT2019B posterior estimates of X_{CO_2} averaged over the 5° latitude by 10° longitude coincidence regions centered at each ground site (using actual coordinate of the ground site as center) to Eq. 1 in the manuscript, as well as corresponding standard errors, $\bar{\sigma}$, used in fit optimization.

Site	$\bar{\sigma}$ ppm	a_0 ppm	σ_{a_0} ppm	a_1 ppm days^{-1}	σ_{a_1} ppm days^{-1}	a_2 ppm	σ_{a_2} ppm	a_3 days	σ_{a_3} days	a_4	σ_{a_4}	a_5 days	σ_{a_5} days
BIA	0.250	395.281	3.1e-03	6.865e-03	1.8e-09	4.616	1.3e-03	56.954	0.270	-0.581	1.5e-04	-64.754	2.316
BRE	0.250	395.467	2.4e-03	6.867e-03	1.4e-09	4.455	1.2e-03	67.109	0.241	-0.663	1.1e-04	-60.689	1.486
ETL	0.250	395.074	2.1e-03	6.830e-03	1.3e-09	5.338	1.3e-03	67.239	0.125	-0.757	4.2e-05	-78.853	0.562
SOD	0.250	394.684	2.2e-03	6.941e-03	1.3e-09	5.422	1.2e-03	64.203	0.164	-0.721	5.8e-05	-64.829	0.797
UAF	0.250	394.858	1.7e-03	7.067e-03	1.0e-09	5.273	1.1e-03	72.621	0.102	-0.767	3.3e-05	-75.087	0.442
BIA, 5x10	0.344	395.271	2.5e-03	6.866e-03	1.5e-09	4.630	1.1e-03	57.407	0.218	-0.585	1.2e-04	-64.931	1.842
BRE, 5x10	0.364	395.410	1.9e-03	6.880e-03	1.1e-09	4.473	9.4e-04	66.100	0.191	-0.658	8.5e-05	-61.289	1.205
ETL, 5x10	0.277	395.158	1.7e-03	6.841e-03	1.0e-09	5.236	1.1e-03	67.391	0.104	-0.749	3.6e-05	-79.926	0.485
SOD, 5x10	0.270	394.689	1.9e-03	6.946e-03	1.1e-09	5.393	9.9e-04	64.461	0.138	-0.718	4.9e-05	-64.654	0.678
UAF, 5x10	0.226	394.788	1.4e-03	7.060e-03	8.6e-10	5.229	9.2e-04	72.734	0.086	-0.765	2.8e-05	-75.256	0.377

Table S4. Seasonal cycle fit parameters, a_i, with uncertainty estimates, σ_{a_i}, for fits of GC-CT2019 estimated X_{CO_2} from the grid-points nearest to the ground sites (see Table 1, in the manuscript, for exact coordinates) and GC-CT2019 estimated X_{CO_2} averaged over the 5° latitude by 10° longitude coincidence regions centered at each ground site (using actual coordinate of the ground site as center) to Eq. 1 in the manuscript, as well as corresponding standard errors, $\bar{\sigma}$, used in fit optimization. Note that daily values from GC-CT2019 are used, so daily standard deviations for the data in the 5° by 10° coincidence regions represent spatial variability and are used directly as standard error in the fit optimization, whereas the single grid points near the ground sites have no spatial variability and are assigned the standard error of 0.250 ppm.

Site	$\bar{\sigma}$ ppm	a_0 ppm	σ_{a_0} ppm	a_1 ppm days^{-1}	σ_{a_1} ppm days^{-1}	a_2 ppm	σ_{a_2} ppm	a_3 days	σ_{a_3} days	a_4	σ_{a_4}	a_5 days	σ_{a_5} days
BIA	0.250	392.433	6.7e-03	6.603e-03	1.3e-08	4.734	2.9e-03	59.926	0.594	-0.595	3.3e-04	-59.223	4.759
BRE	0.250	392.644	6.6e-03	6.379e-03	1.3e-08	4.717	3.2e-03	66.694	0.601	-0.668	2.7e-04	-59.752	3.597
ETL	0.250	392.542	4.8e-03	6.102e-03	9.1e-09	5.374	2.9e-03	70.342	0.273	-0.771	9.1e-05	-75.665	1.158
SOD	0.250	392.000	6.1e-03	6.243e-03	1.2e-08	5.782	3.0e-03	63.652	0.390	-0.687	1.6e-04	-62.111	2.143
UAF	0.250	391.762	3.9e-03	6.305e-03	7.6e-09	5.740	2.4e-03	70.623	0.204	-0.777	6.6e-05	-74.030	0.838
BIA, 5x10	0.368	392.506	6.2e-03	6.593e-03	1.2e-08	4.656	2.6e-03	58.697	0.545	-0.570	3.2e-04	-60.196	4.902
BRE, 5x10	0.341	392.747	6.0e-03	6.389e-03	1.2e-08	4.625	3.0e-03	68.183	0.553	-0.673	2.5e-04	-60.683	3.281
ETL, 5x10	0.299	392.549	4.0e-03	6.075e-03	7.7e-09	5.353	2.4e-03	70.216	0.232	-0.766	7.9e-05	-75.365	1.004
SOD, 5x10	0.238	392.043	5.6e-03	6.228e-03	1.1e-08	5.734	2.7e-03	63.442	0.364	-0.681	1.6e-04	-61.605	2.053
UAF, 5x10	0.209	391.730	3.6e-03	6.228e-03	7.0e-09	5.895	2.2e-03	70.268	0.181	-0.781	5.7e-05	-73.842	0.733
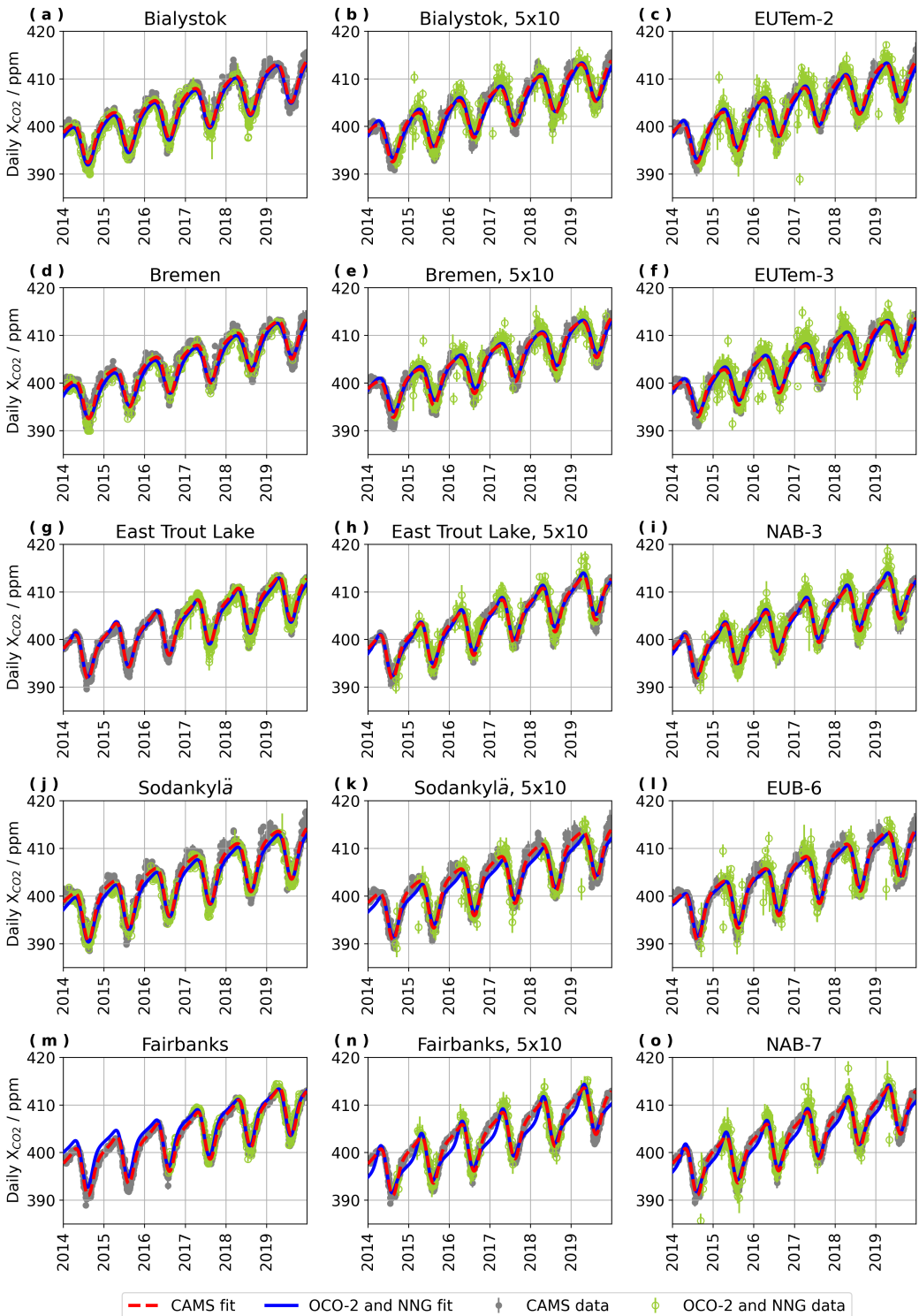
Figure S2. Daily average time-series and seasonal cycle fits of CAMS model estimates (2014-2019) and observations (OCO-2 2014-2019 and NNG as available 2014-2019) at ground sites, within the 5° latitude by 10° longitude coincidence region, and within the 5° latitude by 20° longitude zone encompassing the ground site.
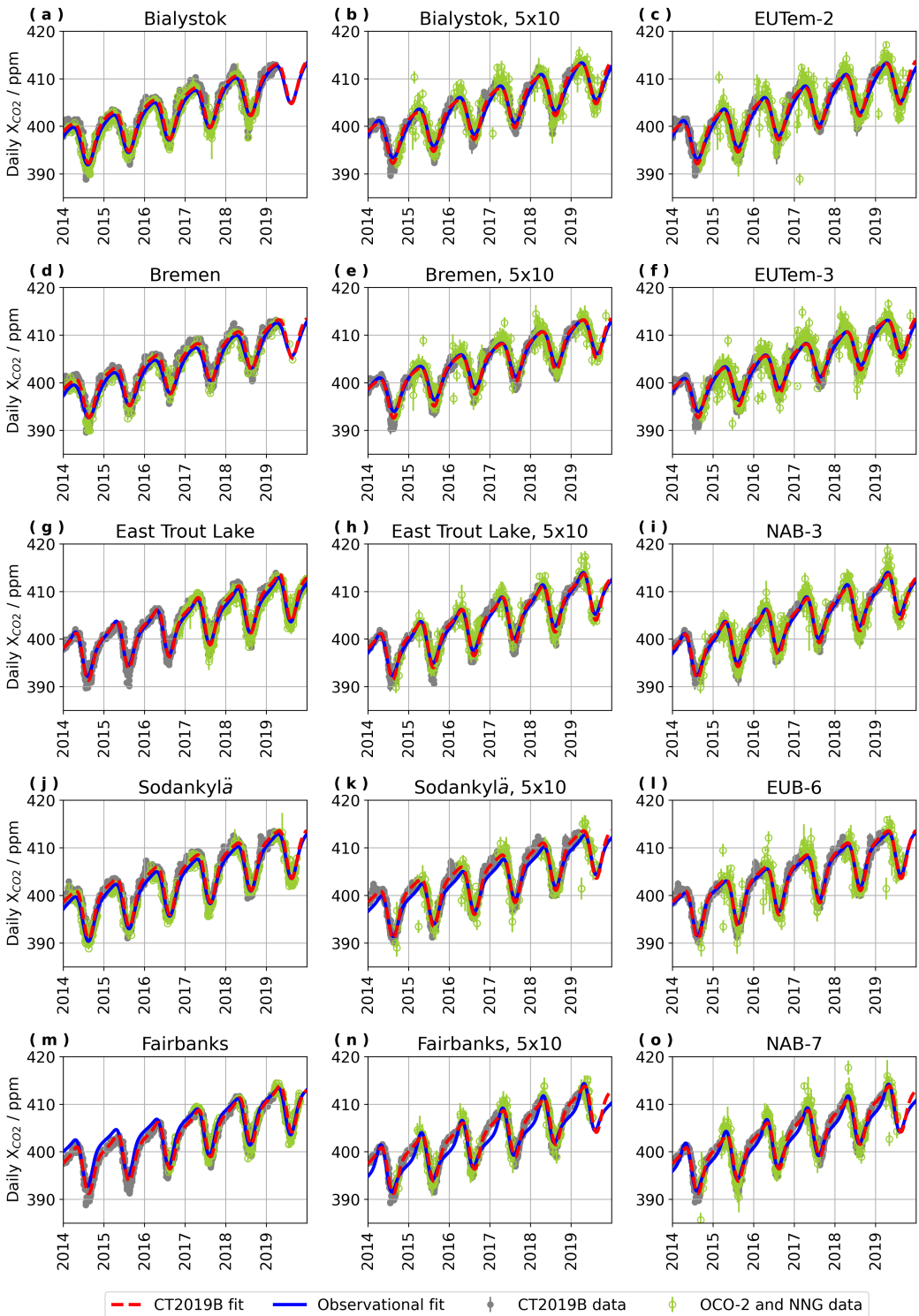
Figure S3. Daily average time-series and seasonal cycle fits of CT2019B model estimates (2014-2019) and observations (OCO-2 2014-2019 and NNG as available 2014-2019) at ground sites, within the 5° latitude by 10° longitude coincidence region, and within the 5° latitude by 20° longitude zone encompassing the ground site.
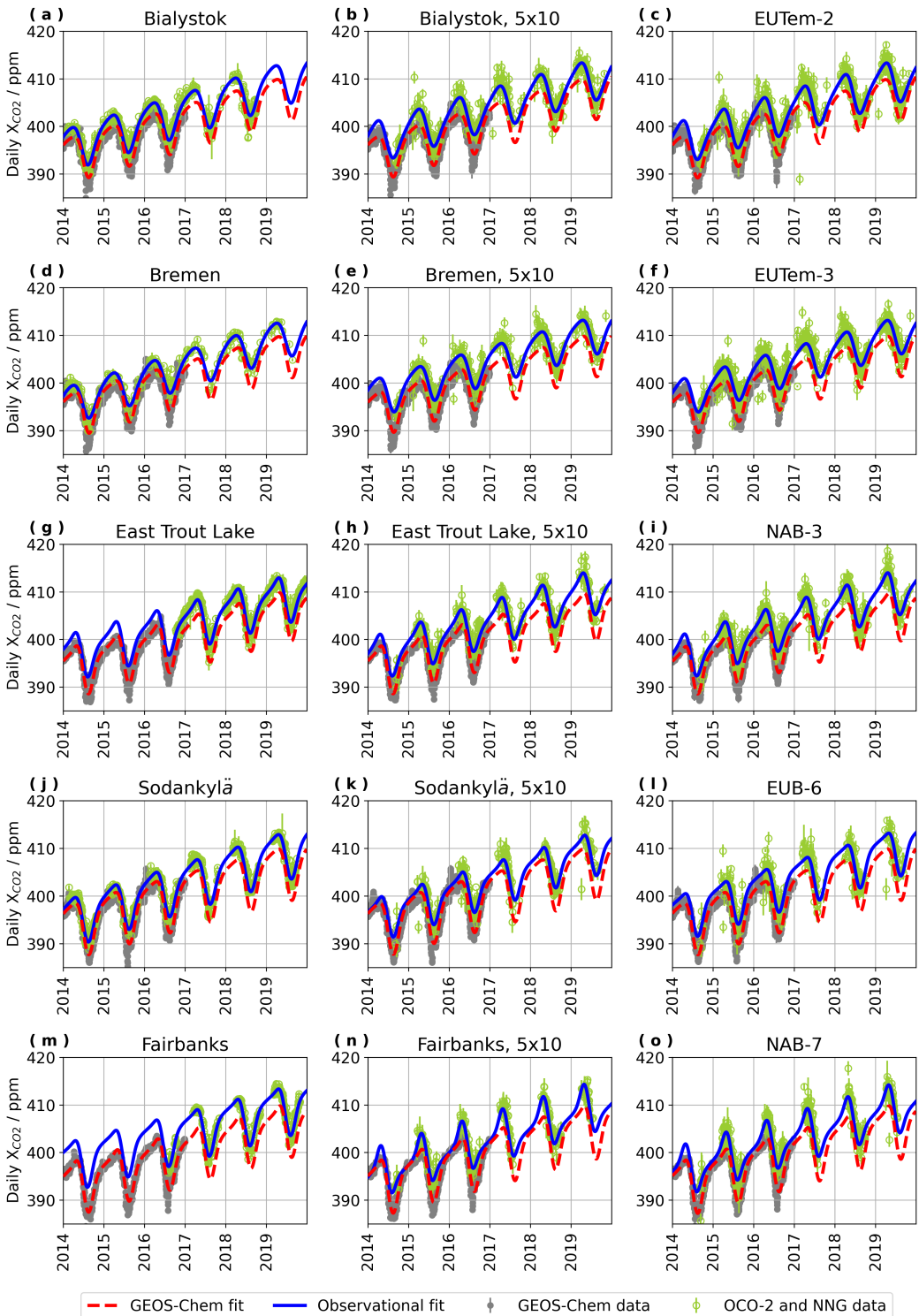
Figure S4. Daily average time-series and seasonal cycle fits of GC-CT2019 model estimates (2014-2016) and observations (OCO-2 2014-2019 and NNG as available 2014-2019) at ground sites, within the 5° latitude by 10° longitude coincidence region, and within the 5° latitude by 20° longitude zone encompassing the ground site.

7

## S1.2 Seasonal cycle fits for OCO-2 data in 5° latitude by 20° longitude zones

In this section, details of seasonal cycle fits to OCO-2 daily averages (see details of data handling in Sect. 2.1 of the manuscript) within all 5° latitude by 20° longitude zones are provided. Figures S5 through S12 show plots of time-series of OCO-2 data and the corresponding fits, and Tables S5 and S6 report standard errors used in each fit, the seasonal fit parameters calculated, and an estimate of parameter uncertainty.
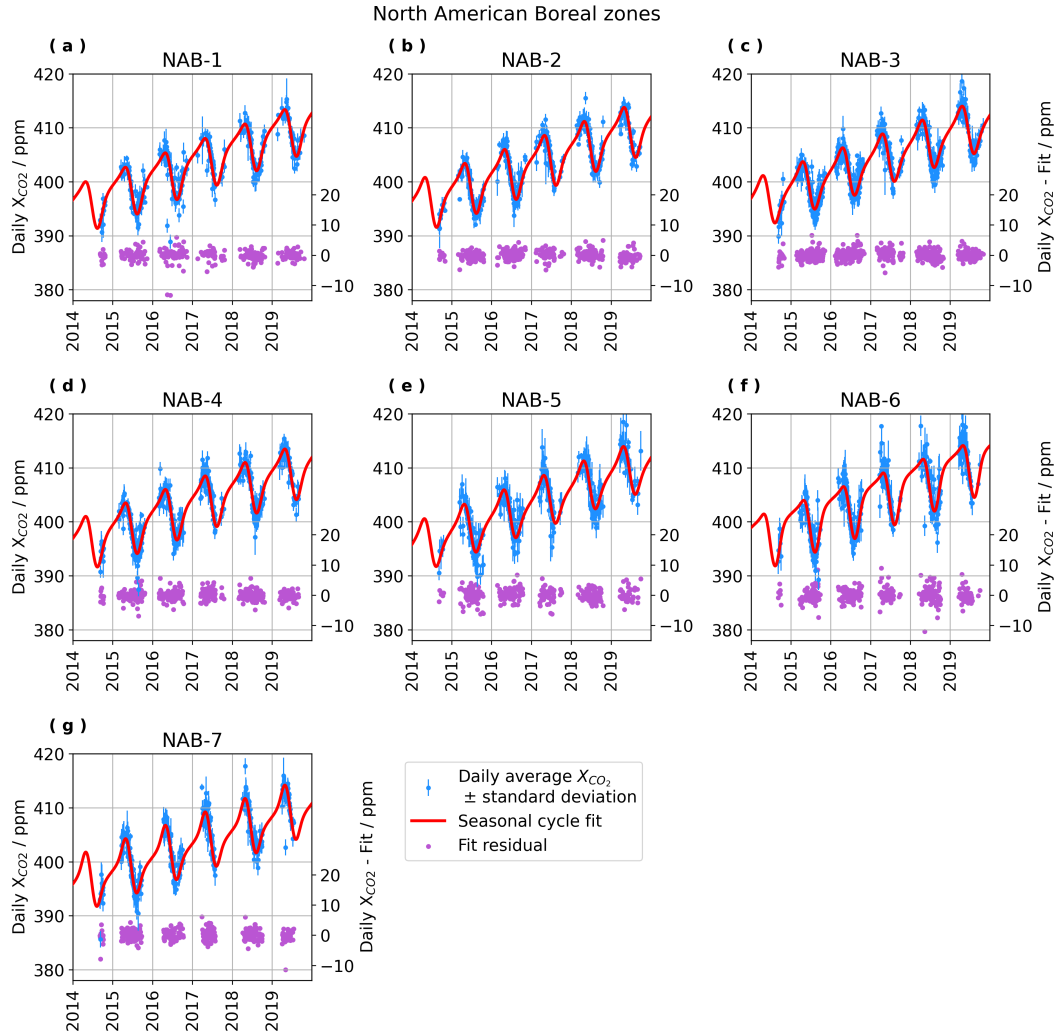

Figure S5. Daily average time-series of OCO-2 observations by zone in the North American Boreal region, with seasonal cycle fits and fit residuals.
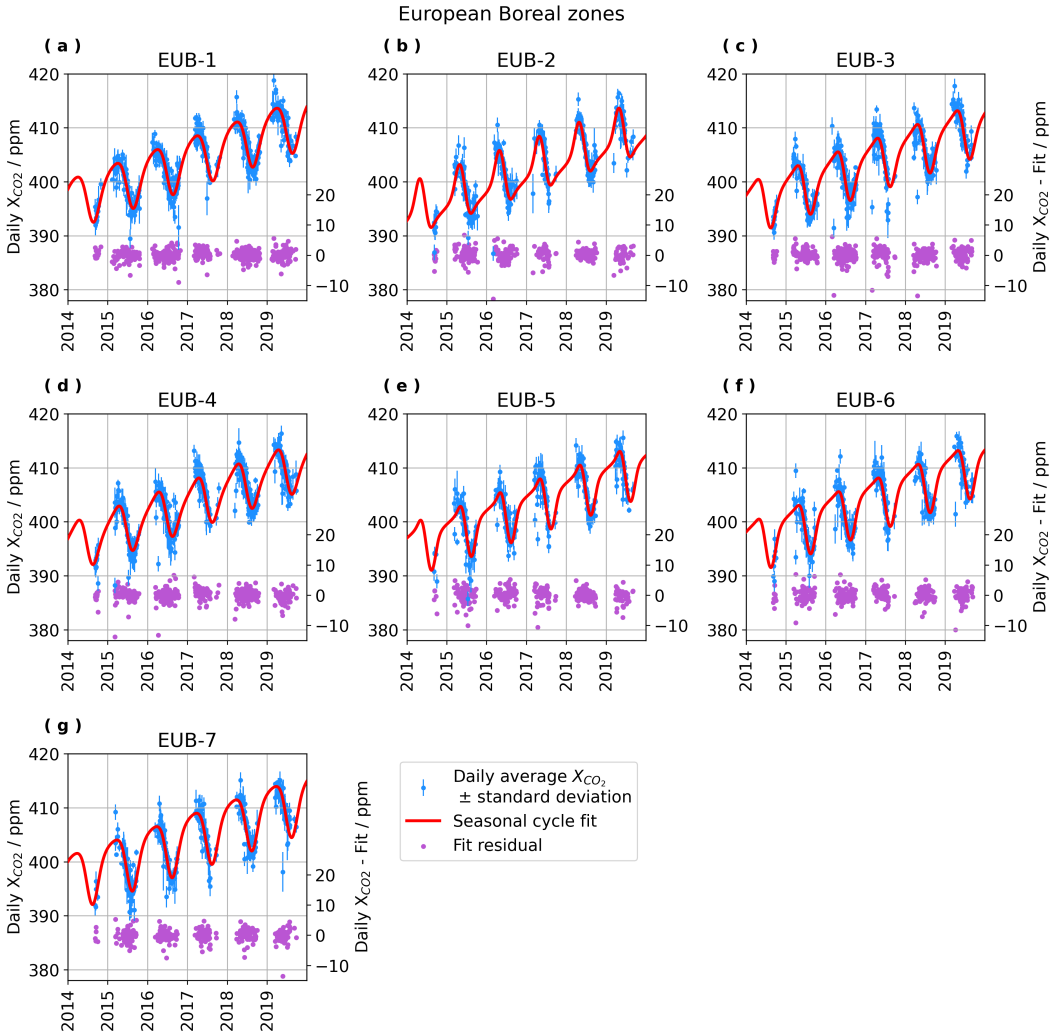
Figure S6. Daily average time-series of OCO-2 observations by zone in the European Boreal region, with seasonal cycle fits and fit residuals.
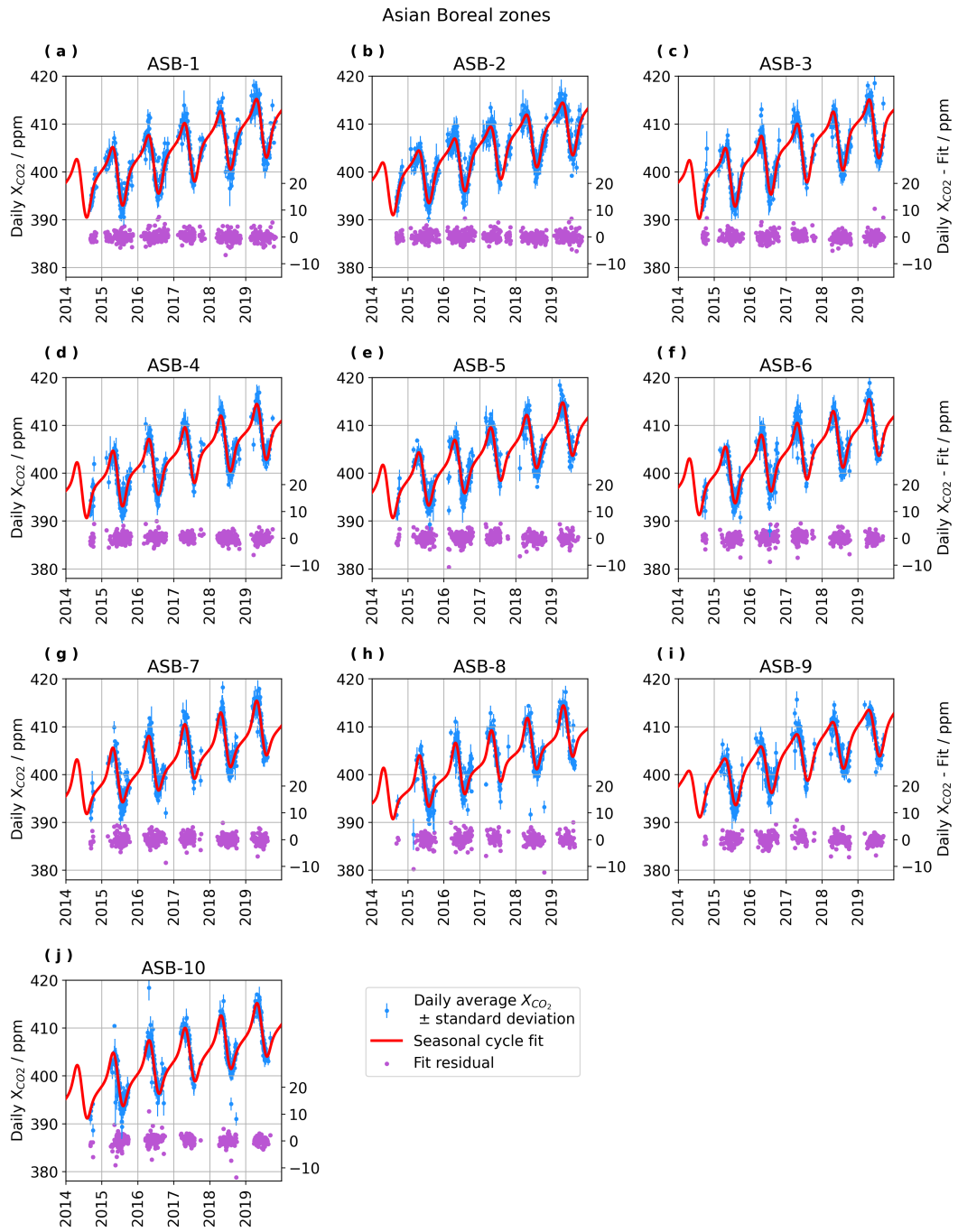
Figure S7. Daily average time-series of OCO-2 observations by zone in the Asian Boreal region, with seasonal cycle fits and fit residuals.
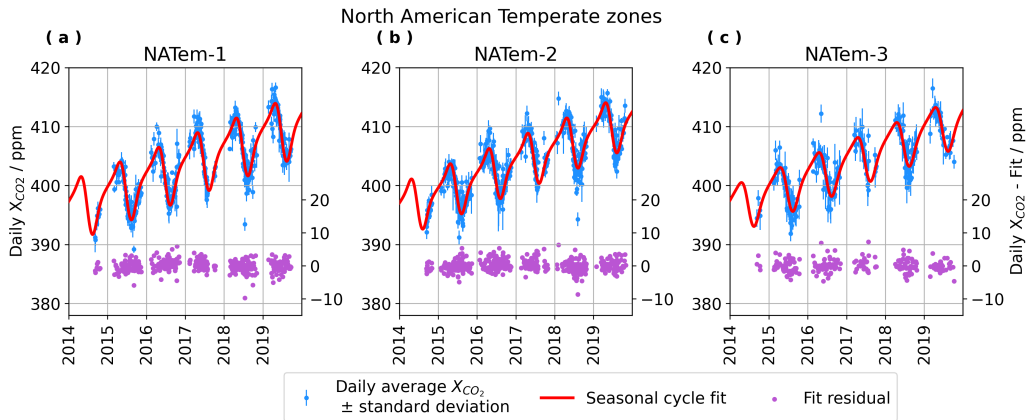
Figure S8. Daily average time-series of OCO-2 observations by zone in the North American Temperate region, with seasonal cycle fits and fit residuals.
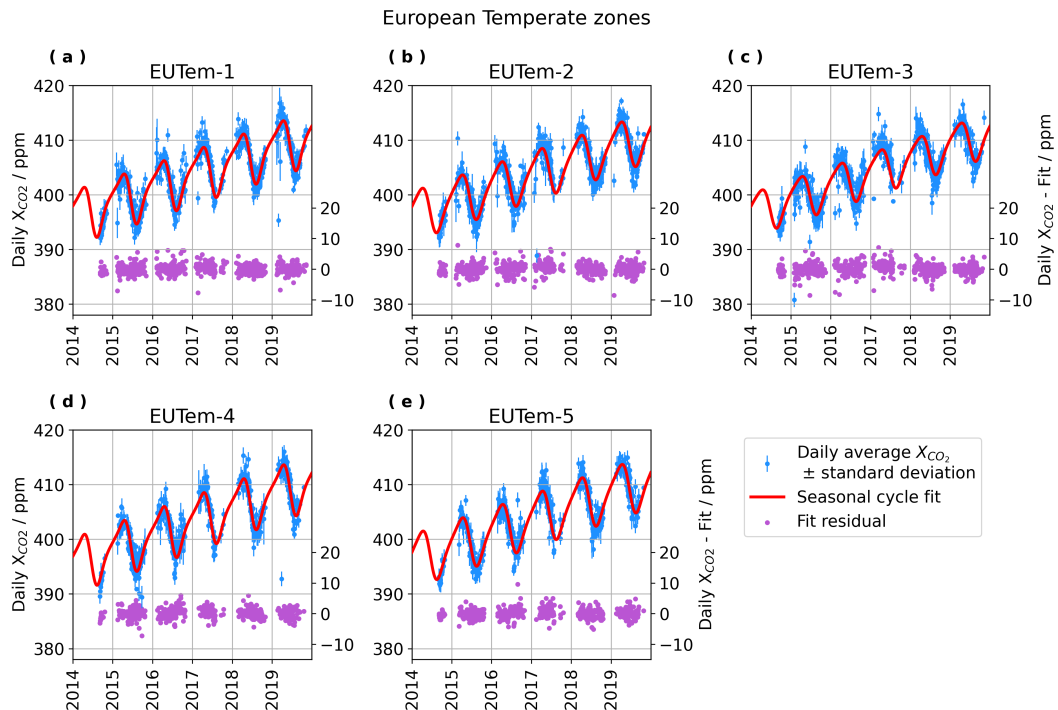

Figure S9. Daily average time-series of OCO-2 observations by zone in the European Temperate region, with seasonal cycle fits and fit residuals.
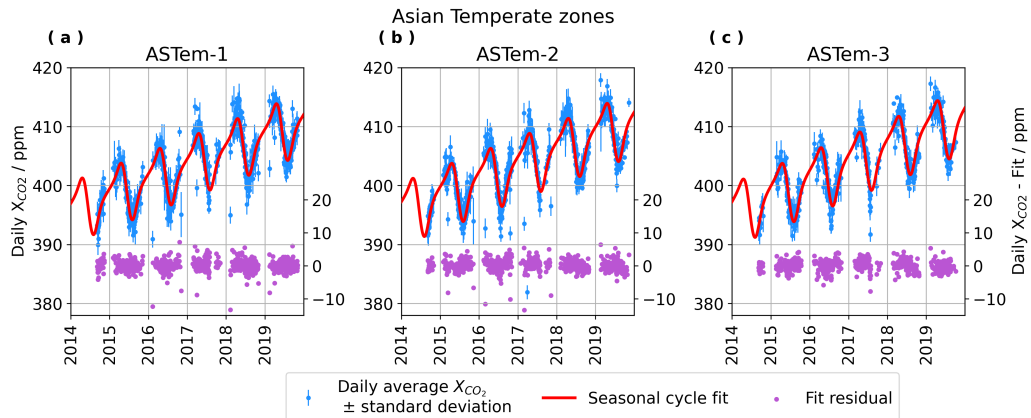
Figure S10. Daily average time-series of OCO-2 observations by zone in the Asian Temperate region, with seasonal cycle fits and fit residuals.
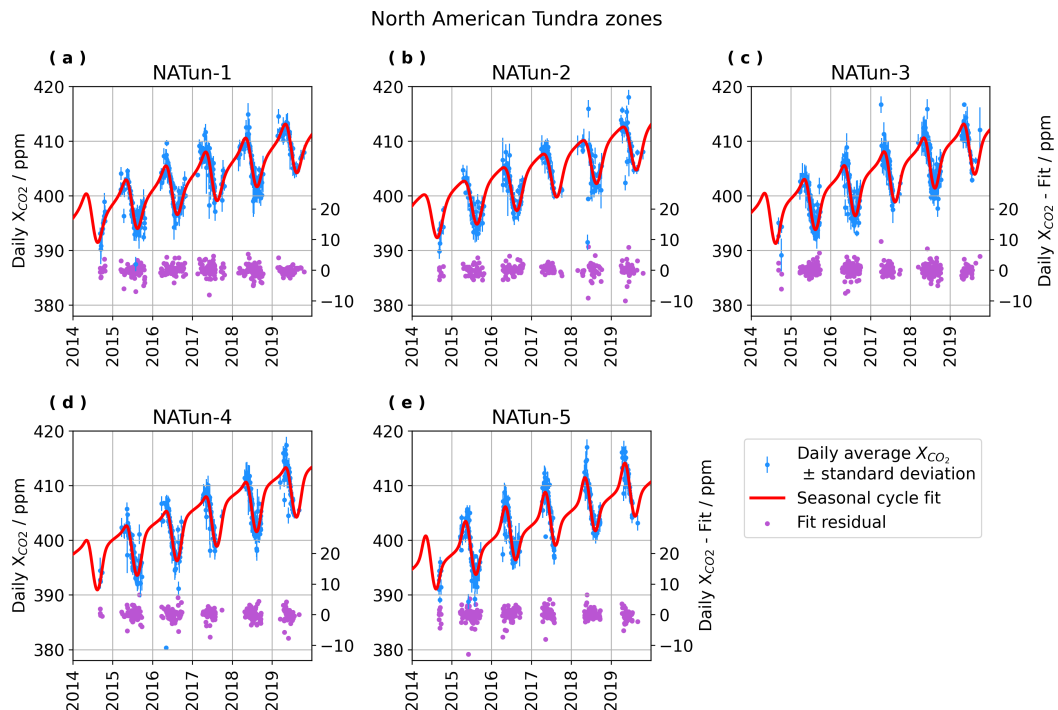
Figure S11. Daily average time-series of OCO-2 observations by zone in the North American Tundra region, with seasonal cycle fits and fit residuals.
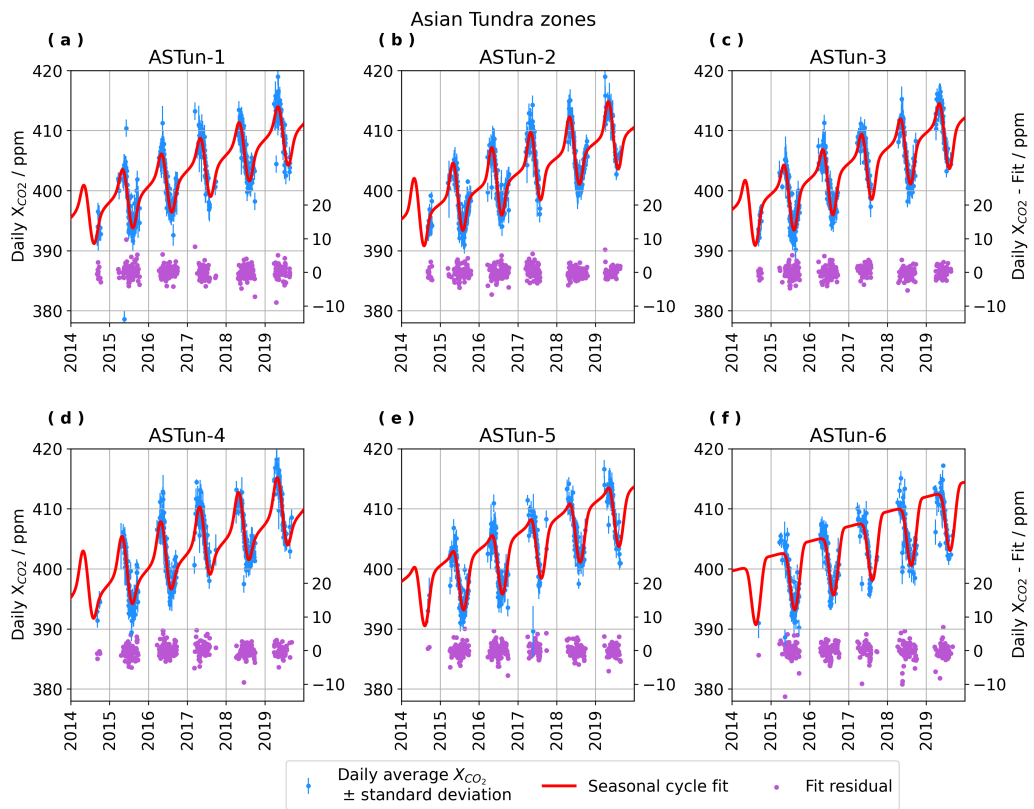
Figure S12. Daily average time-series of OCO-2 observations by zone in the Asian Tundra region, with seasonal cycle fits and fit residuals.

Table S5. Seasonal cycle fit parameters, a_i, with uncertainty estimates, σ_{a_i}, for fits of OCO-2 data to Eq. 1 in the manuscript, and standard errors, $\bar{\sigma}$, for zones in Boreal regions.

Zone	$\bar{\sigma}$ ppm	a_0 ppm	σ_{a_0} ppm	a_1 ppm days^{-1}	σ_{a_1} ppm days^{-1}	a_2 ppm	σ_{a_2} ppm	a_3 days	σ_{a_3} days	a_4	σ_{a_4}	a_5 days	σ_{a_5} days
NAB-1	1.309	394.424	0.088	7.313e-03	4.2e-08	4.736	0.024	69.228	12.414	-0.720	2.1e-03	-82.840	53.518
NAB-2	1.142	394.940	0.039	7.095e-03	1.8e-08	5.018	9.6e-03	75.812	3.488	-0.728	6.4e-04	-89.050	17.666
NAB-3	1.307	395.582	0.046	7.037e-03	2.1e-08	4.791	0.012	69.649	4.253	-0.679	9.8e-04	-99.473	26.146
NAB-4	1.246	395.131	0.040	6.835e-03	1.9e-08	5.063	9.3e-03	72.906	5.725	-0.729	7.0e-04	-88.260	25.271
NAB-5	1.857	394.898	0.088	7.319e-03	3.9e-08	4.842	0.020	74.901	15.873	-0.691	2.2e-03	-99.808	75.563
NAB-6	1.911	395.439	0.082	6.946e-03	3.9e-08	5.182	0.019	61.724	39.469	-0.811	1.7e-03	-75.845	99.621
NAB-7	1.495	395.610	0.056	6.792e-03	2.9e-08	5.384	0.015	78.378	19.863	-0.789	1.5e-03	-104.100	54.686
EUB-1	1.236	395.536	0.037	6.984e-03	1.8e-08	4.696	0.011	64.245	9.376	-0.437	2.1e-03	-59.368	96.246
EUB-2	1.349	394.820	0.088	7.153e-03	3.7e-08	4.907	0.019	91.721	27.545	-0.780	2.5e-03	-123.620	82.368
EUB-3	1.353	394.752	0.067	6.962e-03	3.0e-08	4.912	0.014	67.243	19.300	-0.658	2.2e-03	-77.140	83.666
EUB-4	1.425	394.993	0.061	7.122e-03	2.8e-08	4.572	0.014	70.456	20.578	-0.510	2.7e-03	-84.720	162.578
EUB-5	1.327	394.421	0.099	6.977e-03	4.7e-08	4.999	0.023	71.225	33.419	-0.840	2.4e-03	-78.370	80.599
EUB-6	1.357	394.797	0.088	6.951e-03	3.8e-08	4.879	0.019	65.890	63.993	-0.752	4.6e-03	-68.156	158.712
EUB-7	1.442	395.768	0.114	6.790e-03	4.0e-08	5.240	0.091	52.871	91.071	-0.537	6.3e-03	-59.561	396.314
ASB-1	1.264	395.424	0.028	6.871e-03	1.3e-08	6.464	9.5e-03	63.227	1.150	-0.800	2.3e-04	-100.237	4.346
ASB-2	1.390	395.324	0.024	6.844e-03	1.0e-08	5.864	7.8e-03	60.427	1.154	-0.767	2.6e-04	-93.244	4.979
ASB-3	1.442	395.156	0.034	6.937e-03	1.6e-08	6.469	9.9e-03	63.938	2.325	-0.846	2.4e-04	-95.673	6.667
ASB-4	1.424	395.339	0.034	6.675e-03	1.6e-08	6.150	9.6e-03	69.088	2.305	-0.857	2.9e-04	-107.016	6.419
ASB-5	1.252	395.007	0.047	7.132e-03	2.2e-08	5.923	0.013	68.766	3.628	-0.799	5.0e-04	-108.636	13.228
ASB-6	1.343	396.020	0.041	6.777e-03	2.0e-08	6.249	0.011	71.355	3.861	-0.830	3.8e-04	-104.828	11.199
ASB-7	1.277	396.337	0.049	6.714e-03	2.3e-08	6.038	0.013	77.818	5.721	-0.826	7.9e-04	-118.412	15.742
ASB-8	1.320	394.833	0.090	7.140e-03	4.3e-08	5.702	0.024	80.547	8.527	-0.890	8.6e-04	-114.119	20.753
ASB-9	1.261	394.745	0.064	6.974e-03	2.7e-08	5.252	0.014	63.698	14.839	-0.696	1.5e-03	-86.592	58.752
ASB-10	1.375	395.467	0.069	7.087e-03	3.0e-08	5.942	0.015	78.892	16.782	-0.797	1.4e-03	-110.634	44.932

**Table S6.** Seasonal cycle fit parameters, a_i, with uncertainty estimates, σ_{a_i}, for fits of OCO-2 data to Eq. 1 in the manuscript, and standard errors, $\bar{\sigma}$, for zones in Temperate and Tundra regions.

| Zone	$\bar{\sigma}$ ppm	a_0 ppm	σ_{a_0} ppm	a_1 ppm days^{-1}	σ_{a_1} ppm days^{-1}	a_2 ppm	σ_{a_2} ppm	a_3 days	σ_{a_3} days	a_4	σ_{a_4}	a_5 days	σ_{a_5} days
NATem-1	1.133	395.442	0.060	6.801e-03	2.5e-08	5.287	0.014	72.451	4.189	-0.711	8.8e-04	-88.732	21.763
NATem-2	1.185	395.671	0.046	7.082e-03	2.1e-08	4.638	0.014	70.616	3.239	-0.733	8.1e-04	-96.405	17.635
NATem-3	1.667	395.620	0.122	6.971e-03	5.3e-08	4.146	0.029	68.076	22.576	-0.590	4.9e-03	-85.342	169.476
EUTem-1	1.218	395.707	0.028	6.664e-03	1.2e-08	4.972	7.6e-03	63.771	2.310	-0.639	6.3e-04	-92.198	15.929
EUTem-2	1.278	396.047	0.033	6.631e-03	1.4e-08	4.513	8.1e-03	66.479	3.739	-0.488	1.3e-03	-93.991	43.361
EUTem-3	1.298	396.247	0.042	6.693e-03	1.8e-08	3.953	0.010	73.428	5.441	-0.487	2.3e-03	-77.441	65.002
EUTem-4	1.318	395.101	0.053	6.949e-03	2.3e-08	5.069	0.013	68.180	6.815	-0.634	1.3e-03	-95.369	41.831
EUTem-5	1.354	395.952	0.034	6.672e-03	1.5e-08	4.863	7.8e-03	70.659	6.163	-0.492	1.3e-03	-92.903	58.922
ASTem-1	1.437	395.357	0.035	6.895e-03	1.5e-08	5.182	0.011	65.308	2.291	-0.737	5.7e-04	-102.263	11.351
ASTem-2	1.184	395.154	0.042	6.959e-03	1.8e-08	5.317	0.012	64.538	2.682	-0.730	6.0e-04	-96.134	13.894
ASTem-3	1.231	394.967	0.042	7.282e-03	1.9e-08	5.357	9.7e-03	63.557	3.845	-0.696	6.9e-04	-94.909	20.344
NATun-1	1.322	394.687	0.059	6.976e-03	2.8e-08	4.831	0.015	78.833	6.449	-0.743	9.6e-04	-88.775	29.139
NATun-2	1.384	395.105	0.181	6.780e-03	8.2e-08	4.353	0.059	65.755	114.069	-0.656	8.8e-03	-62.542	431.229
NATun-3	1.517	394.656	0.073	6.929e-03	3.5e-08	4.960	0.017	72.774	38.565	-0.806	1.9e-03	-80.739	93.305
NATun-4	1.293	394.174	0.132	7.280e-03	5.7e-08	4.905	0.030	65.522	110.023	-0.866	4.6e-03	-72.810	199.418
NATun-5	1.411	394.663	0.083	7.287e-03	4.3e-08	5.216	0.023	83.498	50.340	-0.893	1.1e-03	-100.016	99.098
ASTun-1	1.460	394.805	0.093	7.150e-03	4.3e-08	5.217	0.022	77.825	29.123	-0.866	1.5e-03	-98.625	61.286
ASTun-2	1.584	395.245	0.044	7.003e-03	2.3e-08	5.954	0.013	77.232	4.501	-0.929	2.7e-04	-106.731	8.310
ASTun-3	1.364	395.087	0.053	7.003e-03	2.5e-08	5.767	0.014	72.203	19.452	-0.907	4.6e-04	-92.975	36.032
ASTun-4	1.469	396.249	0.057	6.685e-03	2.5e-08	5.943	0.013	81.223	13.380	-0.857	1.0e-03	-115.640	27.800
ASTun-5	1.473	394.144	0.091	7.233e-03	4.0e-08	5.244	0.022	60.559	78.331	-0.892	2.0e-03	-74.444	135.349
ASTun-6	1.283	394.435	0.453	6.756e-03	5.2e-08	5.261	0.506	37.145	257.813	-0.913	5.5e-03	-39.714	333.726

S1.3 Seasonal cycle fits for CAMS estimates in 5° latitude by 20° longitude zones

In this section, details of seasonal cycle fits to CAMS daily averages (Chevallier (2020b); Chevallier (2020a); see Sect. 2.5 of the manuscript) within all 5° latitude by 20° longitude zones are provided. Figures S13 through S20 show plots of time-series of CAMS model estimates, the corresponding fits to CAMS estimates, and the fit to OCO-2 data (to allow for easier direct comparison between the model-derived and OCO-2 observational fits). Tables S7 and S8 report standard errors used in each CAMS fit, the seasonal fit parameters calculated, and an estimate of parameter uncertainty.
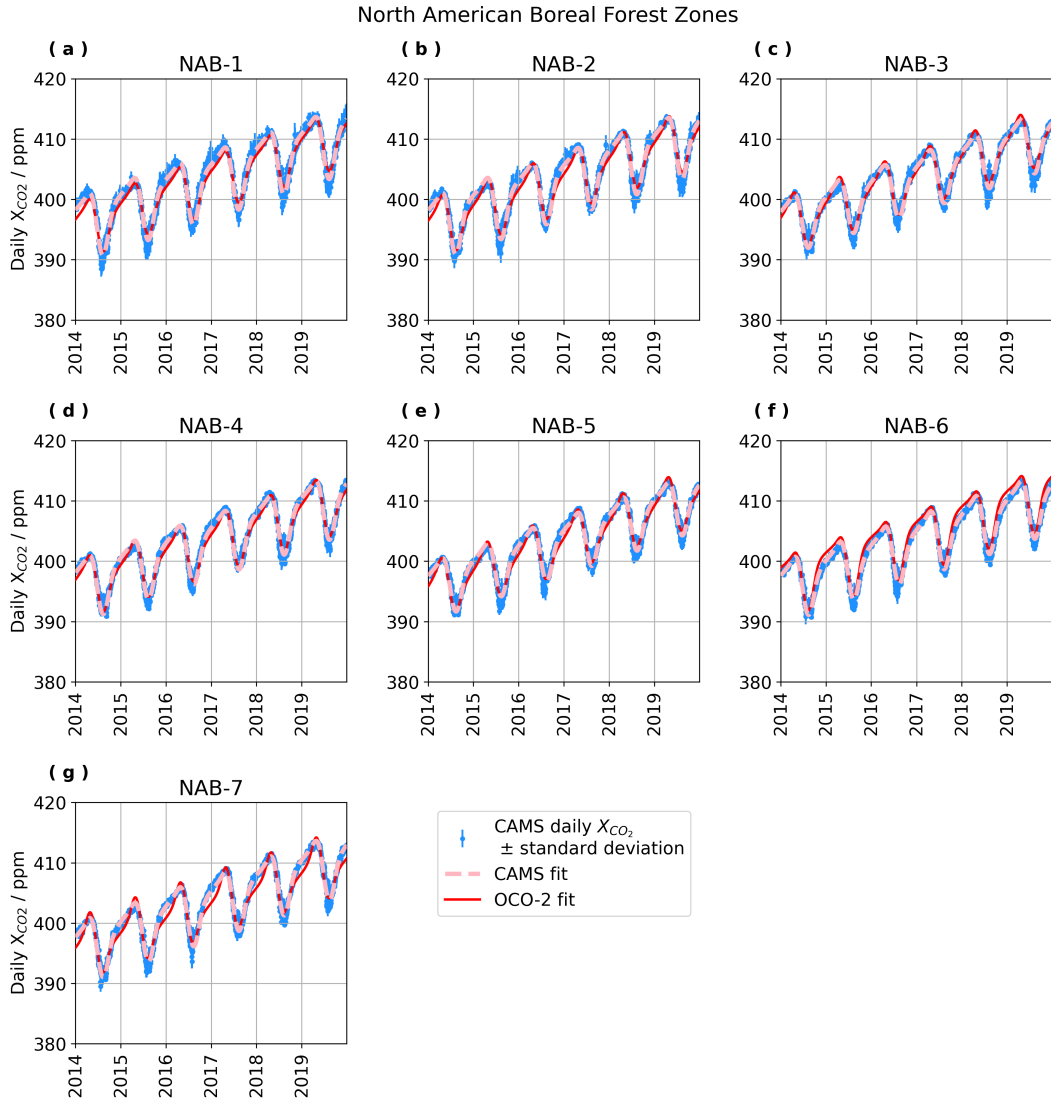
Figure S13. Time-series of CAMS X_{CO_2} by zone in the North American Boreal region, with seasonal cycle fits to CAMS and OCO-2.
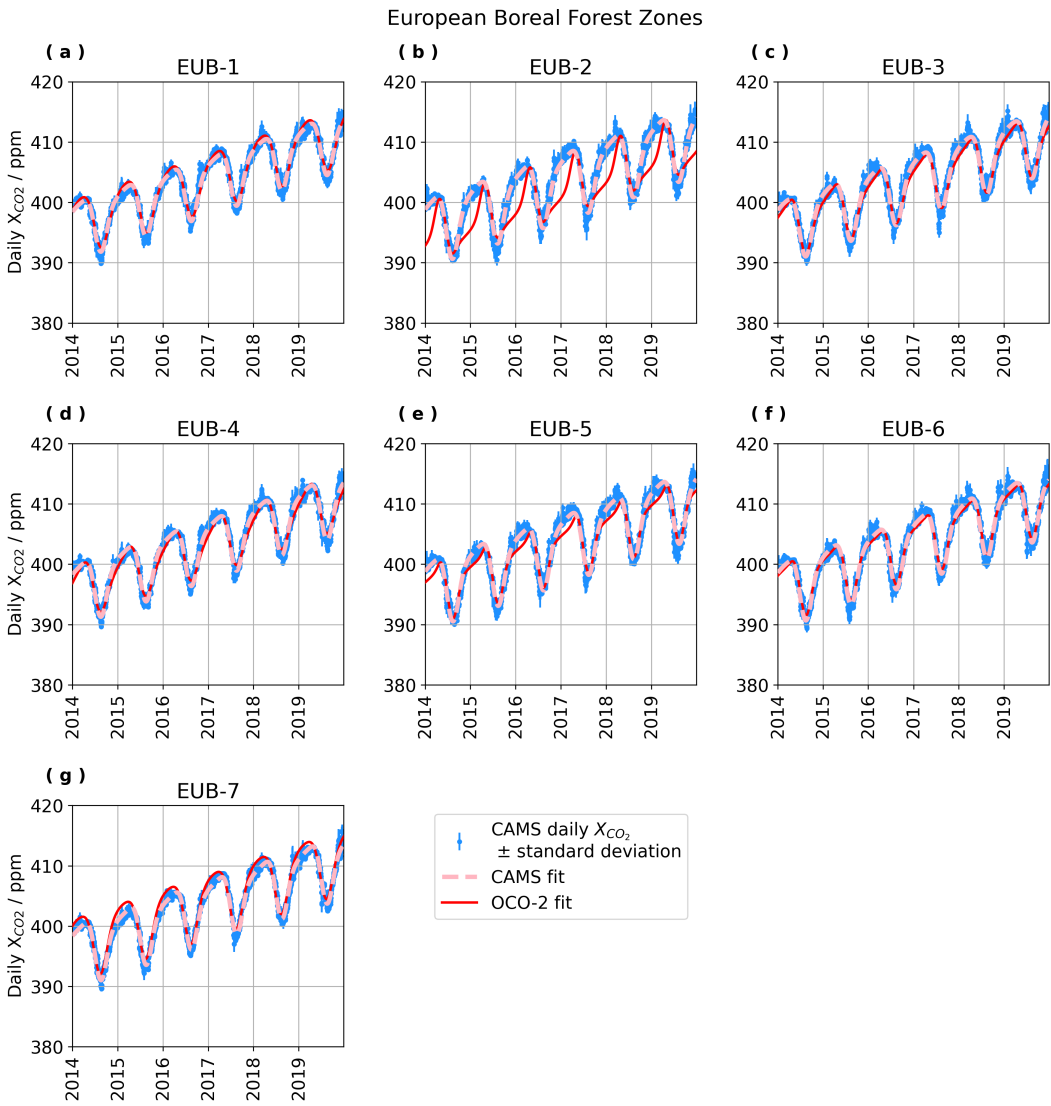
Figure S14. Time-series of CAMS X_{CO_2} by zone in the European Boreal region, with seasonal cycle fits to CAMS and OCO-2.
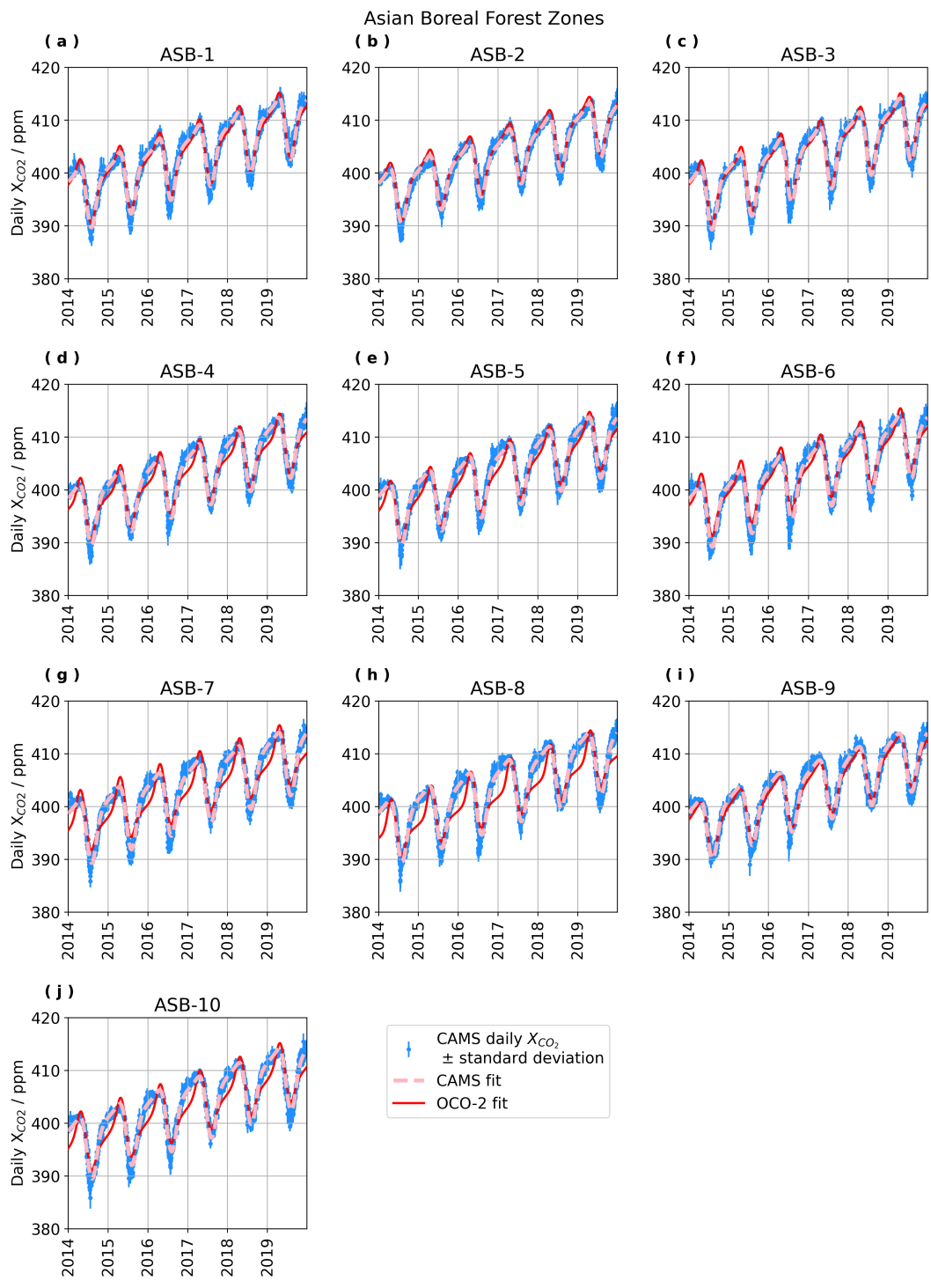
Figure S15. Time-series of CAMS X_{CO_2} by zone in the Asian Boreal region, with seasonal cycle fits to CAMS and OCO-2.
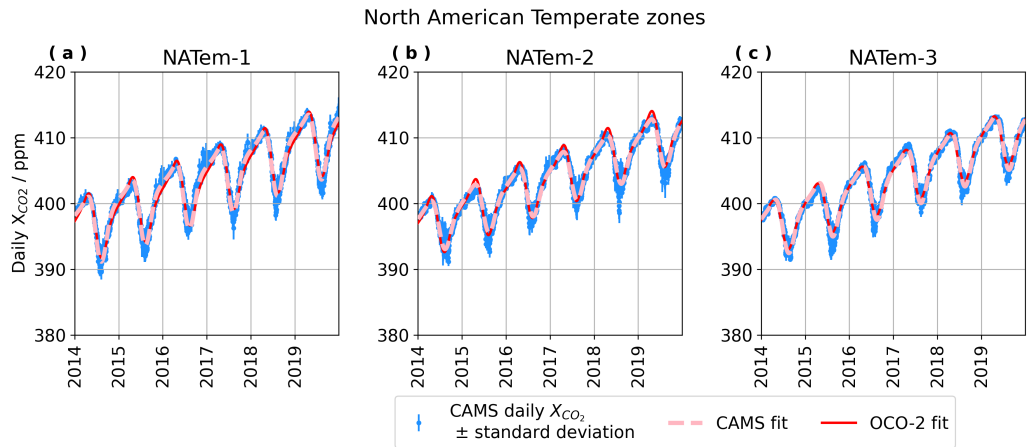
Figure S16. Time-series of CAMS X_{CO_2} by zone in the North American Temperate region, with seasonal cycle fits to CAMS and OCO-2.
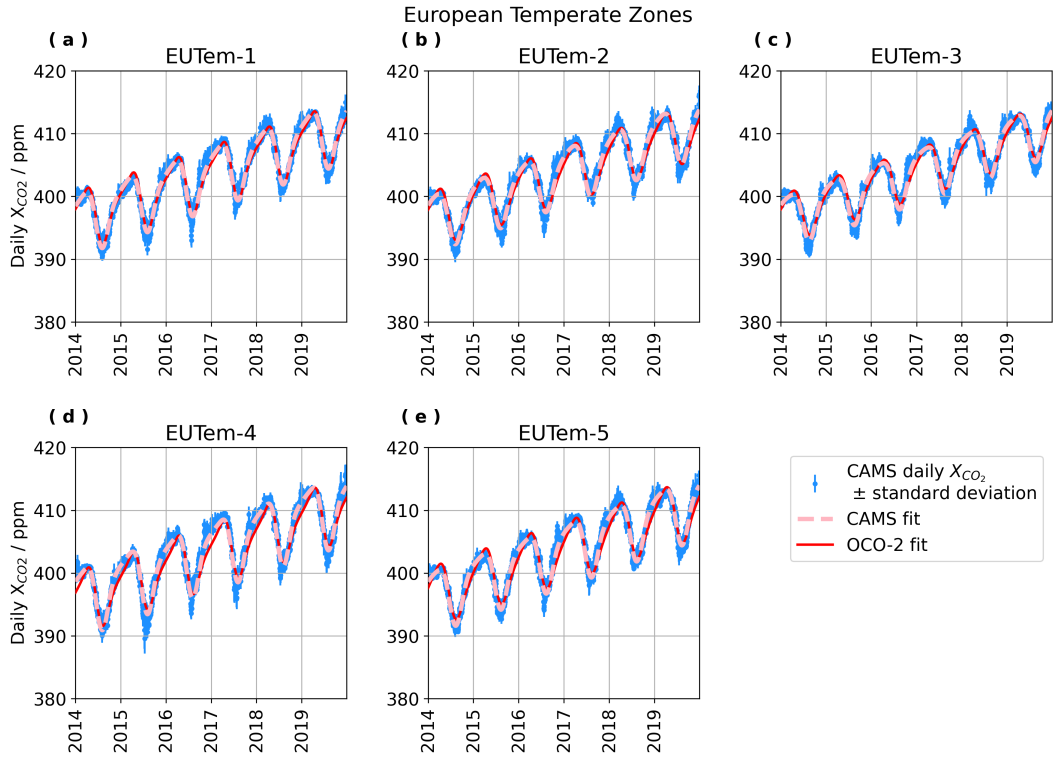

Figure S17. Time-series of CAMS X_{CO_2} by zone in the European Temperate region, with seasonal cycle fits to CAMS and OCO-2.
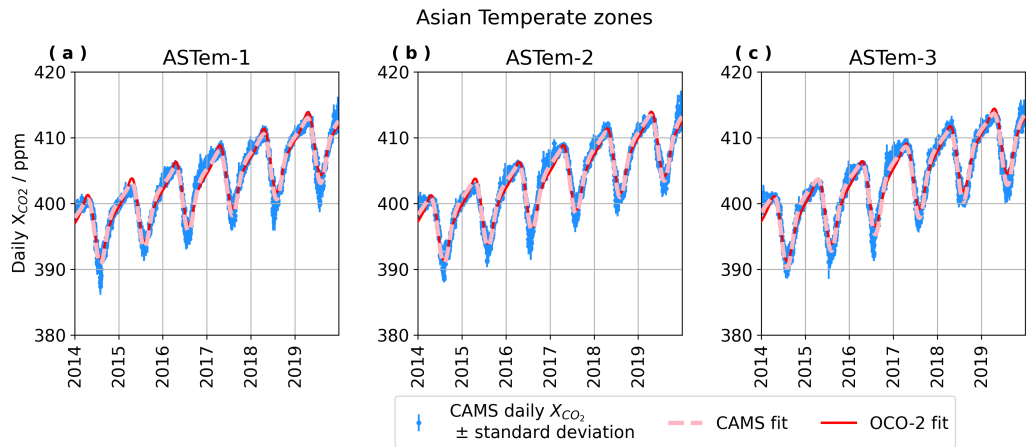
Figure S18. Time-series of CAMS X_{CO_2} by zone in the Asian Temperate region, with seasonal cycle fits to CAMS and OCO-2.
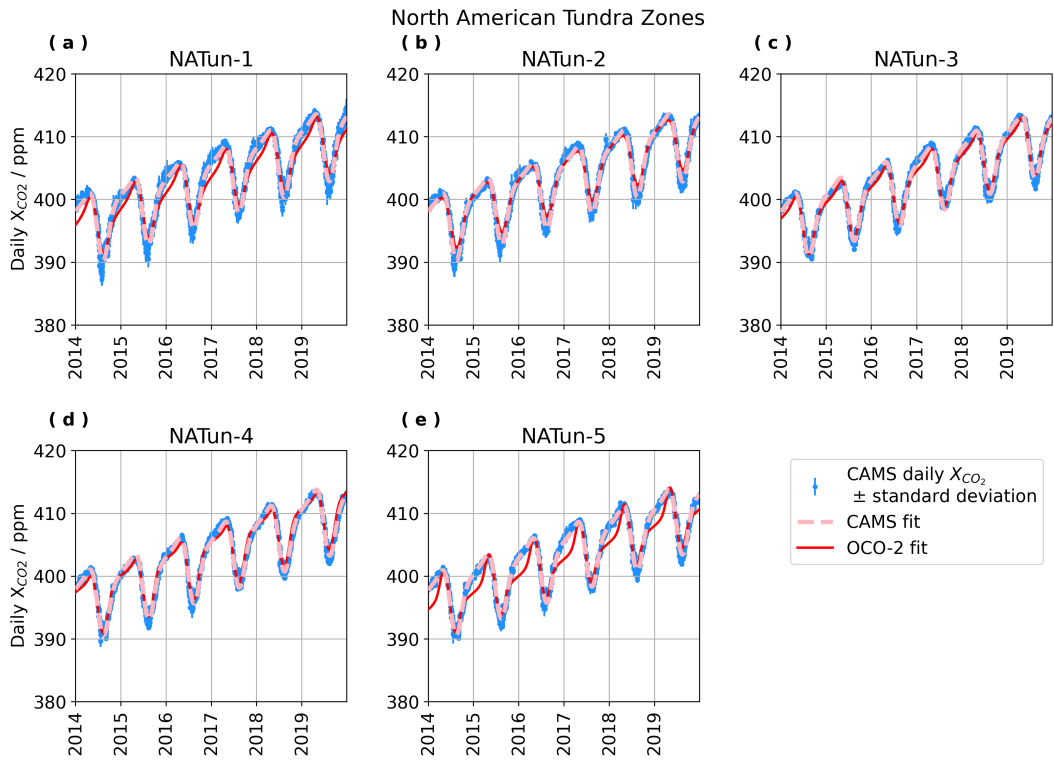
Figure S19. Time-series of CAMS X_{CO_2} by zone in the North American Tundra region, with seasonal cycle fits to CAMS and OCO-2.
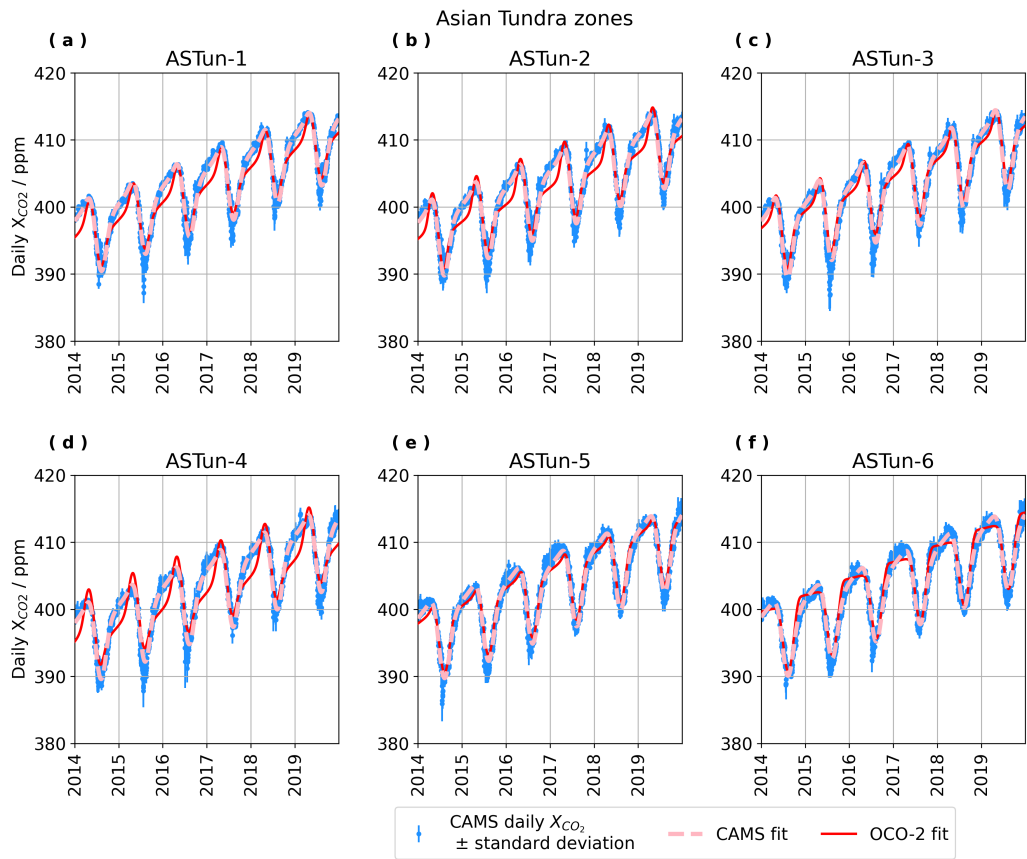
Figure S20. Time-series of CAMS X_{CO_2} by zone in the Asian Tundra region, with seasonal cycle fits to CAMS and OCO-2.

Table S7. Seasonal cycle fit parameters, a_i, with uncertainty estimates, σ_{a_i}, for fits of CAMS estimated X_{CO_2} to Eq. 1 in the manuscript, and standard errors, $\bar{\sigma}$, for zones in Boreal regions.

| Zone	$\bar{\sigma}$ ppm	a_0 ppm	σ_{a_0} ppm	a_1 ppm days^{-1}	σ_{a_1} ppm days^{-1}	a_2 ppm	σ_{a_2} ppm	a_3 days	σ_{a_3} days	a_4	σ_{a_4}	a_5 days	σ_{a_5} days
NAB-1	0.496	394.702	1.5e-03	6.924e-03	6.8e-10	5.541	8.6e-04	62.109	0.088	-0.755	3.0e-05	-77.557	0.389
NAB-2	0.400	394.826	1.2e-03	6.806e-03	5.6e-10	5.471	7.1e-04	64.413	0.072	-0.752	2.5e-05	-76.771	0.325
NAB-3	0.444	395.219	1.3e-03	6.765e-03	5.7e-10	4.795	7.0e-04	64.498	0.087	-0.706	3.7e-05	-80.527	0.477
NAB-4	0.333	394.938	1.0e-03	6.755e-03	4.8e-10	5.243	5.9e-04	65.031	0.066	-0.730	2.5e-05	-76.053	0.323
NAB-5	0.372	394.885	1.1e-03	6.908e-03	5.0e-10	4.795	6.3e-04	68.124	0.078	-0.727	3.1e-05	-76.614	0.396
NAB-6	0.325	394.725	9.7e-04	6.905e-03	4.4e-10	5.184	5.7e-04	67.284	0.059	-0.747	2.1e-05	-78.015	0.275
NAB-7	0.326	394.717	1.0e-03	7.018e-03	4.7e-10	5.285	6.1e-04	67.187	0.060	-0.744	2.2e-05	-78.335	0.286
EUB-1	0.445	394.902	1.5e-03	6.958e-03	6.6e-10	4.705	6.6e-04	61.624	0.134	-0.647	6.2e-05	-61.590	0.867
EUB-2	0.520	394.621	2.4e-03	6.991e-03	1.1e-09	5.561	1.1e-03	54.521	0.151	-0.663	6.8e-05	-72.991	0.931
EUB-3	0.445	394.624	1.9e-03	7.075e-03	8.6e-10	5.202	8.3e-04	56.855	0.143	-0.638	6.8e-05	-64.540	0.960
EUB-4	0.400	394.627	1.4e-03	6.977e-03	6.2e-10	4.957	6.4e-04	62.702	0.114	-0.667	5.0e-05	-62.361	0.682
EUB-5	0.485	394.495	2.1e-03	7.041e-03	9.7e-10	5.573	1.0e-03	57.937	0.147	-0.676	6.2e-05	-65.659	0.844
EUB-6	0.432	394.435	1.9e-03	7.078e-03	8.5e-10	5.381	8.6e-04	59.659	0.139	-0.676	5.8e-05	-63.406	0.793
EUB-7	0.361	394.574	1.4e-03	6.953e-03	6.3e-10	5.166	6.7e-04	64.378	0.110	-0.692	4.4e-05	-61.405	0.594
ASB-1	0.613	394.385	1.9e-03	7.082e-03	8.9e-10	6.228	1.2e-03	55.116	0.092	-0.810	2.4e-05	-87.346	0.328
ASB-2	0.543	394.632	1.6e-03	6.782e-03	7.3e-10	5.525	9.7e-04	55.343	0.088	-0.769	2.9e-05	-89.816	0.377
ASB-3	0.574	394.081	1.8e-03	7.090e-03	8.3e-10	6.357	1.1e-03	55.573	0.084	-0.805	2.2e-05	-85.590	0.305
ASB-4	0.544	394.244	1.6e-03	6.907e-03	7.6e-10	6.116	9.7e-04	53.098	0.084	-0.763	2.7e-05	-85.412	0.357
ASB-5	0.522	394.395	2.0e-03	6.839e-03	9.5e-10	6.137	1.2e-03	52.824	0.108	-0.758	3.5e-05	-83.369	0.464
ASB-6	0.549	394.018	2.0e-03	7.106e-03	9.2e-10	6.408	1.2e-03	56.426	0.093	-0.793	2.6e-05	-83.356	0.352
ASB-7	0.463	394.115	1.9e-03	7.002e-03	8.9e-10	6.354	1.1e-03	54.146	0.098	-0.763	3.1e-05	-80.595	0.409
ASB-8	0.488	394.271	2.3e-03	6.949e-03	1.1e-09	6.248	1.3e-03	53.796	0.123	-0.743	4.2e-05	-79.387	0.557
ASB-9	0.497	394.505	2.4e-03	6.942e-03	1.1e-09	5.949	1.3e-03	55.038	0.137	-0.714	5.2e-05	-77.311	0.694
ASB-10	0.474	394.117	2.0e-03	7.082e-03	9.4e-10	6.227	1.1e-03	57.442	0.106	-0.752	3.5e-05	-77.056	0.466

Table S8. Seasonal cycle fit parameters, a_i, with uncertainty estimates, σ_{a_i}, for fits of CAMS estimated X_{CO_2} to Eq. 1 in the manuscript, and standard errors, $\bar{\sigma}$, for zones in Temperate and Tundra regions.

Zone	$\bar{\sigma}$ ppm	a_0 ppm	σ_{a_0} ppm	a_1 ppm days^{-1}	σ_{a_1} ppm days^{-1}	a_2 ppm	σ_{a_2} ppm	a_3 days	σ_{a_3} days	a_4	σ_{a_4}	a_5 days	σ_{a_5} days
NATem-1	0.465	394.934	1.3e-03	6.836e-03	6.1e-10	5.312	7.9e-04	62.548	0.082	-0.760	2.8e-05	-80.058	0.361
NATem-2	0.506	395.577	1.4e-03	6.791e-03	6.1e-10	4.063	7.2e-04	68.041	0.120	-0.650	6.2e-05	-80.590	0.838
NATem-3	0.380	395.301	1.2e-03	6.935e-03	5.2e-10	4.461	6.3e-04	71.892	0.089	-0.693	4.0e-05	-74.749	0.517
EUTem-1	0.553	395.145	1.7e-03	6.934e-03	7.9e-10	4.903	8.4e-04	53.246	0.117	-0.610	6.5e-05	-84.139	0.933
EUTem-2	0.569	395.309	1.8e-03	6.983e-03	8.2e-10	4.490	7.6e-04	52.840	0.143	-0.526	9.7e-05	-75.840	1.631
EUTem-3	0.531	395.441	1.6e-03	6.885e-03	7.2e-10	4.155	6.6e-04	59.597	0.177	-0.591	9.7e-05	-59.269	1.453
EUTem-4	0.583	394.801	2.2e-03	6.962e-03	1.0e-09	5.411	1.1e-03	53.155	0.141	-0.668	6.4e-05	-80.186	0.869
EUTem-5	0.533	394.945	1.7e-03	7.013e-03	7.7e-10	4.913	7.5e-04	55.643	0.132	-0.610	7.0e-05	-69.266	1.013
ASTem-1	0.605	394.659	1.7e-03	6.736e-03	7.7e-10	5.306	1.0e-03	55.966	0.100	-0.752	3.5e-05	-89.016	0.455
ASTem-2	0.482	394.798	1.9e-03	6.848e-03	8.6e-10	5.349	1.0e-03	55.593	0.114	-0.702	4.7e-05	-84.082	0.624
ASTem-3	0.526	394.595	2.0e-03	6.867e-03	9.4e-10	5.806	1.1e-03	53.928	0.117	-0.724	4.3e-05	-81.036	0.574
NATun-1	0.452	394.455	1.4e-03	6.887e-03	6.3e-10	5.717	8.0e-04	63.923	0.079	-0.765	2.5e-05	-74.707	0.335
NATun-2	0.334	394.407	1.1e-03	6.884e-03	5.0e-10	5.723	6.2e-04	67.646	0.064	-0.755	2.1e-05	-69.225	0.278
NATun-3	0.250	394.750	8.9e-04	6.824e-03	4.0e-10	5.403	5.0e-04	68.146	0.054	-0.739	1.9e-05	-72.190	0.254
NATun-4	0.277	394.590	8.3e-04	6.957e-03	3.8e-10	5.636	4.8e-04	68.352	0.045	-0.750	1.6e-05	-73.490	0.206
NATun-5	0.309	394.575	8.0e-04	7.012e-03	3.6e-10	5.534	4.7e-04	68.950	0.044	-0.750	1.6e-05	-74.306	0.203
ASTun-1	0.341	394.677	1.9e-03	6.983e-03	8.9e-10	5.796	1.2e-03	66.091	0.096	-0.780	3.0e-05	-80.092	0.392
ASTun-2	0.438	394.251	1.9e-03	7.102e-03	8.9e-10	6.041	1.2e-03	62.383	0.089	-0.807	2.4e-05	-84.530	0.328
ASTun-3	0.466	394.211	2.2e-03	7.152e-03	1.0e-09	6.320	1.4e-03	62.990	0.096	-0.803	2.7e-05	-82.345	0.356
ASTun-4	0.540	394.149	2.0e-03	7.105e-03	9.2e-10	6.119	1.2e-03	60.281	0.098	-0.777	3.0e-05	-81.113	0.396
ASTun-5	0.542	394.215	1.9e-03	7.049e-03	8.8e-10	6.047	1.0e-03	56.946	0.111	-0.733	3.9e-05	-73.568	0.517
ASTun-6	0.483	394.409	2.2e-03	7.013e-03	1.0e-09	5.894	1.1e-03	57.867	0.135	-0.705	5.2e-05	-69.976	0.695

S1.4 Seasonal cycle fits for CT2019B estimates in 5° latitude by 20° longitude zones

In this section, we provide details of seasonal cycle fits to CT2019B daily X_{CO_2} estimates (see Sect. 2.6 of the manuscript) averaged across each 5° latitude by 20° longitude zone. Figures S21 through S28 show plots of time-series of CT2019B model estimates, the corresponding seasonal cycle fits, as well as the fit to OCO-2 data (to allow for easier direct comparison between the model-derived and OCO-2 observational fits). Tables S9 and S10 report standard errors used in each CT2019B fit, the seasonal fit parameters calculated, and an estimate of parameter uncertainty.
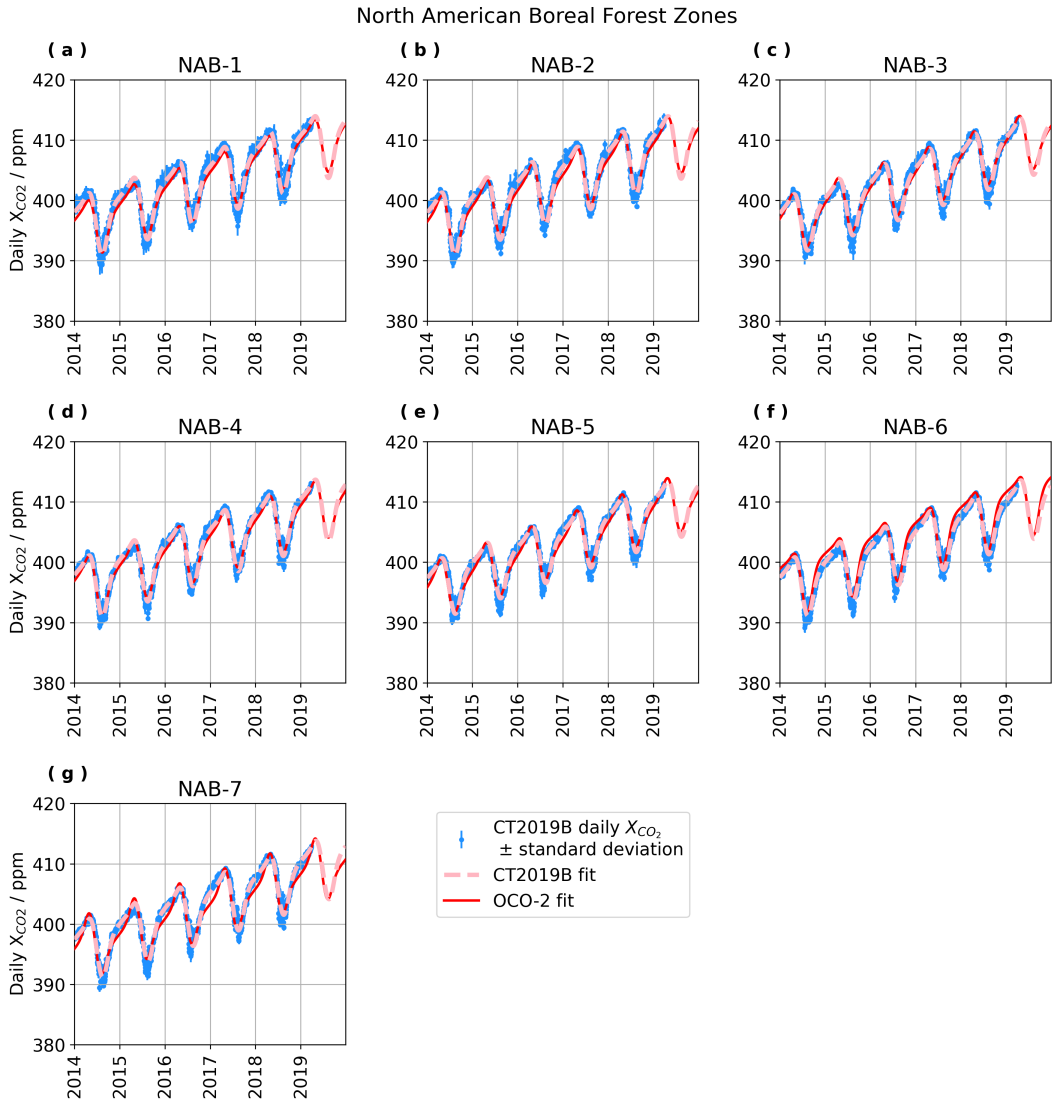
Figure S21. Time-series of CT2019B X_{CO_2} by zone in the North American Boreal region, with seasonal cycle fits to CT2019B and OCO-2.
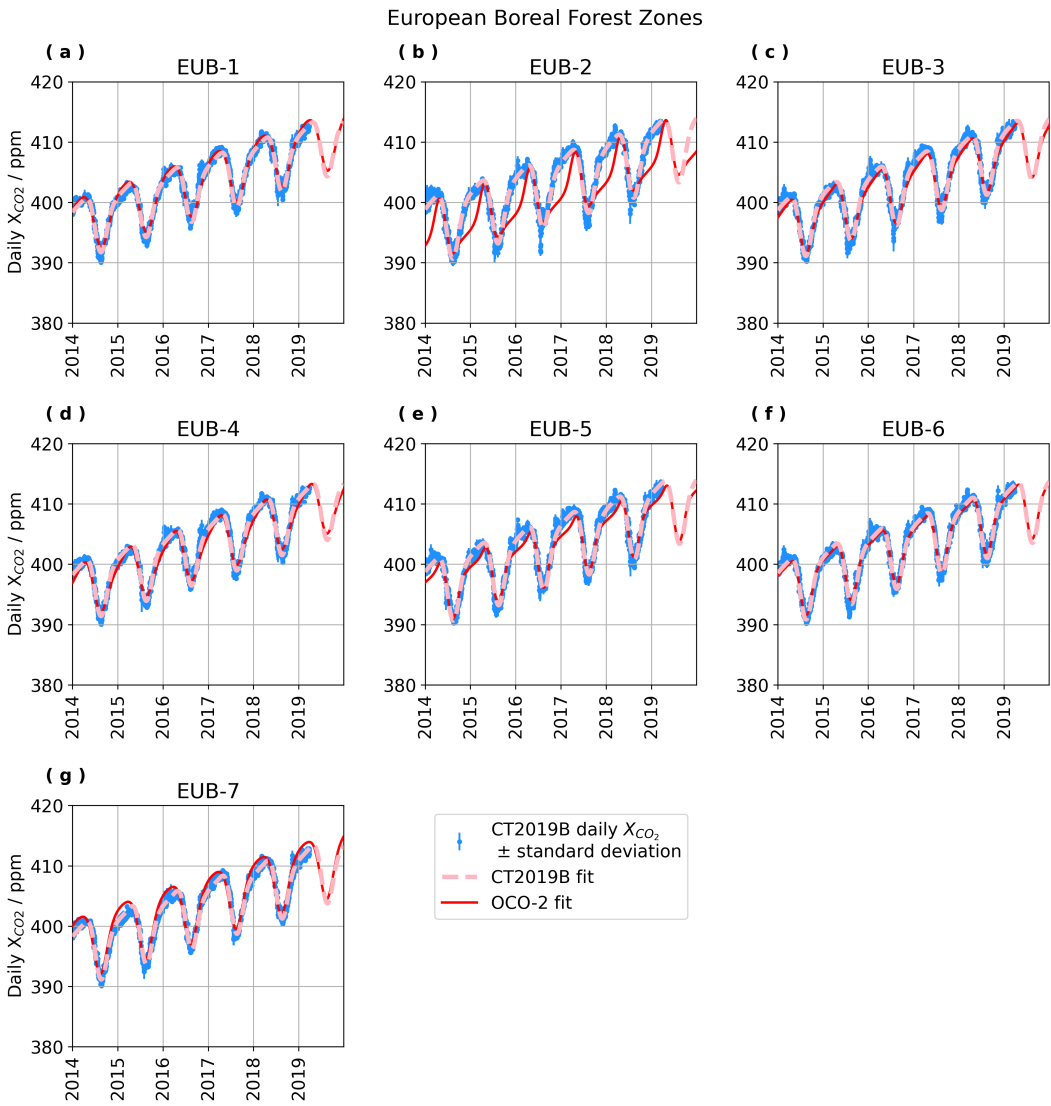
Figure S22. Time-series of CT2019B X_{CO_2} by zone in the European Boreal region, with seasonal cycle fits to CT2019B and OCO-2.
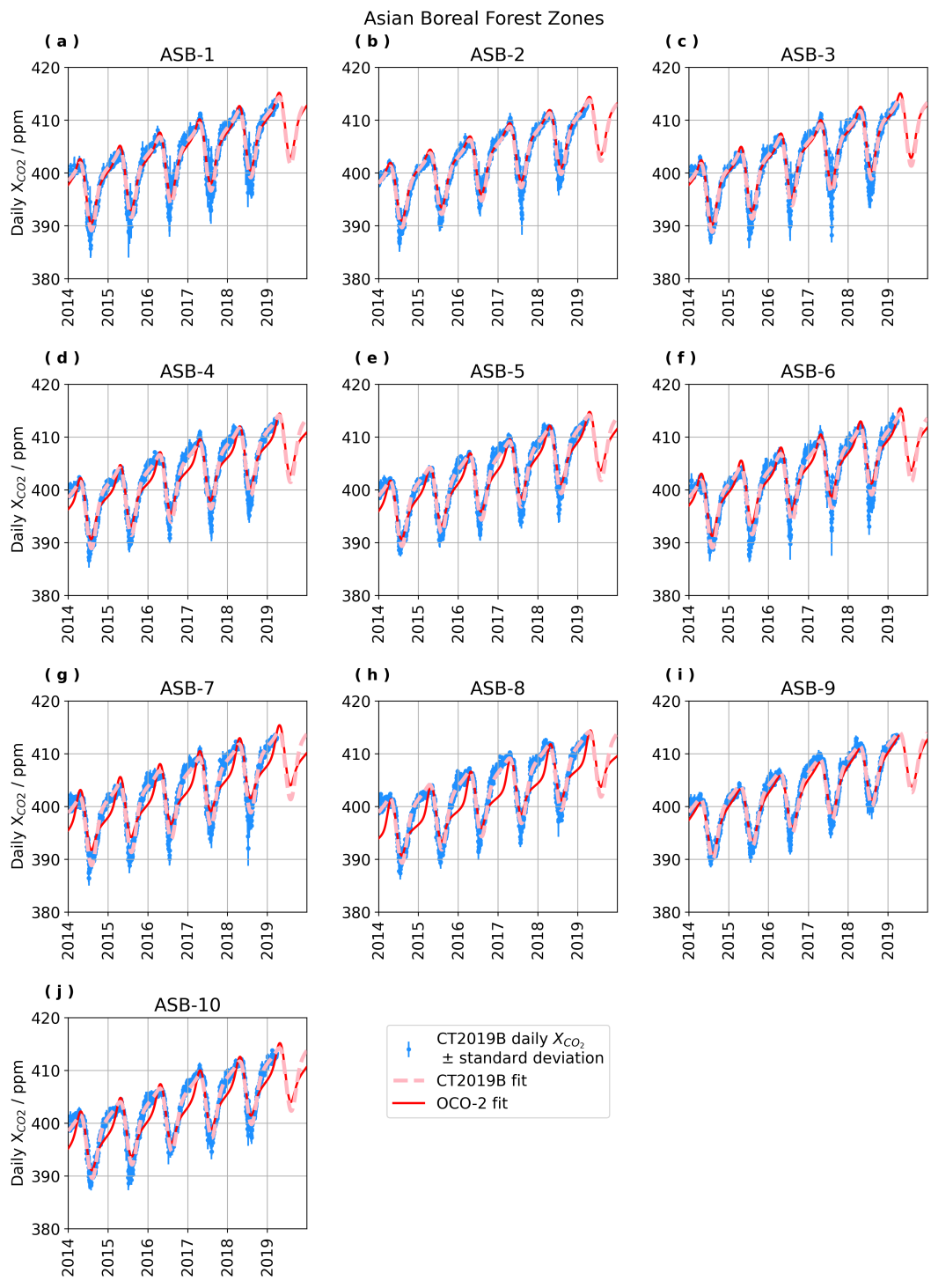
Figure S23. Time-series of CT2019B X_{CO_2} by zone in the Asian Boreal region, with seasonal cycle fits to CT2019B and OCO-2.
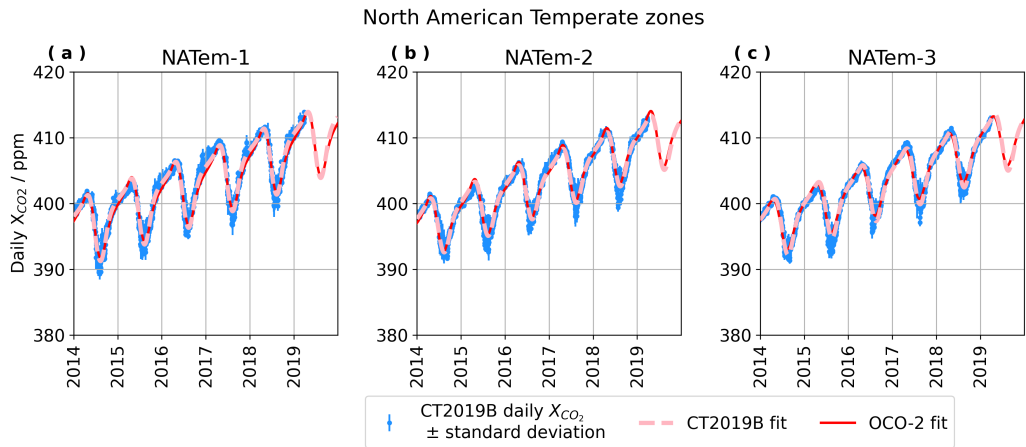
Figure S24. Time-series of CT2019B X_{CO_2} by zone in the North American Temperate region, with seasonal cycle fits to CT2019B and OCO-2.
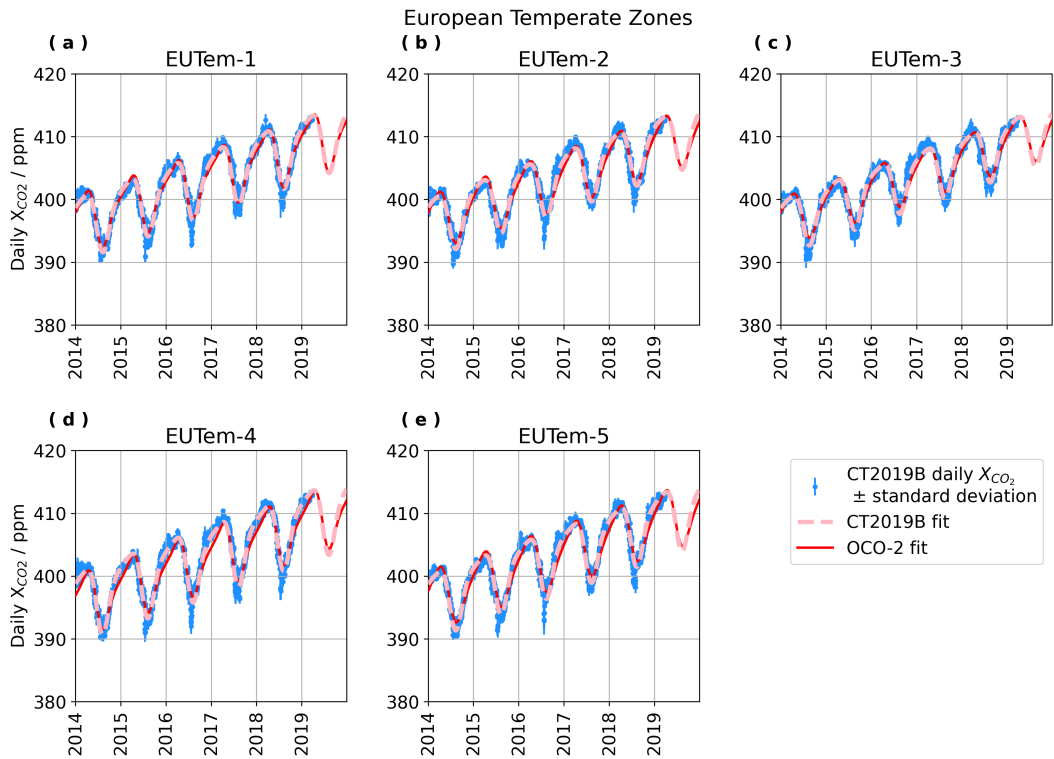
Figure S25. Time-series of CT2019B X_{CO_2} by zone in the European Temperate region, with seasonal cycle fits to CT2019B and OCO-2.
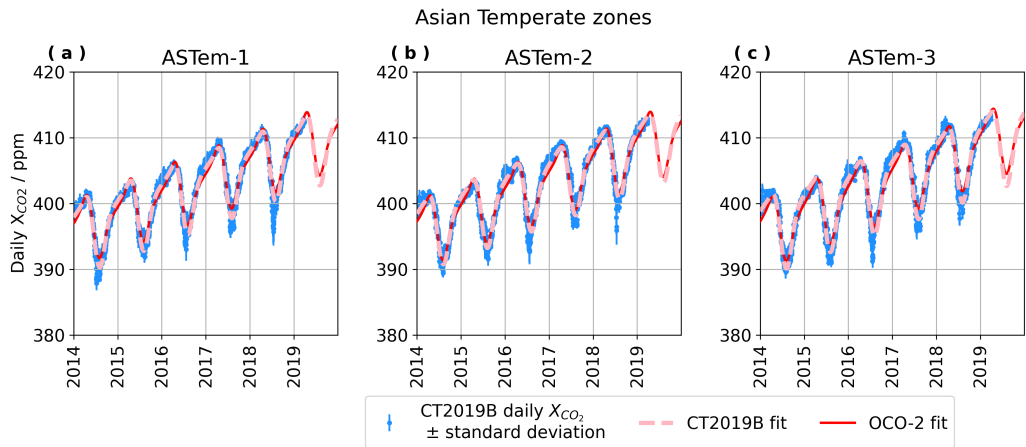
Figure S26. Time-series of CT2019B X_{CO_2} by zone in the Asian Temperate region, with seasonal cycle fits to CT2019B and OCO-2.
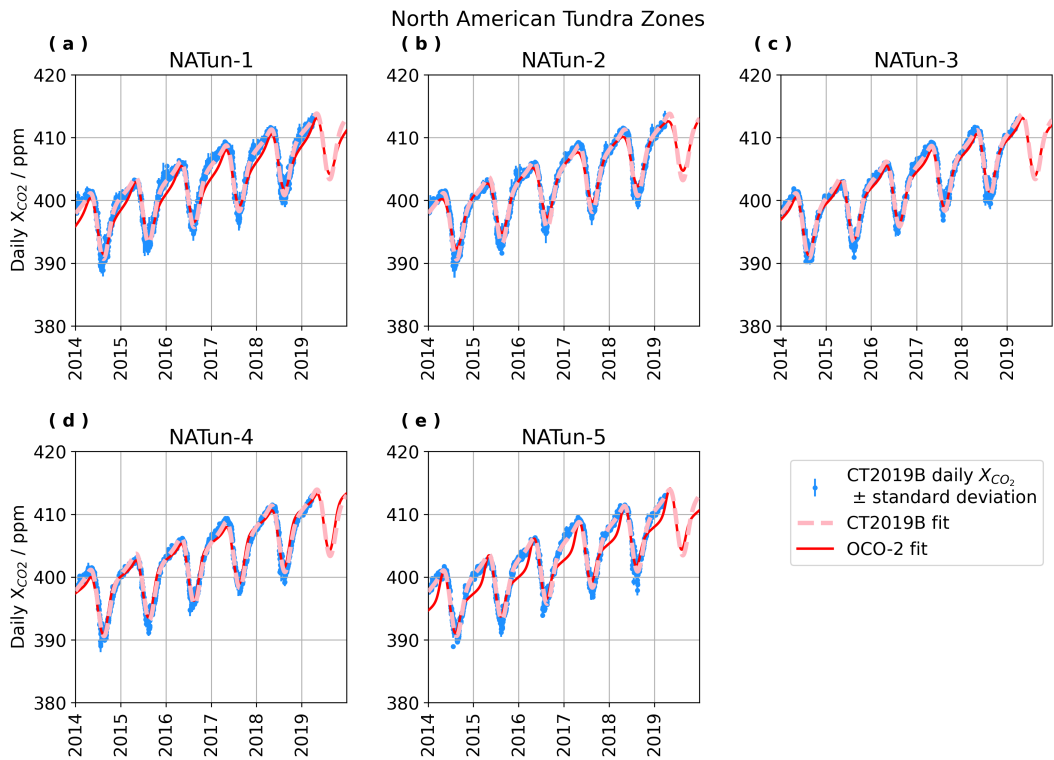
Figure S27. Time-series of CT2019B X_{CO_2} by zone in the North American Tundra region, with seasonal cycle fits to CT2019B and OCO-2.
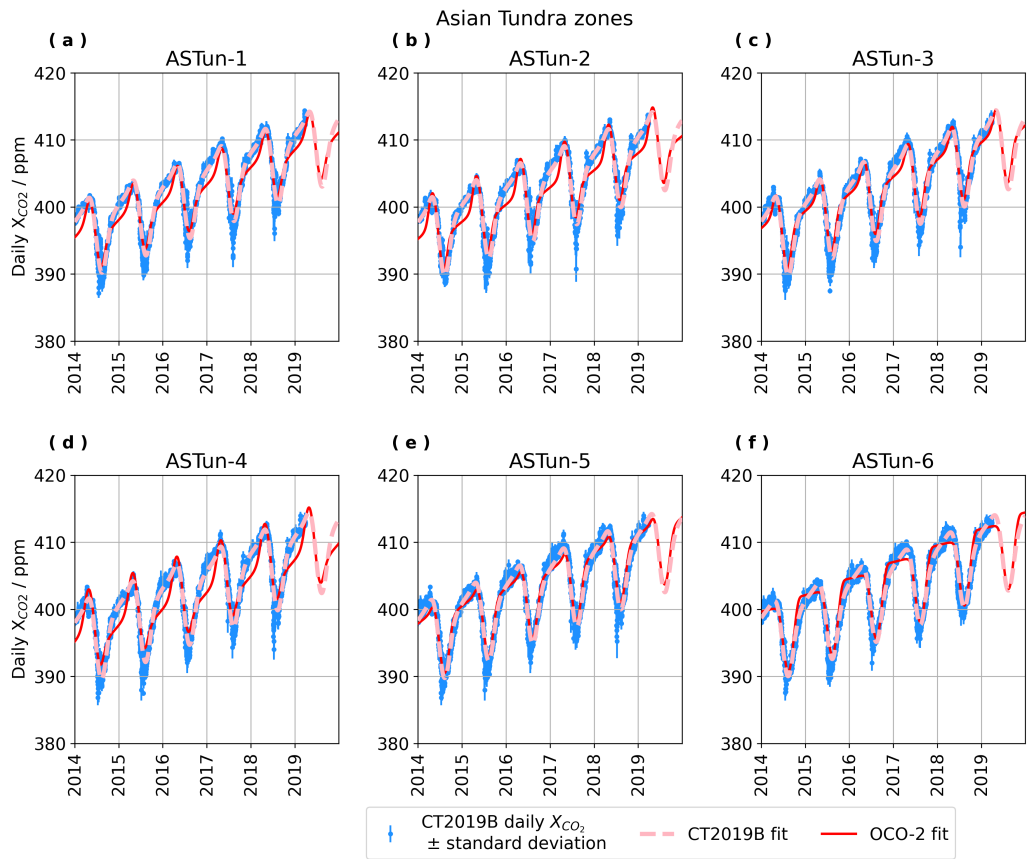
Figure S28. Time-series of CT2019B X_{CO_2} by zone in the Asian Tundra region, with seasonal cycle fits to CT2019B and OCO-2.

Table S9. Seasonal cycle fit parameters, a_i, with uncertainty estimates, σ_{a_i}, for fits of CT2019B estimated X_{CO_2} to Eq. 1 in the manuscript, and standard errors, $\bar{\sigma}$, for zones in Boreal regions.

Zone	$\bar{\sigma}$ ppm	a_0 ppm	σ_{a_0} ppm	a_1 ppm days^{-1}	σ_{a_1} ppm days^{-1}	a_2 ppm	σ_{a_2} ppm	a_3 days	σ_{a_3} days	a_4	σ_{a_4}	a_5 days	σ_{a_5} days
NAB-1	0.461	394.895	2.0e-03	6.976e-03	1.2e-09	5.503	1.3e-03	66.614	0.115	-0.772	3.6e-05	-78.061	0.483
NAB-2	0.343	394.925	1.6e-03	6.922e-03	9.4e-10	5.544	1.0e-03	68.211	0.087	-0.769	2.7e-05	-77.841	0.371
NAB-3	0.406	395.173	1.5e-03	6.873e-03	9.2e-10	5.041	9.4e-04	67.885	0.097	-0.734	3.6e-05	-79.993	0.481
NAB-4	0.305	394.864	1.3e-03	6.877e-03	8.0e-10	5.448	8.4e-04	68.644	0.077	-0.759	2.5e-05	-76.753	0.343
NAB-5	0.321	394.839	1.5e-03	6.997e-03	8.9e-10	4.993	9.4e-04	71.797	0.097	-0.749	3.4e-05	-76.408	0.454
NAB-6	0.298	394.746	1.4e-03	6.981e-03	8.5e-10	5.227	9.1e-04	71.016	0.085	-0.765	2.8e-05	-77.097	0.373
NAB-7	0.252	394.802	1.5e-03	7.074e-03	8.9e-10	5.219	9.5e-04	72.710	0.089	-0.764	2.9e-05	-75.314	0.393
EUB-1	0.365	395.008	1.6e-03	6.897e-03	9.2e-10	4.896	8.0e-04	66.315	0.128	-0.685	5.3e-05	-64.391	0.726
EUB-2	0.397	394.742	2.3e-03	6.928e-03	1.4e-09	5.651	1.2e-03	58.177	0.144	-0.679	6.0e-05	-71.518	0.831
EUB-3	0.338	394.814	1.9e-03	6.943e-03	1.1e-09	5.296	9.5e-04	61.012	0.142	-0.685	5.7e-05	-66.383	0.795
EUB-4	0.333	394.832	1.3e-03	6.913e-03	7.8e-10	5.049	7.1e-04	67.601	0.104	-0.707	4.0e-05	-64.390	0.542
EUB-5	0.340	394.645	2.1e-03	6.977e-03	1.3e-09	5.606	1.1e-03	62.793	0.148	-0.705	5.5e-05	-64.373	0.762
EUB-6	0.276	394.660	1.9e-03	6.952e-03	1.1e-09	5.426	9.8e-04	64.782	0.136	-0.720	4.8e-05	-64.216	0.661
EUB-7	0.263	394.752	1.4e-03	6.908e-03	8.0e-10	5.223	7.4e-04	69.286	0.102	-0.725	3.6e-05	-62.706	0.492
ASB-1	0.619	394.336	3.8e-03	6.880e-03	2.3e-09	6.731	2.5e-03	56.839	0.159	-0.802	4.2e-05	-86.361	0.585
ASB-2	0.515	394.333	2.5e-03	6.906e-03	1.5e-09	6.161	1.6e-03	57.342	0.117	-0.773	3.6e-05	-87.479	0.488
ASB-3	0.536	394.150	3.6e-03	6.861e-03	2.2e-09	6.826	2.4e-03	57.302	0.146	-0.814	3.6e-05	-85.939	0.512
ASB-4	0.478	394.114	2.7e-03	6.866e-03	1.6e-09	6.718	1.7e-03	54.807	0.118	-0.792	3.2e-05	-85.746	0.448
ASB-5	0.376	394.372	2.6e-03	6.840e-03	1.6e-09	6.560	1.6e-03	54.479	0.118	-0.757	3.7e-05	-84.176	0.511
ASB-6	0.566	394.247	3.3e-03	6.893e-03	2.0e-09	6.767	2.2e-03	58.234	0.140	-0.801	3.6e-05	-83.779	0.514
ASB-7	0.437	394.183	3.3e-03	6.847e-03	2.0e-09	6.843	2.1e-03	54.774	0.141	-0.784	3.9e-05	-83.912	0.546
ASB-8	0.382	394.346	3.0e-03	6.860e-03	1.8e-09	6.541	1.8e-03	54.614	0.141	-0.749	4.6e-05	-82.015	0.628
ASB-9	0.420	394.594	2.5e-03	6.909e-03	1.5e-09	6.101	1.3e-03	56.552	0.131	-0.708	4.9e-05	-76.838	0.679
ASB-10	0.391	394.375	2.6e-03	6.982e-03	1.6e-09	6.350	1.6e-03	60.758	0.125	-0.752	4.1e-05	-77.768	0.558

Table S10. Seasonal cycle fit parameters, a_i, with uncertainty estimates, σ_{a_i}, for fits of CT2019B estimated X_{CO_2} to Eq. 1 in the manuscript, and standard errors, $\bar{\sigma}$, for zones in Temperate and Tundra regions.

| Zone	$\bar{\sigma}$ ppm	a_0 ppm	σ_{a_0} ppm	a_1 ppm days^{-1}	σ_{a_1} ppm days^{-1}	a_2 ppm	σ_{a_2} ppm	a_3 days	σ_{a_3} days	a_4	σ_{a_4}	a_5 days	σ_{a_5} days
NATem-1	0.405	395.076	1.9e-03	6.924e-03	1.2e-09	5.394	1.2e-03	65.899	0.112	-0.767	3.6e-05	-80.968	0.484
NATem-2	0.428	395.495	1.5e-03	6.867e-03	8.9e-10	4.496	8.8e-04	69.737	0.112	-0.693	4.9e-05	-80.753	0.660
NATem-3	0.335	395.208	1.4e-03	7.005e-03	8.0e-10	4.645	8.0e-04	74.061	0.097	-0.706	4.1e-05	-74.233	0.542
EUTem-1	0.394	395.061	2.1e-03	6.903e-03	1.2e-09	5.031	9.6e-04	56.386	0.144	-0.605	7.7e-05	-74.465	1.145
EUTem-2	0.399	395.209	2.3e-03	6.920e-03	1.3e-09	4.700	9.8e-04	56.059	0.187	-0.565	1.1e-04	-67.910	1.738
EUTem-3	0.453	395.453	1.8e-03	6.869e-03	1.1e-09	4.403	8.5e-04	64.357	0.185	-0.636	8.8e-05	-60.894	1.272
EUTem-4	0.424	394.787	2.3e-03	6.914e-03	1.4e-09	5.581	1.1e-03	55.302	0.140	-0.655	6.3e-05	-76.191	0.897
EUTem-5	0.392	394.921	2.3e-03	6.919e-03	1.3e-09	5.146	1.1e-03	57.734	0.164	-0.638	7.8e-05	-69.567	1.120
ASTem-1	0.473	394.532	2.1e-03	6.813e-03	1.3e-09	5.721	1.3e-03	58.218	0.109	-0.741	3.8e-05	-86.702	0.516
ASTem-2	0.377	394.801	2.1e-03	6.819e-03	1.3e-09	5.569	1.2e-03	57.878	0.122	-0.688	5.1e-05	-80.407	0.701
ASTem-3	0.408	394.649	2.3e-03	6.863e-03	1.3e-09	6.060	1.2e-03	55.699	0.117	-0.707	4.5e-05	-80.131	0.615
NATun-1	0.400	394.685	1.7e-03	6.951e-03	1.0e-09	5.610	1.1e-03	68.948	0.095	-0.784	2.8e-05	-74.673	0.379
NATun-2	0.284	394.639	1.3e-03	6.918e-03	7.9e-10	5.668	8.3e-04	72.188	0.075	-0.768	2.4e-05	-69.814	0.318
NATun-3	0.255	394.766	1.2e-03	6.881e-03	7.3e-10	5.536	7.7e-04	70.871	0.068	-0.761	2.3e-05	-74.005	0.302
NATun-4	0.207	394.642	1.2e-03	6.989e-03	7.0e-10	5.670	7.4e-04	72.579	0.064	-0.765	2.1e-05	-71.474	0.277
NATun-5	0.219	394.593	1.3e-03	7.035e-03	7.6e-10	5.604	8.0e-04	72.833	0.069	-0.768	2.2e-05	-72.083	0.298
ASTun-1	0.324	394.567	1.3e-03	7.027e-03	7.8e-10	5.964	8.5e-04	69.508	0.062	-0.782	1.9e-05	-77.413	0.254
ASTun-2	0.355	394.454	1.4e-03	6.945e-03	8.6e-10	6.198	9.6e-04	66.578	0.062	-0.797	1.7e-05	-82.162	0.240
ASTun-3	0.314	394.431	1.3e-03	7.053e-03	7.6e-10	6.266	8.3e-04	68.107	0.055	-0.785	1.6e-05	-78.763	0.221
ASTun-4	0.375	394.397	1.4e-03	7.039e-03	8.5e-10	6.406	9.2e-04	65.514	0.060	-0.780	1.8e-05	-80.325	0.244
ASTun-5	0.418	394.407	1.4e-03	7.008e-03	8.2e-10	6.222	8.2e-04	62.241	0.066	-0.751	2.2e-05	-77.756	0.295
ASTun-6	0.379	394.476	1.3e-03	6.995e-03	7.5e-10	6.022	6.9e-04	60.549	0.071	-0.719	2.6e-05	-72.182	0.351

S1.5 Seasonal cycle fits for GC-CT2019 estimates in 5° latitude by 20° longitude zones

In this section, we provide details of seasonal cycle fits to GC-CT2019 daily X_{CO_2} estimates (see Sect. 2.7 of the manuscript) averaged across each 5° latitude by 20° longitude zone. Figures S29 through S36 show plots of time-series of GC-CT2019 model estimates, the corresponding seasonal cycle fits (with three years of extrapolation to cover 2014-2019), and the fit to OCO-2 data (to allow for easier direct comparison between the model-derived and OCO-2 observational fits). Tables S11 and S12 report standard errors used in each GC-CT2019 fit, the seasonal fit parameters calculated, and an estimate of parameter uncertainty.
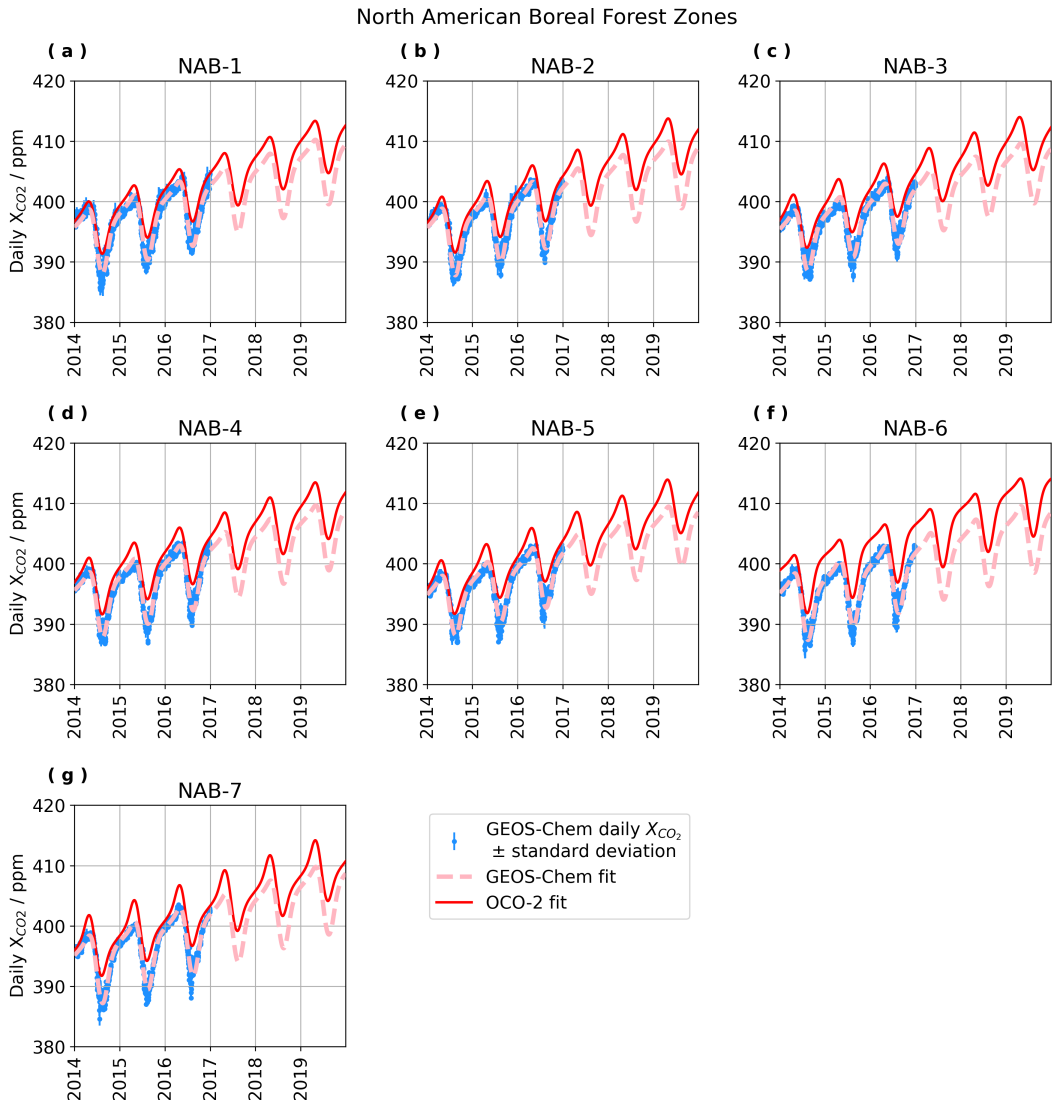
Figure S29. Time-series of GC-CT2019 X_{CO_2} by zone in the North American Boreal region, with seasonal cycle fits to GC-CT2019 and OCO-2.

European Boreal Forest Zones
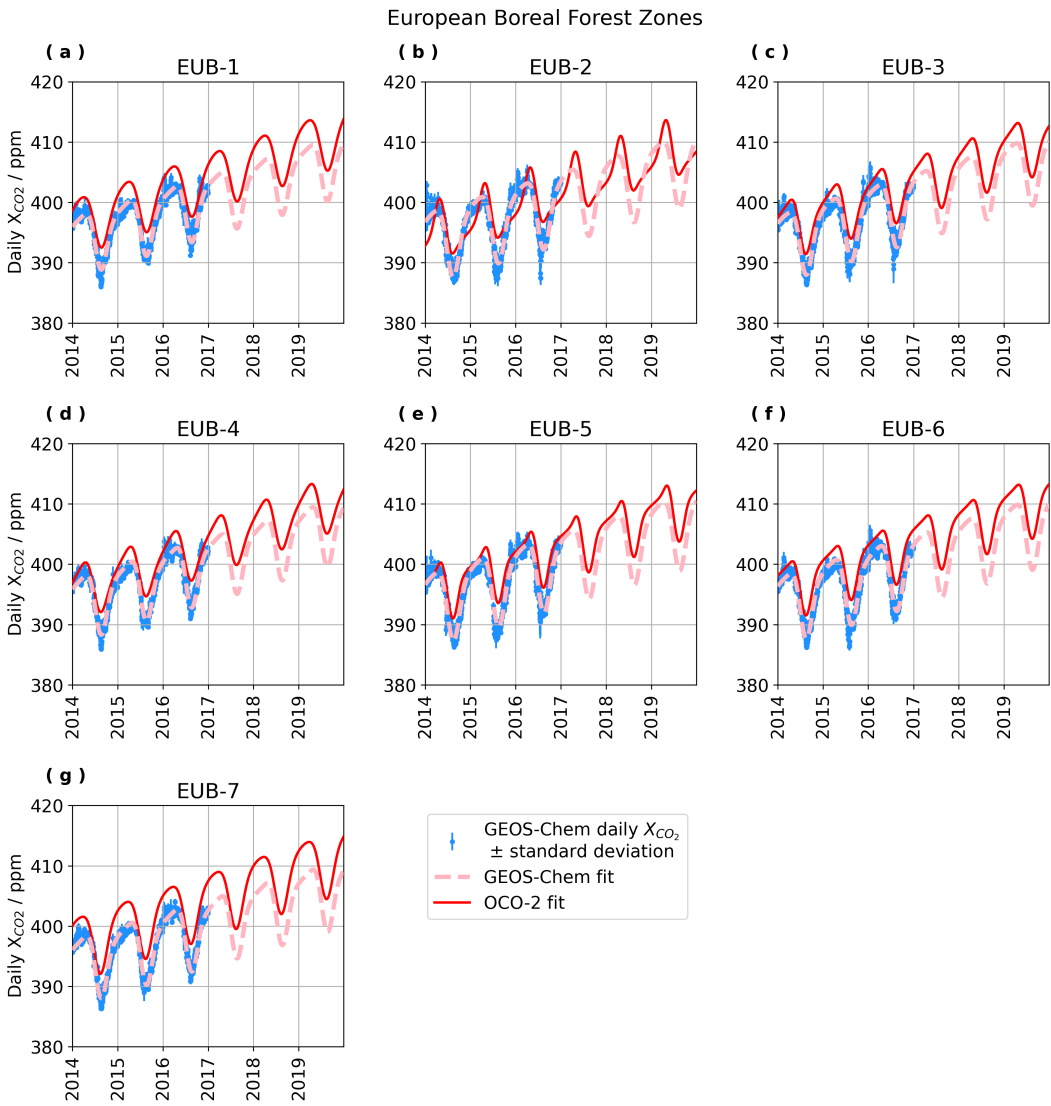
Figure S30. Time-series of GC-CT2019 X_{CO_2} by zone in the European Boreal region, with seasonal cycle fits to GC-CT2019 and OCO-2.
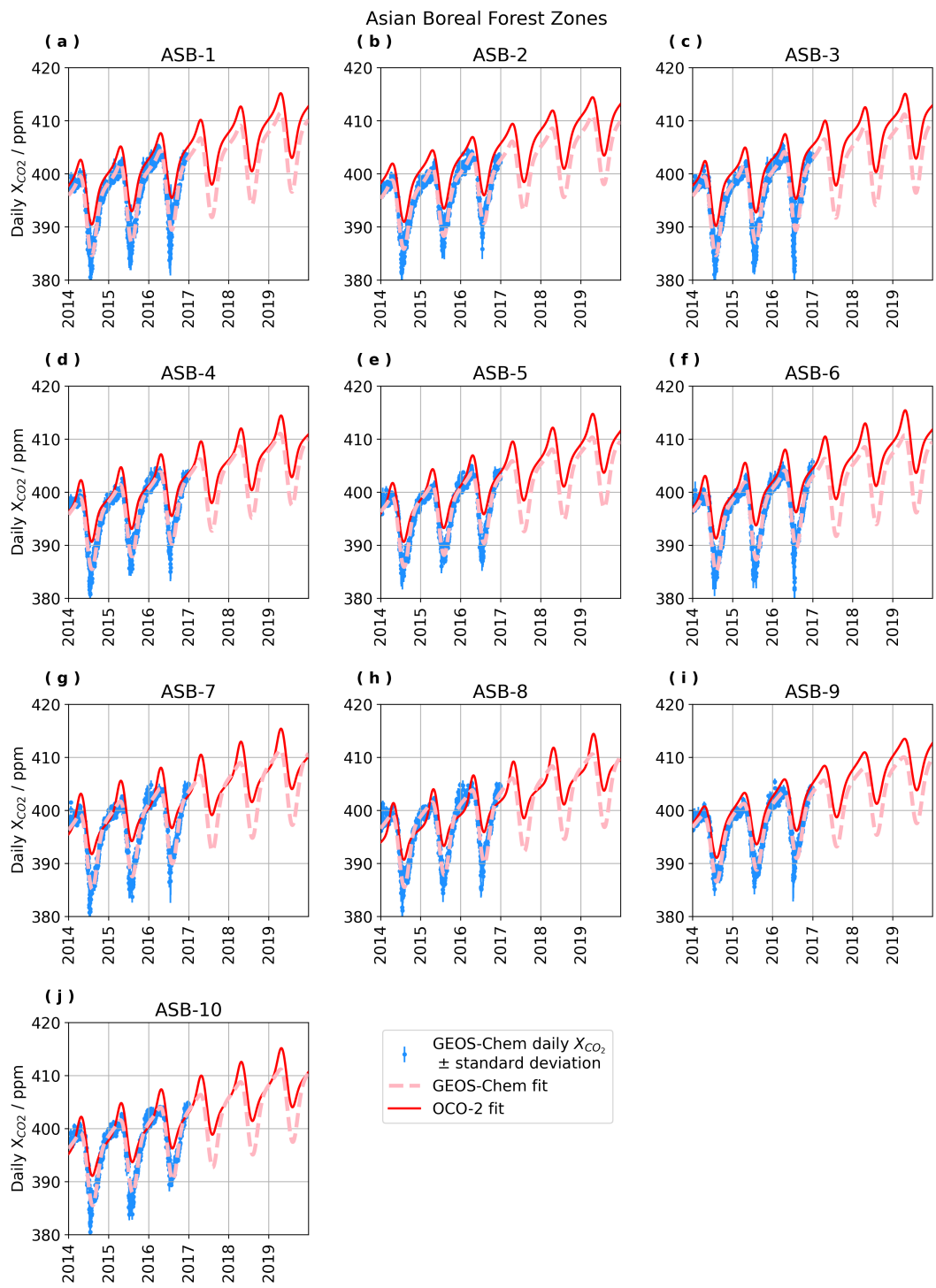
Figure S31. Time-series of GC-CT2019 X_{CO_2} by zone in the Asian Boreal region, with seasonal cycle fits to GC-CT2019 and OCO-2.
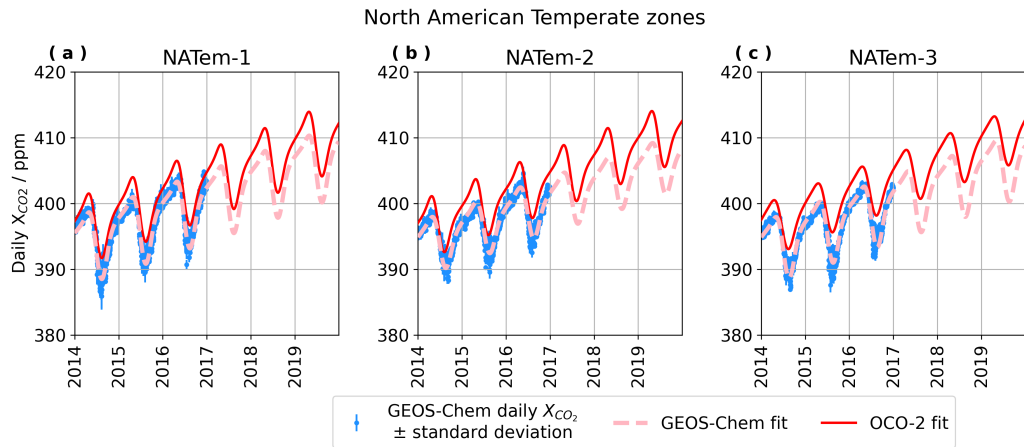
Figure S32. Time-series of GC-CT2019 X_{CO_2} by zone in the North American Temperate region, with seasonal cycle fits to GC-CT2019 and OCO-2.
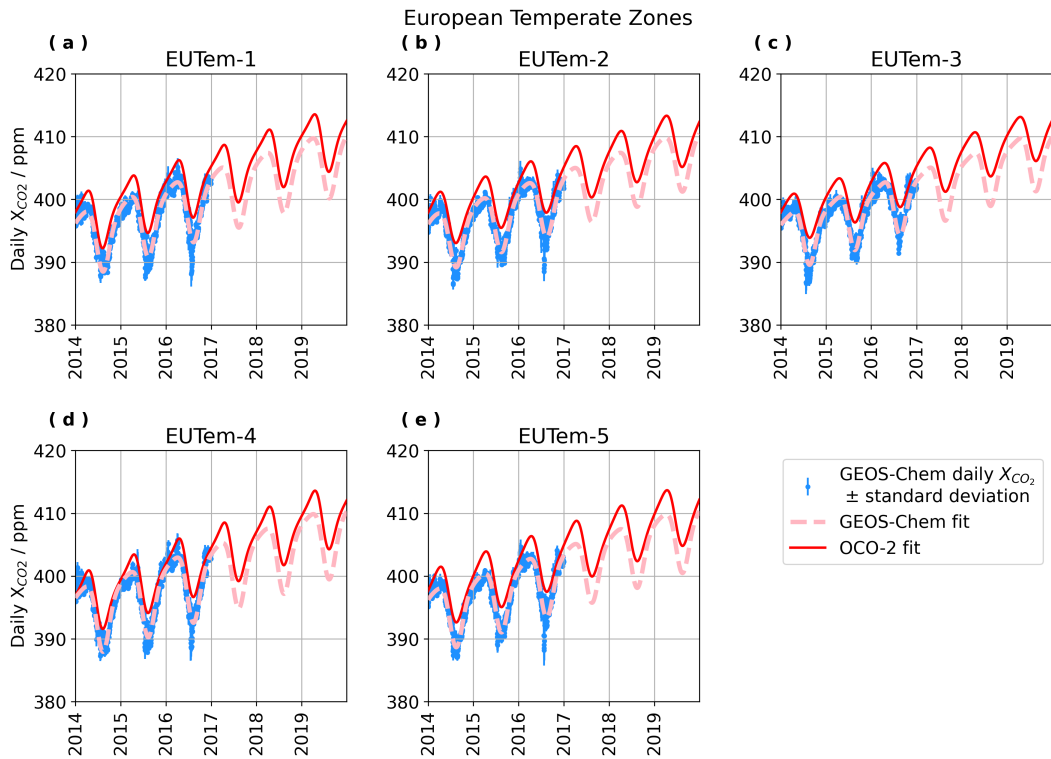
Figure S33. Time-series of GC-CT2019 X_{CO_2} by zone in the European Temperate region, with seasonal cycle fits to GC-CT2019 and OCO-2.
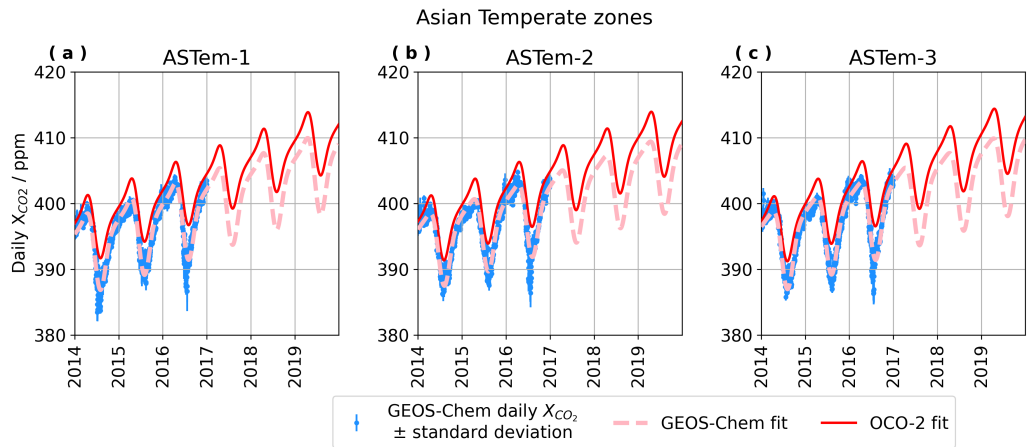
Figure S34. Time-series of GC-CT2019 X_{CO_2} by zone in the Asian Temperate region, with seasonal cycle fits to GC-CT2019 and OCO-2.
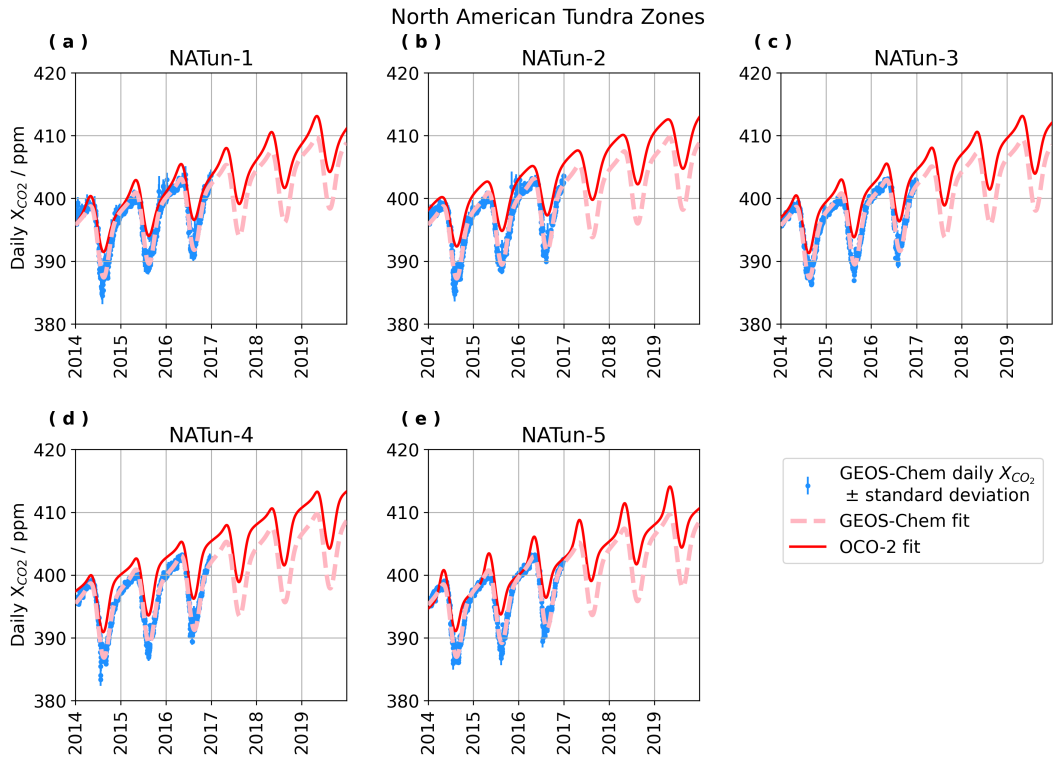
Figure S35. Time-series of GC-CT2019 X_{CO_2} by zone in the North American Tundra region, with seasonal cycle fits to GC-CT2019 and OCO-2.
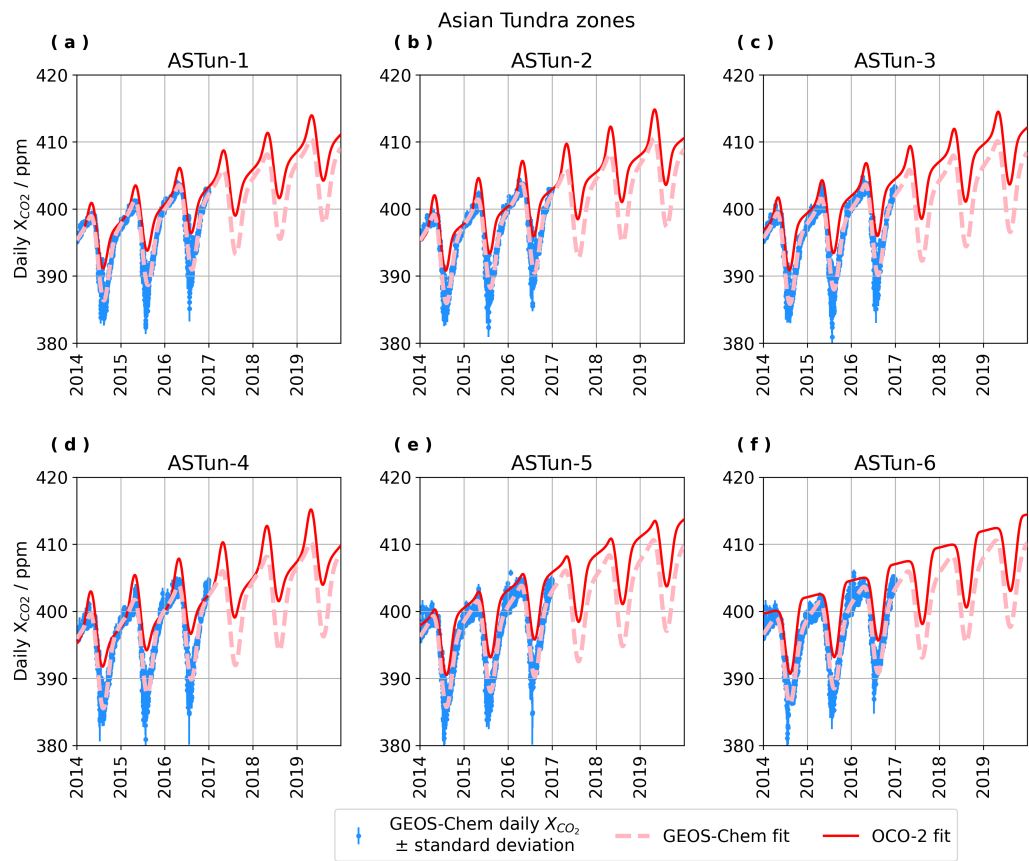
Figure S36. Time-series of GC-CT2019 X_{CO_2} by zone in the Asian Tundra region, with seasonal cycle fits to GC-CT2019 and OCO-2.

Table S11. Seasonal cycle fit parameters, a_i, with uncertainty estimates, σ_{a_i}, for fits of GC-CT2019 estimated X_{CO_2} to Eq. 1 in the manuscript, and standard errors, $\bar{\sigma}$, for zones in Boreal regions.

Zone	$\bar{\sigma}$ ppm	a_0 ppm	σ_{a_0} ppm	a_1 ppm days^{-1}	σ_{a_1} ppm days^{-1}	a_2 ppm	σ_{a_2} ppm	a_3 days	σ_{a_3} days	a_4	σ_{a_4}	a_5 days	σ_{a_5} days
NAB-1	0.451	392.288	5.3e-03	6.302e-03	1.0e-08	5.683	3.2e-03	66.819	0.297	-0.771	9.6e-05	-74.678	1.238
NAB-2	0.320	392.234	3.7e-03	6.082e-03	7.1e-09	5.855	2.2e-03	69.566	0.189	-0.778	6.0e-05	-73.380	0.769
NAB-3	0.372	392.451	4.0e-03	6.111e-03	7.6e-09	5.315	2.4e-03	70.094	0.235	-0.764	8.0e-05	-74.872	1.019
NAB-4	0.302	392.160	3.4e-03	6.057e-03	6.6e-09	5.711	2.1e-03	69.529	0.192	-0.785	5.9e-05	-71.902	0.758
NAB-5	0.324	391.960	3.7e-03	6.274e-03	7.2e-09	5.274	2.2e-03	72.473	0.225	-0.765	7.7e-05	-72.299	0.971
NAB-6	0.330	391.813	3.5e-03	6.098e-03	6.6e-09	5.844	2.1e-03	70.823	0.176	-0.787	5.4e-05	-73.061	0.692
NAB-7	0.266	391.718	3.5e-03	6.229e-03	6.7e-09	5.939	2.1e-03	70.234	0.172	-0.782	5.4e-05	-73.551	0.693
EUB-1	0.389	392.397	4.6e-03	6.224e-03	8.9e-09	5.024	2.3e-03	66.998	0.372	-0.682	1.6e-04	-60.576	2.103
EUB-2	0.425	392.102	6.3e-03	6.221e-03	1.3e-08	5.920	2.8e-03	57.191	0.376	-0.620	1.9e-04	-62.973	2.700
EUB-3	0.387	392.107	5.3e-03	6.289e-03	1.0e-08	5.582	2.4e-03	60.374	0.374	-0.647	1.7e-04	-58.499	2.375
EUB-4	0.348	392.177	3.7e-03	6.175e-03	7.1e-09	5.313	1.9e-03	67.974	0.262	-0.691	1.1e-04	-61.336	1.439
EUB-5	0.384	391.893	6.2e-03	6.379e-03	1.2e-08	6.096	2.9e-03	60.294	0.368	-0.651	1.7e-04	-60.331	2.308
EUB-6	0.328	391.998	5.4e-03	6.250e-03	1.1e-08	5.793	2.6e-03	62.962	0.356	-0.678	1.5e-04	-60.778	2.012
EUB-7	0.298	392.157	3.8e-03	6.020e-03	7.3e-09	5.519	1.9e-03	68.222	0.260	-0.702	1.0e-04	-59.820	1.358
ASB-1	0.668	391.034	9.5e-03	6.549e-03	1.9e-08	7.800	6.3e-03	54.603	0.294	-0.803	8.2e-05	-88.662	1.083
ASB-2	0.510	391.235	6.9e-03	6.683e-03	1.4e-08	6.852	4.4e-03	55.316	0.259	-0.777	8.3e-05	-90.337	1.071
ASB-3	0.581	390.999	1.0e-02	6.448e-03	2.0e-08	7.745	6.6e-03	55.100	0.309	-0.805	8.5e-05	-88.781	1.132
ASB-4	0.472	391.149	7.4e-03	6.604e-03	1.5e-08	7.115	4.6e-03	53.966	0.276	-0.770	8.9e-05	-87.314	1.156
ASB-5	0.448	391.533	7.4e-03	6.117e-03	1.5e-08	6.968	4.5e-03	53.805	0.306	-0.769	9.7e-05	-84.057	1.268
ASB-6	0.588	391.342	9.1e-03	6.073e-03	1.8e-08	7.622	5.8e-03	57.304	0.304	-0.790	8.9e-05	-83.520	1.166
ASB-7	0.437	391.126	8.5e-03	6.628e-03	1.7e-08	7.455	5.1e-03	55.030	0.314	-0.758	1.0e-04	-81.102	1.349
ASB-8	0.434	391.401	9.0e-03	6.193e-03	1.8e-08	7.230	5.3e-03	54.383	0.370	-0.755	1.2e-04	-79.042	1.586
ASB-9	0.467	391.850	7.3e-03	6.010e-03	1.5e-08	6.604	3.8e-03	55.204	0.354	-0.691	1.5e-04	-73.462	1.935
ASB-10	0.411	391.275	8.2e-03	6.556e-03	1.6e-08	7.220	4.7e-03	58.351	0.316	-0.745	1.1e-04	-77.207	1.424

Table S12. Seasonal cycle fit parameters, a_i, with uncertainty estimates, σ_{a_i}, for fits of GC-CT2019 estimated X_{CO_2} to Eq. 1 in the manuscript, and standard errors, $\bar{\sigma}$, for zones in Temperate and Tundra regions.

| Zone	$\bar{\sigma}$ ppm	a_0 ppm	σ_{a_0} ppm	a_1 ppm days^{-1}	σ_{a_1} ppm days^{-1}	a_2 ppm	σ_{a_2} ppm	a_3 days	σ_{a_3} days	a_4	σ_{a_4}	a_5 days	σ_{a_5} days
NATem-1	0.419	392.482	4.7e-03	6.381e-03	9.1e-09	5.422	2.9e-03	67.755	0.267	-0.768	9.0e-05	-78.184	1.144
NATem-2	0.417	392.986	3.6e-03	6.148e-03	6.8e-09	4.233	2.0e-03	75.135	0.286	-0.685	1.4e-04	-76.536	1.749
NATem-3	0.329	392.169	3.5e-03	6.358e-03	6.6e-09	4.984	2.0e-03	73.868	0.229	-0.735	8.9e-05	-70.551	1.118
EUTem-1	0.449	392.261	5.8e-03	6.393e-03	1.2e-08	5.213	2.6e-03	55.310	0.400	-0.576	2.4e-04	-69.017	3.541
EUTem-2	0.478	392.428	5.9e-03	6.600e-03	1.2e-08	4.763	2.5e-03	56.828	0.474	-0.537	3.1e-04	-62.815	4.980
EUTem-3	0.465	392.691	5.3e-03	6.413e-03	1.0e-08	4.625	2.6e-03	67.158	0.493	-0.664	2.3e-04	-60.538	3.018
EUTem-4	0.454	392.149	6.2e-03	6.315e-03	1.2e-08	5.617	2.8e-03	53.963	0.397	-0.612	2.1e-04	-68.331	2.974
EUTem-5	0.475	392.300	5.3e-03	6.473e-03	1.1e-08	5.115	2.3e-03	57.856	0.400	-0.589	2.3e-04	-62.397	3.310
ASTem-1	0.529	391.663	6.5e-03	6.270e-03	1.3e-08	6.167	4.0e-03	56.399	0.292	-0.752	1.0e-04	-89.350	1.335
ASTem-2	0.434	392.009	6.4e-03	5.990e-03	1.3e-08	5.846	3.5e-03	56.128	0.356	-0.691	1.5e-04	-79.004	2.003
ASTem-3	0.457	391.891	6.4e-03	6.086e-03	1.3e-08	6.261	3.5e-03	54.116	0.336	-0.695	1.4e-04	-77.244	1.830
NATun-1	0.351	392.012	4.7e-03	6.008e-03	9.0e-09	5.991	2.8e-03	68.813	0.246	-0.789	7.2e-05	-71.084	0.943
NATun-2	0.289	391.930	4.1e-03	5.990e-03	7.8e-09	6.078	2.4e-03	70.278	0.209	-0.767	6.8e-05	-67.679	0.873
NATun-3	0.245	391.944	2.8e-03	5.868e-03	5.3e-09	5.980	1.7e-03	71.312	0.149	-0.782	4.5e-05	-67.476	0.585
NATun-4	0.229	391.693	3.1e-03	6.044e-03	6.0e-09	6.244	1.9e-03	70.773	0.147	-0.779	4.6e-05	-69.500	0.590
NATun-5	0.250	391.681	3.0e-03	6.073e-03	5.7e-09	6.104	1.8e-03	71.131	0.141	-0.778	4.5e-05	-71.263	0.572
ASTun-1	0.326	391.569	3.6e-03	6.286e-03	7.0e-09	6.640	2.2e-03	67.517	0.141	-0.776	4.6e-05	-76.895	0.583
ASTun-2	0.449	391.500	3.3e-03	6.227e-03	6.5e-09	6.936	2.1e-03	64.141	0.115	-0.786	3.6e-05	-83.217	0.461
ASTun-3	0.375	391.613	3.6e-03	5.874e-03	6.9e-09	7.082	2.3e-03	65.276	0.123	-0.793	3.7e-05	-80.080	0.476
ASTun-4	0.455	391.572	3.7e-03	5.870e-03	7.3e-09	7.338	2.4e-03	62.606	0.124	-0.790	3.7e-05	-81.230	0.485
ASTun-5	0.476	391.488	3.8e-03	6.204e-03	7.5e-09	7.118	2.3e-03	59.710	0.149	-0.757	5.0e-05	-77.588	0.646
ASTun-6	0.431	391.602	3.7e-03	6.285e-03	7.3e-09	6.811	2.0e-03	58.185	0.167	-0.712	6.5e-05	-72.208	0.846

S2 Comparing observed and model-derived SCA and HDD

The alternative bias correction (ABC) proposed by Jacobs et al. (2020b), which is parameterized to account bias related to temperature at 700 hPa, was applied to OCO-2 data used in this study. Figures S37, S38, and S39 show the direct correlations of SCA and HDD from model estimates in CAMS, CT2019B, and GC-CT2019, respectively, versus observed SCA and HDD

5   from OCO-2. In these figures, OCO-2 B9 retrievals of X_{CO_2} are corrected with either the standard global bias correction for B9 retrievals (B9 BC) or the ABC proposed by Jacobs et al. (2020b), and seasonal cycle fits to OCO-2 B10 retrievals of X_{CO_2} with the standard global B10 bias correction are also considered. These results demonstrate that there is a slight improvement in the agreement between observational (OCO-2) and model-derived (CAMS CT2019B, and GC-CT2019) SCA when the ABC is applied to OCO-2 data.

10   Figure S40 shows the correlations of SCA and HDD from fits to a six-year time-series for 2014-2019 versus SCA and HDD from fits to a three-year time-series for 2014-2016, using OCO-2 observations, as well as CAMS and CT2019B model estimates. Figure S40 tests the possible impact on SCA and HDD of constraining the time-series to the 2014-2016 period, so that we can speculate on the possible impacts of comparing GC-CT2019 model-derived seasonal cycles fit for the 2014-2016 period, to seasonal cycle fits with CAMS, CT2019B, and OCO-2 data that cover 2014-2019.
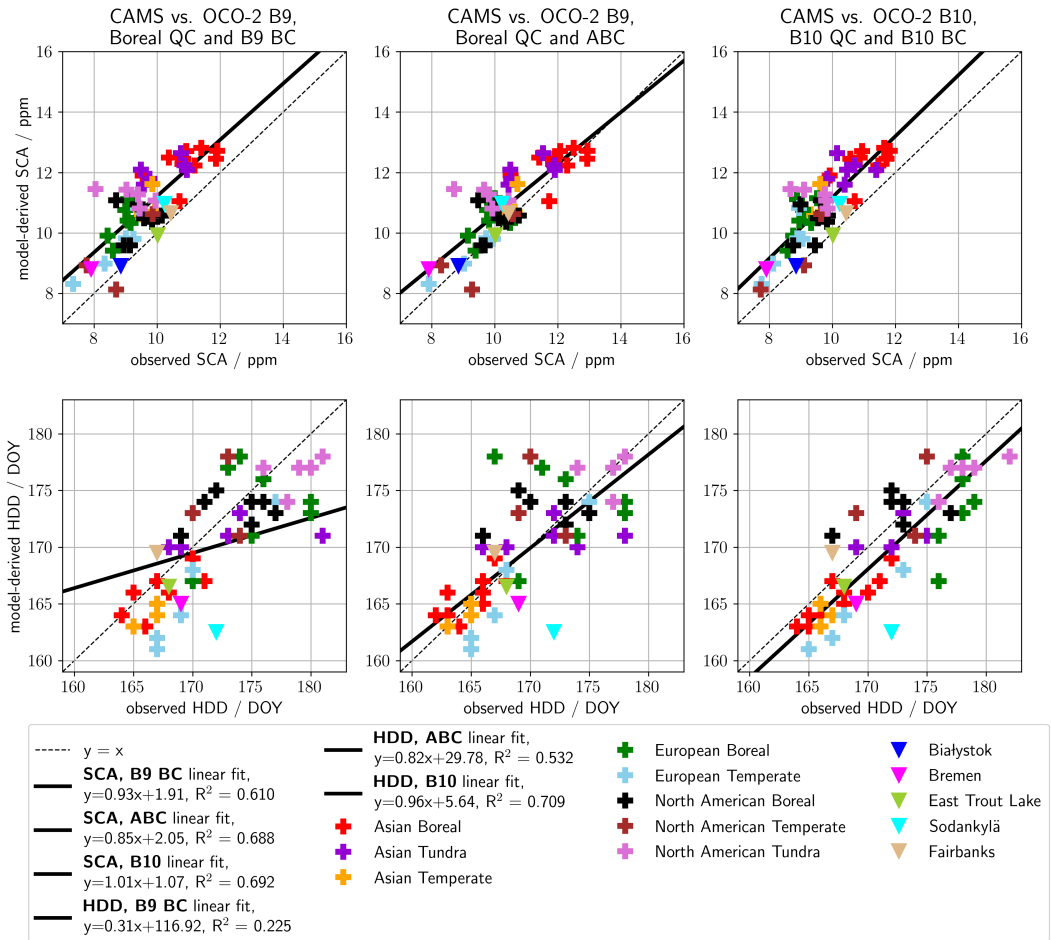
Figure S37. Correlations of CAMS model-derived versus observed (OCO-2 and NNG) SCA and HDD with three different data treatments for OCO-2 retrievals. The left column uses OCO-2 B9 retrievals with quality controls tailored for Boreal Forest regions (Boreal QC), as described by Jacobs et al. (2020b), and the standard B9 bias correction (B9 BC). The center column uses OCO-2 B9 retrievals with Boreal QC and an alternative bias correction for high latitude retrievals (ABC), as described by Jacobs et al. (2020b). The right column uses OCO-2 B10 retrievals with the standard B10 quality controls and bias correction.
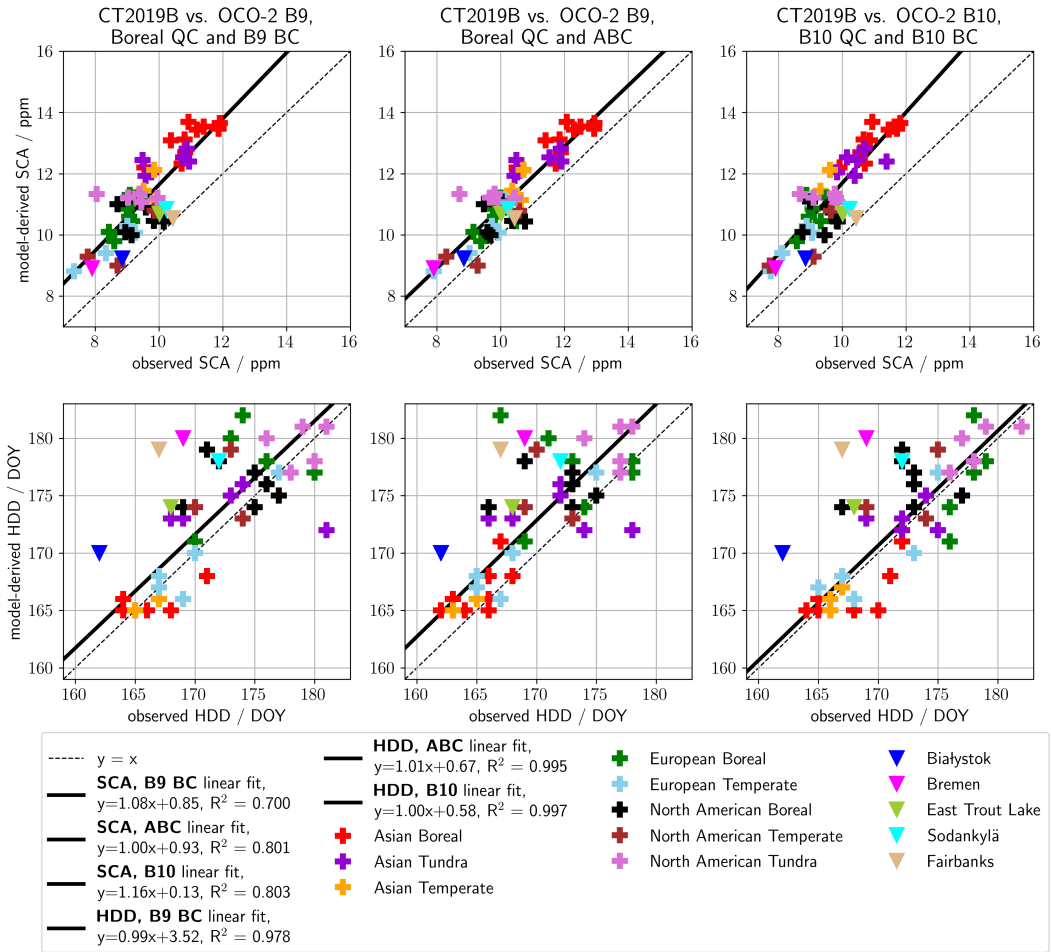
Figure S38. Correlations of CT2019B model-derived versus observed (OCO-2 and NNG) SCA and HDD with three different data treatments for OCO-2 retrievals. The left column uses OCO-2 B9 retrievals with quality controls tailored for Boreal Forest regions (Boreal QC), as described by Jacobs et al. (2020b), and the standard B9 bias correction (B9 BC). The center column uses OCO-2 B9 retrievals with Boreal QC and an alternative bias correction for high latitude retrievals (ABC), as described by Jacobs et al. (2020b). The right column uses OCO-2 B10 retrievals with the standard B10 quality controls and bias correction.
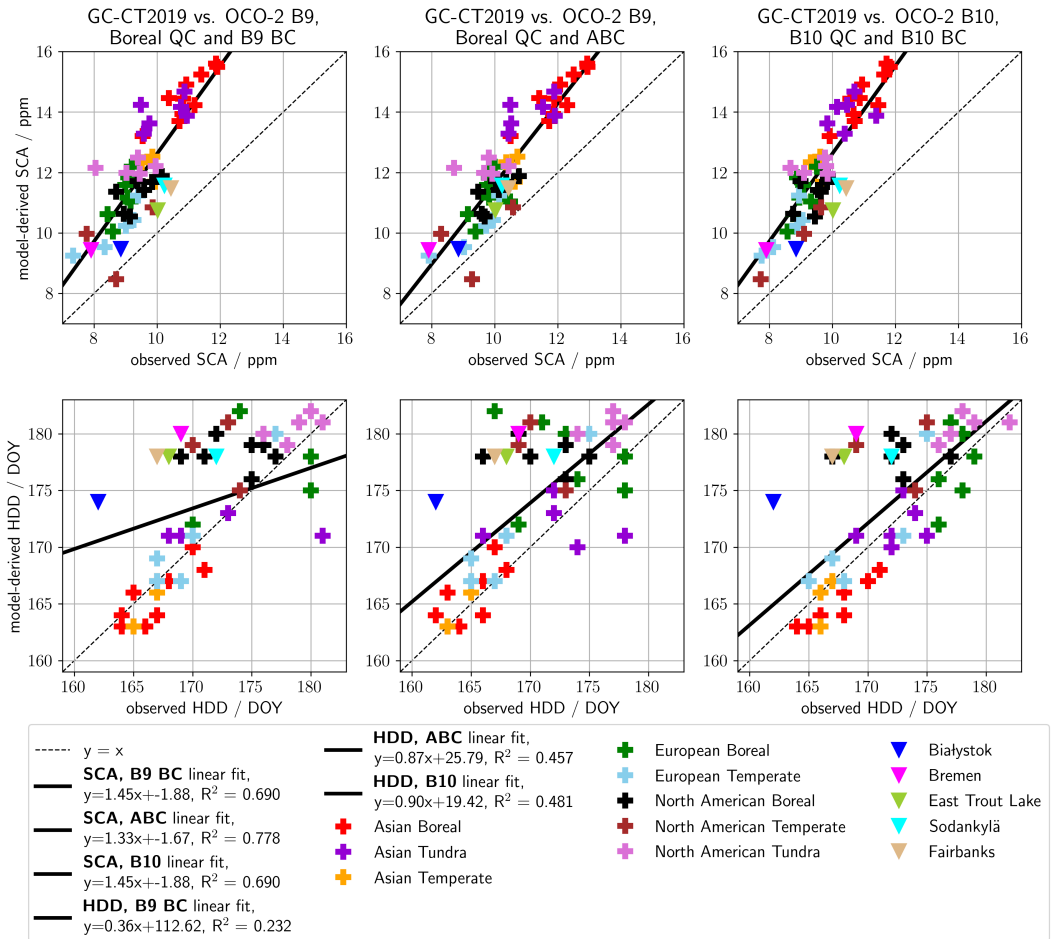
Figure S39. Correlations of GC-CT2019 model-derived versus observed (OCO-2 and NNG) SCA and HDD with three different data treatments for OCO-2 retrievals. The left column uses OCO-2 B9 retrievals with quality controls tailored for Boreal Forest regions (Boreal QC), as described by Jacobs et al. (2020b), and the standard B9 bias correction (B9 BC). The center column uses OCO-2 B9 retrievals with Boreal QC and an alternative bias correction for high latitude retrievals (ABC), as described by Jacobs et al. (2020b). The right column uses OCO-2 B10 retrievals with the standard B10 quality controls and bias correction. Note that the GC-CT2019 model estimates only span 2014-2016, while the OCO-2 observations span 2014-2019 and NNG observations cover various time periods depending on the site (see Table 1 in the manuscript).
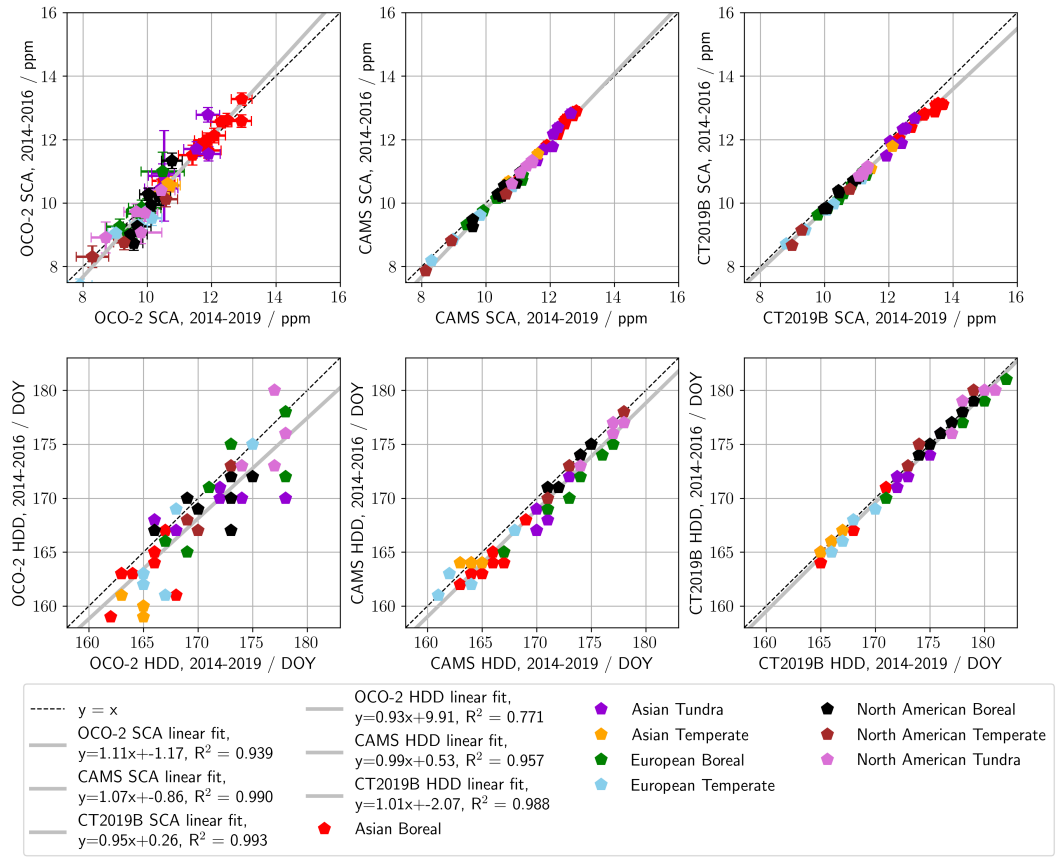
Figure S40. Correlations of SCA and HDD calculated from the time-series for 2014-2016 versus SCA and HDD calculated from the time-series for 2014-2019.

S2.1 A test of temporal sampling effects with CAMS

In this section we present results from a test using CAMS model estimates for 2014-2019. First, seasonal cycle fits are calculated for the full continuous time-series of CAMS daily averaged X_{CO_2}. Then, seasonal cycle fits are calculated for CAMS daily averages for only days that are represented by OCO-2 observations within a given zone. We then compare biases in CAMS SCA with the full time-series, relative to OCO-2 SCA, to the shift in CAMS SCA that results from introducing artificial data gaps that follow those in the OCO-2 data (see Fig. S41 and S42). Results in Fig. S42 demonstrate that the shifts in CAMS SCA that result from imposed data gaps are small (-0.044 ± 0.197 ppm) relative to the biases in CAMS SCA for the full time-series relative to observed OCO-2 SCA (0.547 ± 0.720 ppm). This suggests that the impacts of wintertime data gaps on the resulting observed OCO-2 SCA from seasonal cycle fits with the methods from Lindqvist et al. (2015) are small relative to the cumulative effects of other factors contributing to model discrepancies. These shifts in SCA from imposed data gaps are also small relative to the 5 ppm overall variability in SCA across the northern high latitude regions.
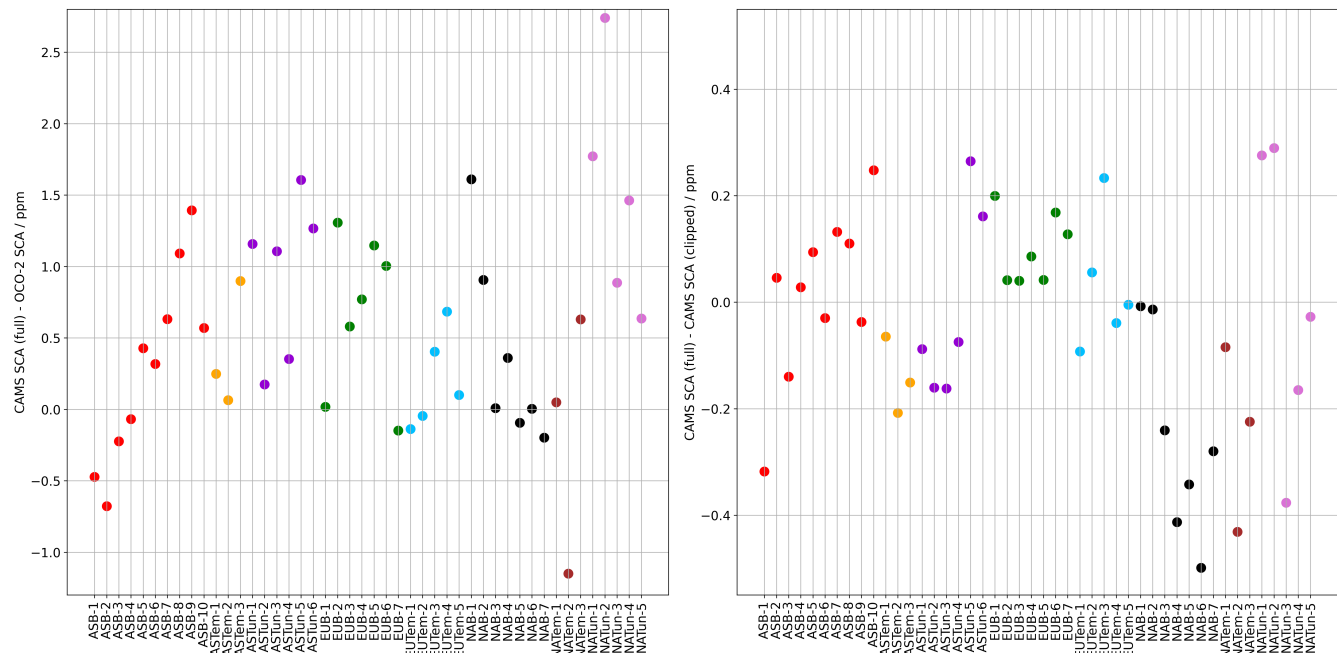
Figure S41. Differences between SCA for the full continuous time-series of CAMS daily averages and SCA for OCO-2 observations (left). Differences between SCA from the full continuous time-series of CAMS daily averages and SCA from the time-series of CAMS daily averages including only days with corresponding OCO-2 observations within a given zone (right).
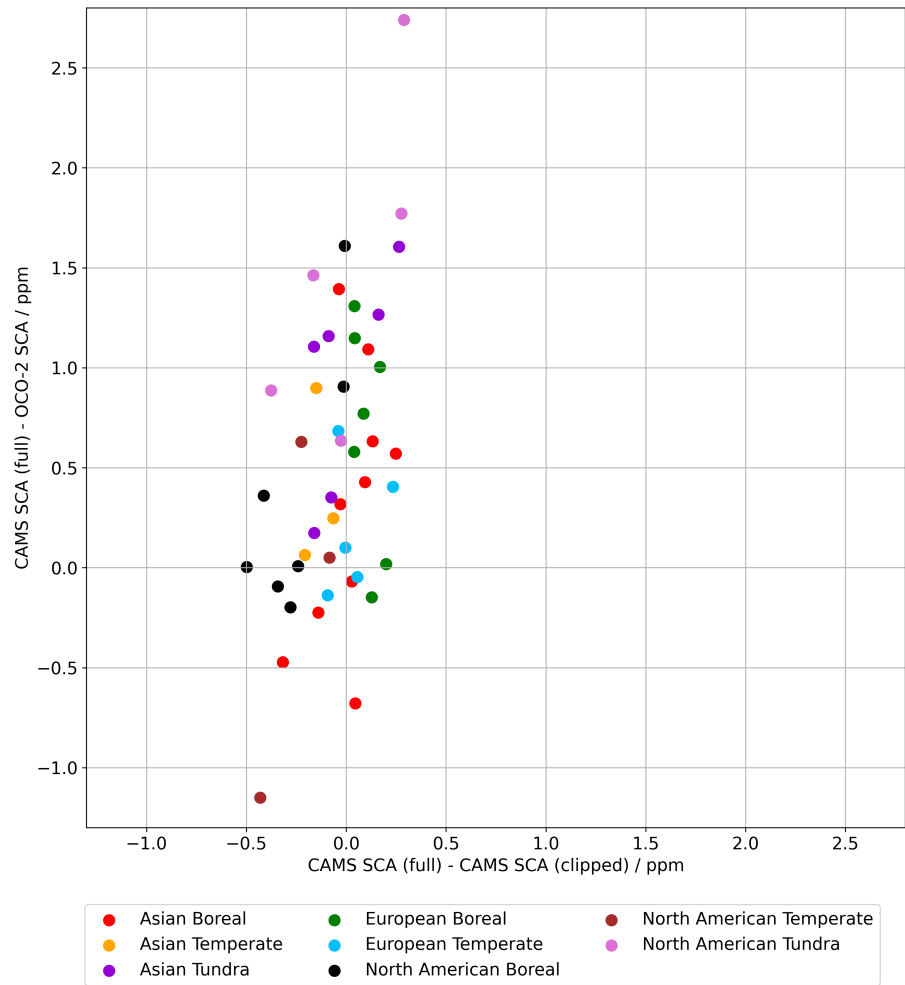
Figure S42. The correlation between SCA differences plotted in Fig. S41, with the difference between SCA for the full continuous time-series of CAMS daily averages and SCA for OCO-2 observations versus the difference between SCA from the full continuous time-series of CAMS daily averages and SCA from the time-series of CAMS daily averages including only days with corresponding OCO-2 observations within a given zone.

S3   CO$_2$ source contributions

Through analysis of X_{CO_2} source attribution in GC-CT2019, we found that the seasonal variability in X_{CO_2} for northern high latitudes is overwhelmingly dominated by seasonality in the contribution of terrestrial NEE. Detrended seasonal cycles of all CO$_2$ sources in GC-CT2019, averaged by region and day of year, are shown in Fig. S43, demonstrating that the seasonal
5   variability in fossil fuel, fire, and ocean source contributions are negligibly small compared to the seasonal variability in the terrestrial NEE contribution. Furthermore, seasonal cycle fits of GC-CT2019 daily average terrestrial NEE contribution within each zone to Eq. 1 of the manuscript yield SCA and HDD that are very strongly correlated to SCA and HDD from GC-CT2019 X_{CO_2} (see Fig. S44). Figure S44 also shows that SCA is slightly larger and HDD is slightly earlier for seasonal cycle fits of the terrestrial NEE contribution than for seasonal cycle fits of X_{CO_2}. Although some zones have large anthropogenic CO$_2$ sources,
10   these sources are not very seasonal, so do not contribute directly to SCA.
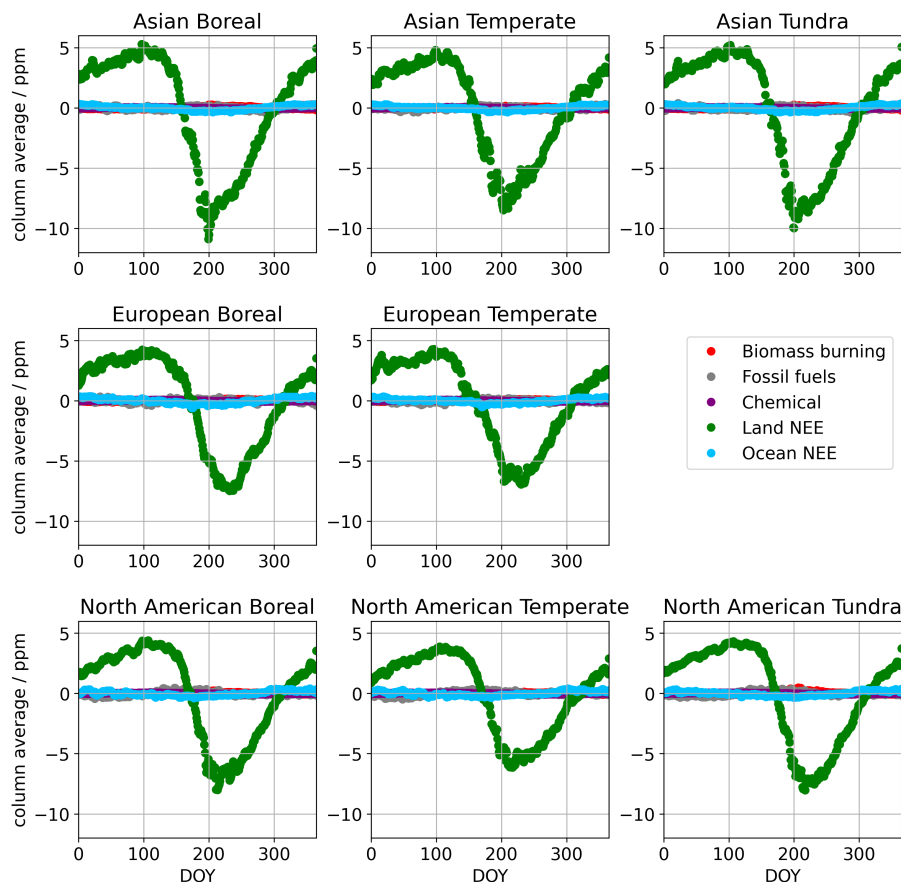
Figure S43. Detrended seasonal cycles of GC-CT2019 source contributions to column-average CO$_2$ averaged by region and day of year.
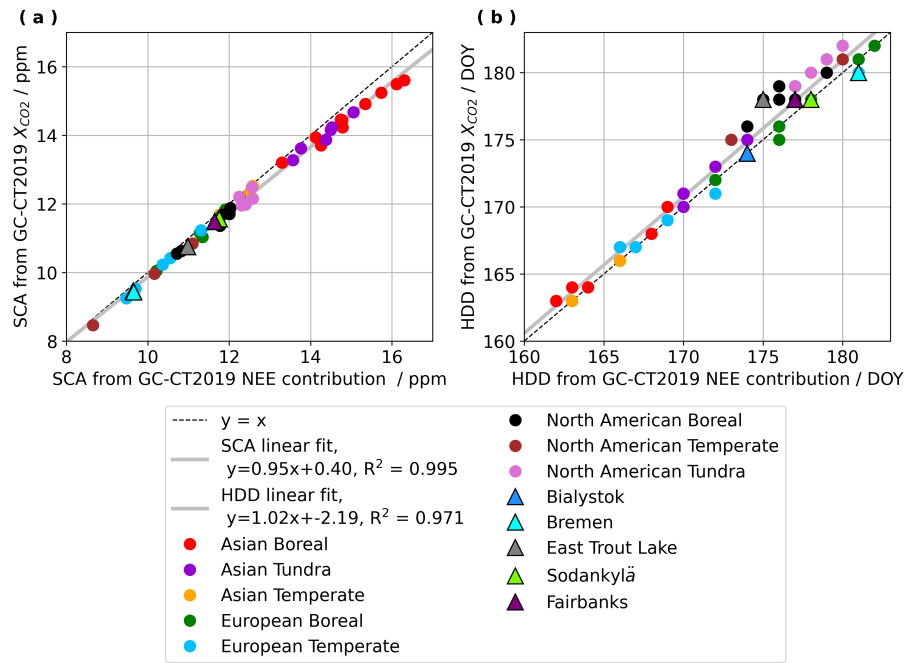
Figure S44. Correlations between SCA (left) and HDD (right) from seasonal cycle fits to GC-CT2019 X_{CO_2} and from seasonal cycle fits to GC-CT2019 source contribution of terrestrial NEE to the column.

S4 GEOS-Chem surface contact tracers plotted against OCO-2 seasonal cycle parameters
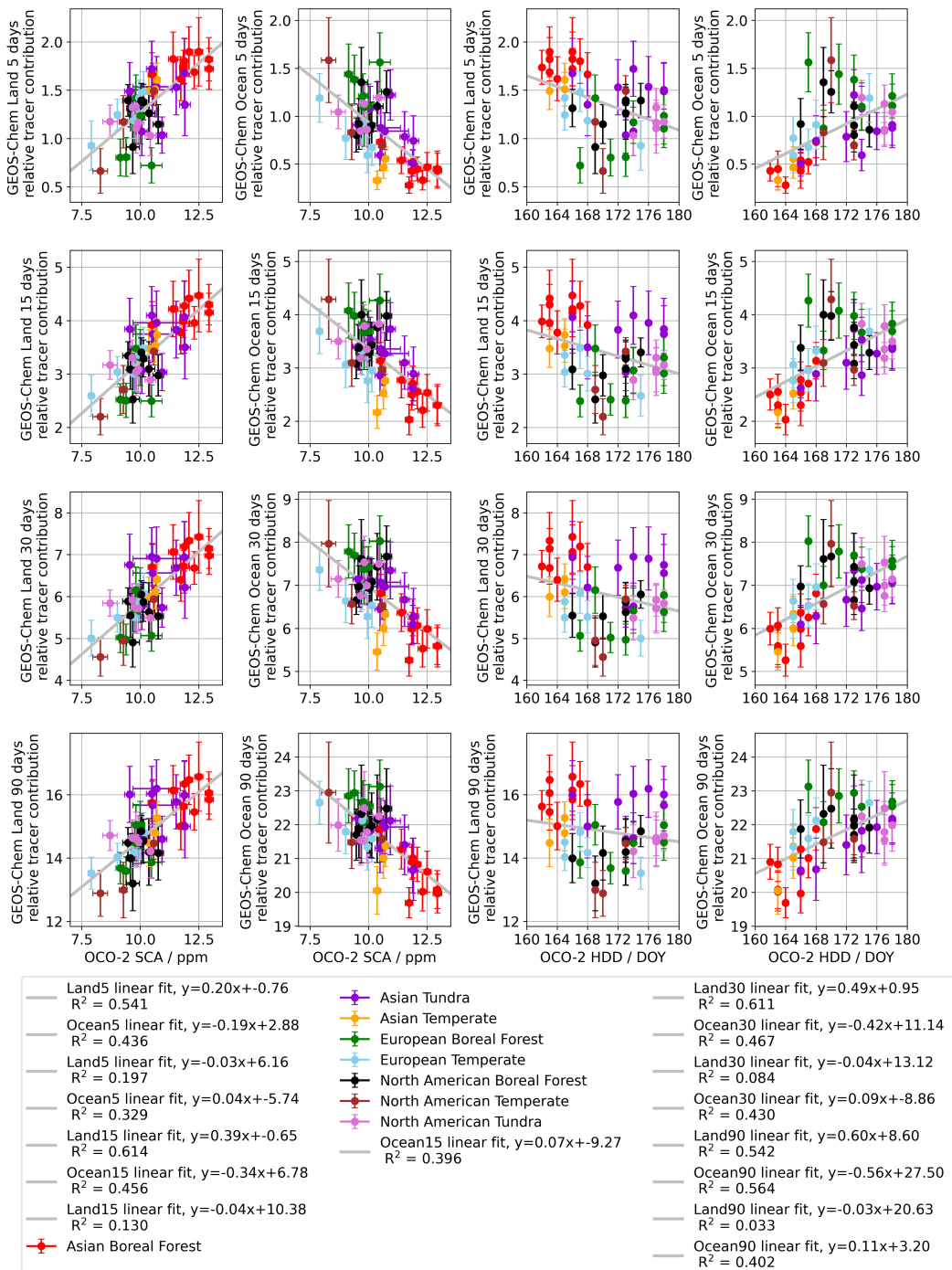
Figure S45. Direct correlations and calculated linear regressions for GEOS-Chem land and ocean tracers correlated against SCA and HDD from seasonal cycle fits to OCO-2 observations in 5° latitude by 20° longitude zones. Error bars for relative tracer contributions represent variability in one annual cycle, while those for SCA are determined by the uncertainty in seasonal cycle fitting parameters.

S5 CO$_2$ fluxes by day of year from CAMS and GC-CT2019

In this section time-series of daily sums of CO$_2$ flux are provided for all 5° latitude by 20° longitude zones and for five northern high latitude sites (see map in Fig. 1 of the manuscript). Before calculating daily sums for zones, fluxes are averaged spatially by timestamp. Next, fluxes are summed for each 24 hour period in UTC and a 15-day rolling mean is calculated.

5   Finally, average annual cycles are obtained by averaging the 15-day rolling mean by day of year across 2014-2019. The annual cycles of CAMS flux estimates are similar to annual cycles of daily CO$_2$ fluxes used in the GC-CT2019 CO$_2$ simulation and the separation of emission sources for fluxes used in GC-CT2019 demonstrates how seasonality in CO$_2$ exchange in northern high latitude regions is dominated by terrestrial net ecosystem exchange (NEE). Results in this section also show that European Temperate zone 3 and Bremen have much larger fossil fuel emissions and much less seasonal uptake from NEE than other zones

10   and sites, and these two factors may be related despite the fact that fossil fuel emissions display limited seasonal variability.
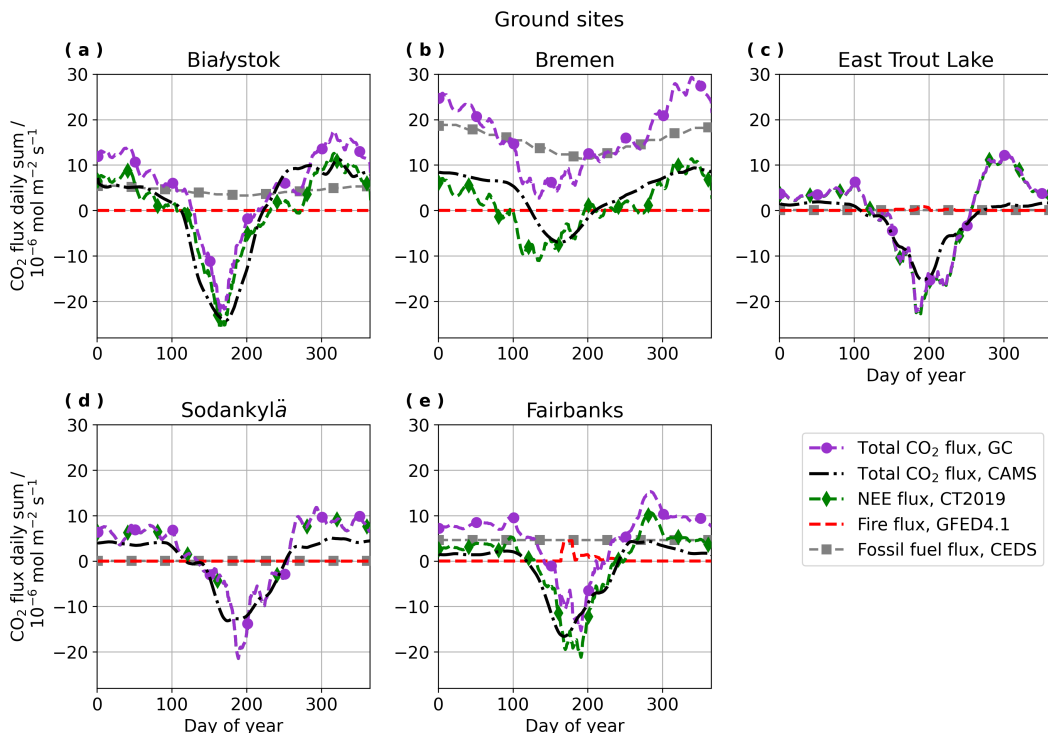
Figure S46. Time-series of CAMS and GC-CT2019 daily sum CO$_2$ flux averaged by day of year (DOY) over 2014-2019 for the nearest model grid-point (see Table 1) to five northern high latitude ground sites.
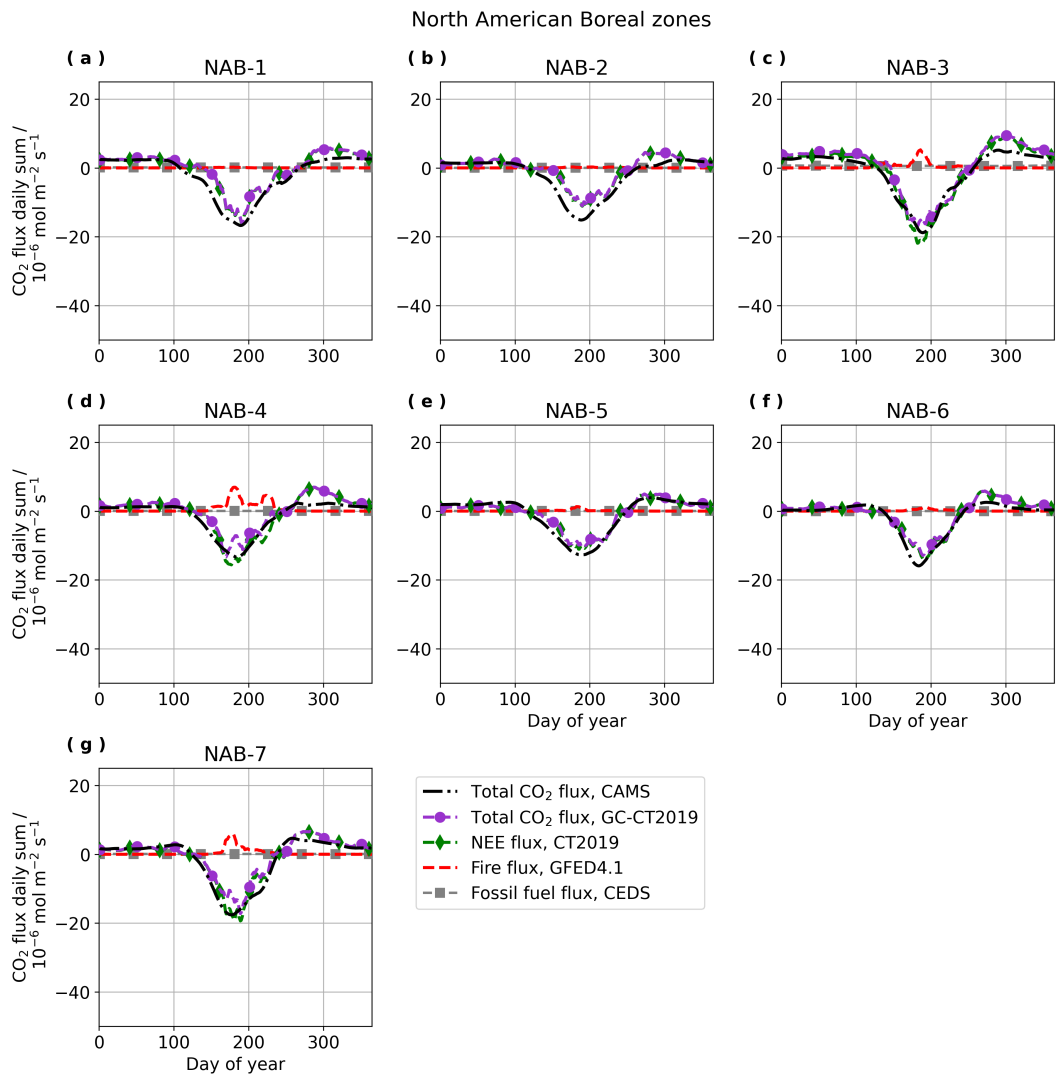
Figure S47. Time-series of CAMS and GC-CT2019 total daily sum CO_2 flux averaged by day of year (DOY) over 2014-2019 and spatially by 5° latitude by 20° longitude zone in the North American Boreal region.

European Boreal zones
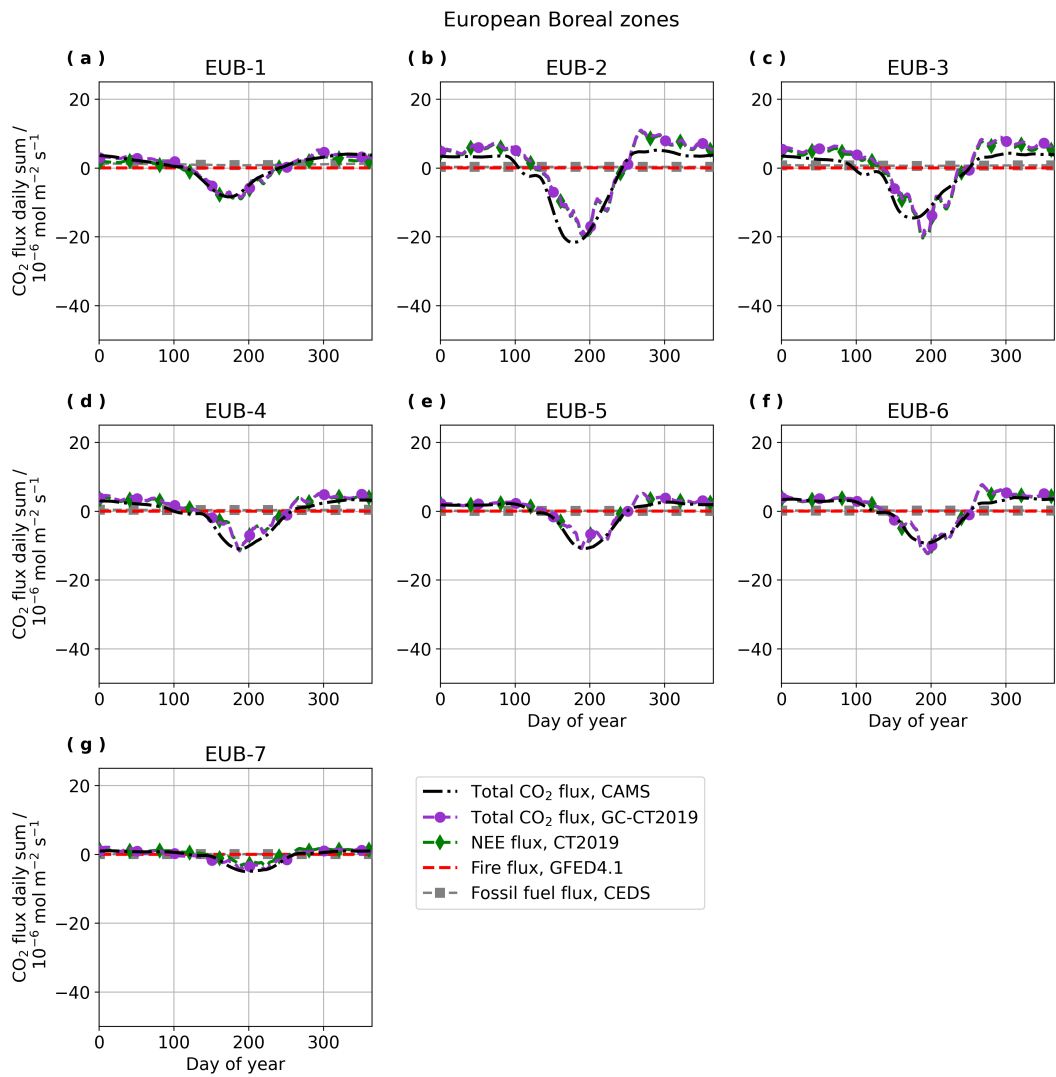
Figure S48. Time-series of CAMS and GC-CT2019 total daily sum CO_2 flux averaged by day of year (DOY) over 2014-2019 and spatially by 5° latitude by 20° longitude zone in the European Boreal region.
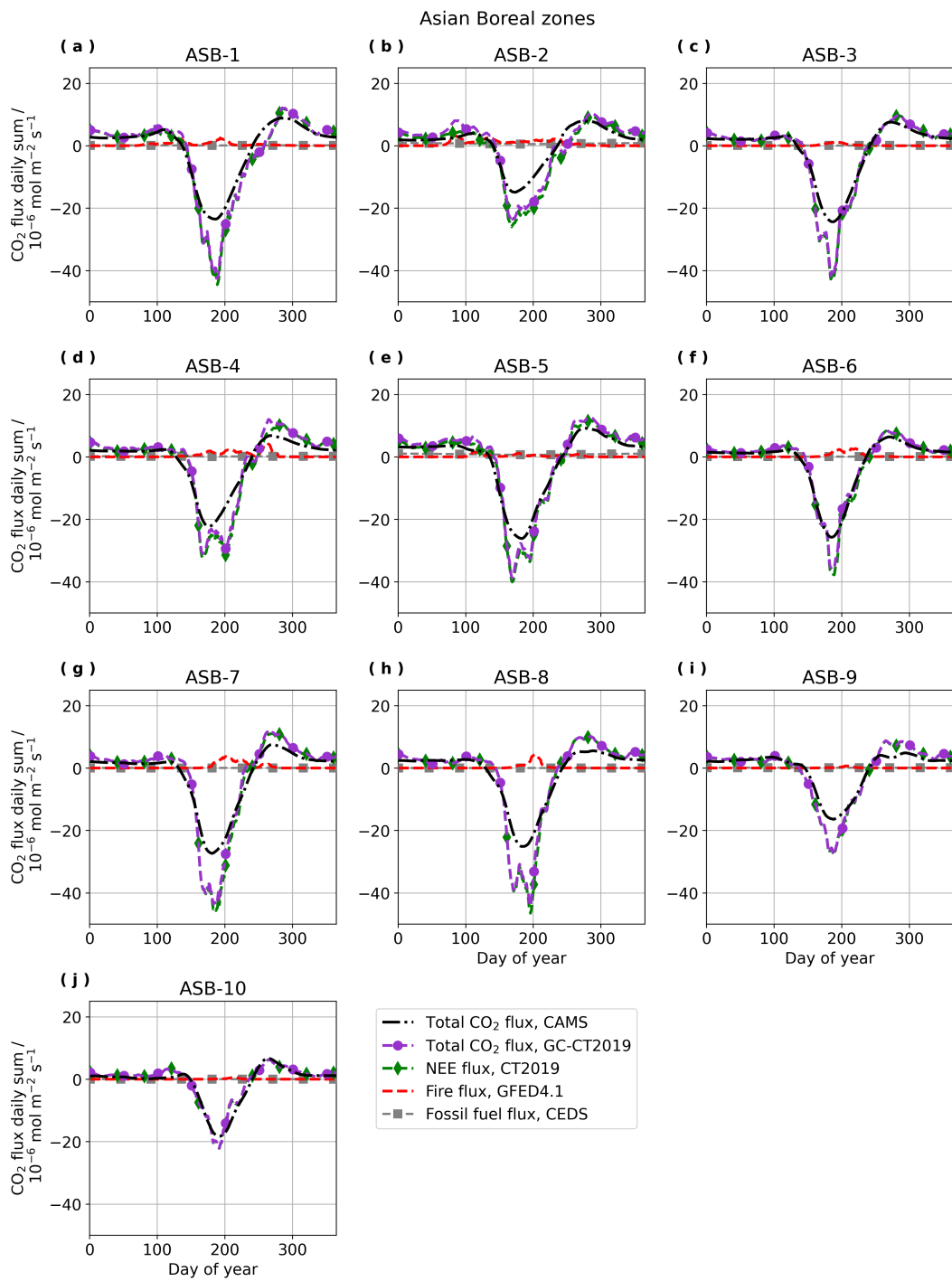
Figure S49. Time-series of CAMS and GC-CT2019 total daily sum CO_2 flux averaged by day of year (DOY) over 2014-2019 and spatially by 5° latitude by 20° longitude zone in the Asian Boreal region.
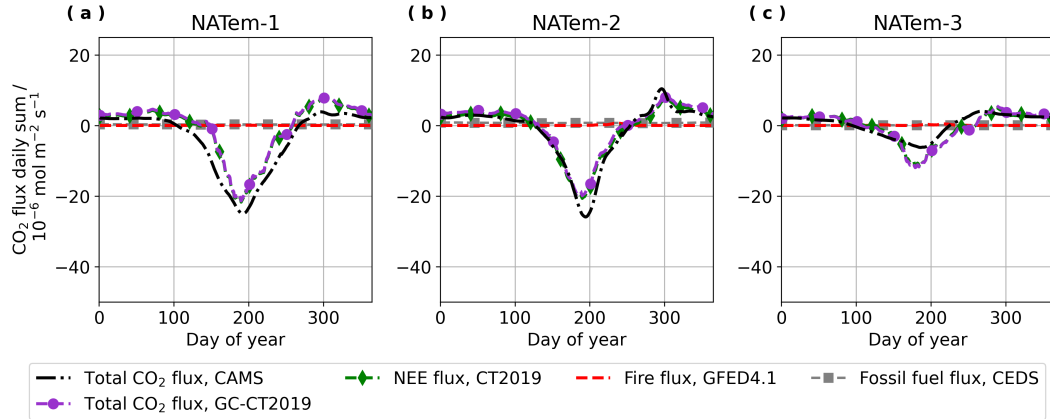
Figure S50. Time-series of CAMS and GC-CT2019 total daily sum CO_2 flux averaged by day of year (DOY) over 2014-2019 and spatially by 5° latitude by 20° longitude zone in the North American Temperate region.
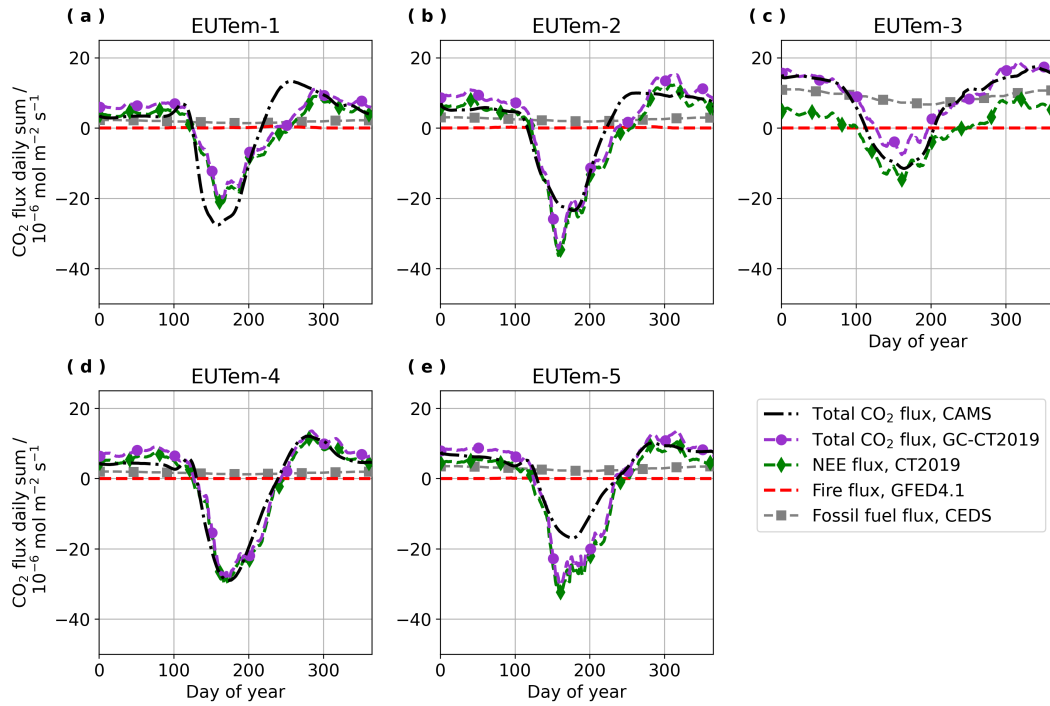
Figure S51. Time-series of CAMS and GC-CT2019 total daily sum CO_2 flux averaged by day of year (DOY) over 2014-2019 and spatially by 5° latitude by 20° longitude zone in the European Temperate region.
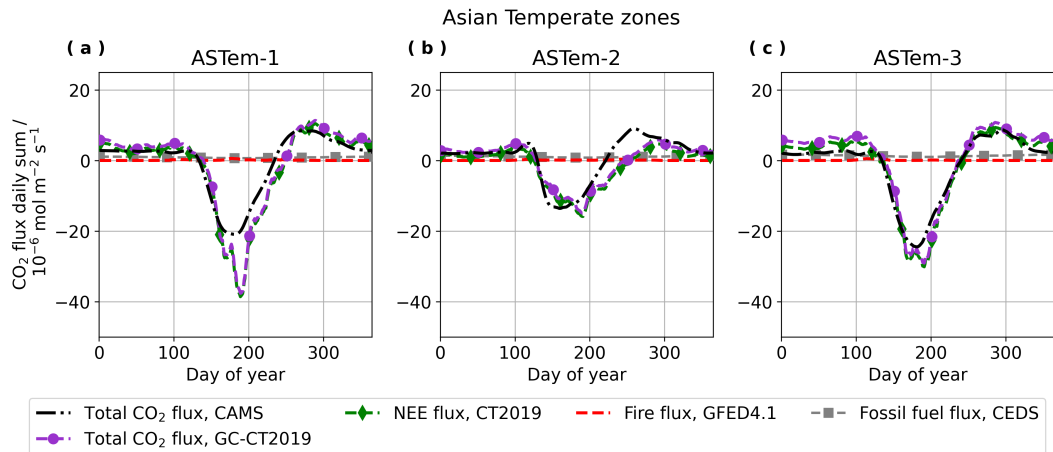
Figure S52. Time-series of CAMS and GC-CT2019 total daily sum CO_2 flux averaged by day of year (DOY) over 2014-2019 and spatially by 5° latitude by 20° longitude zone in the Asian Temperate region.
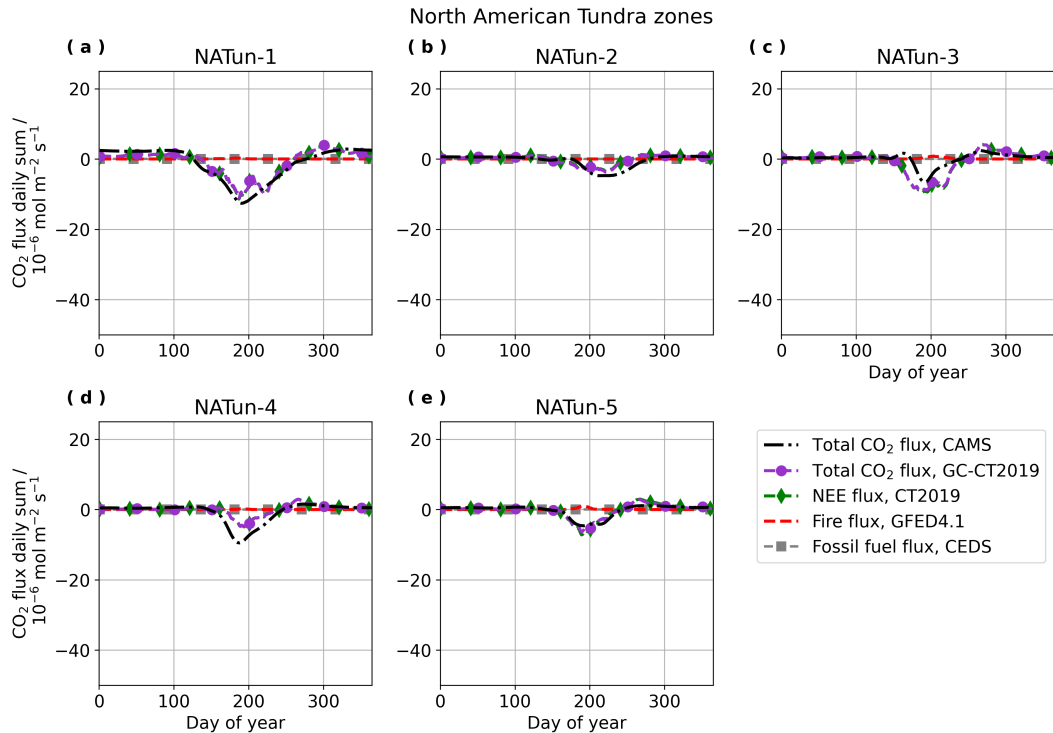
Figure S53. Time-series of CAMS and GC-CT2019 total daily sum CO_2 flux averaged by day of year (DOY) over 2014-2019 and spatially by 5° latitude by 20° longitude zone in the North American Tundra region.
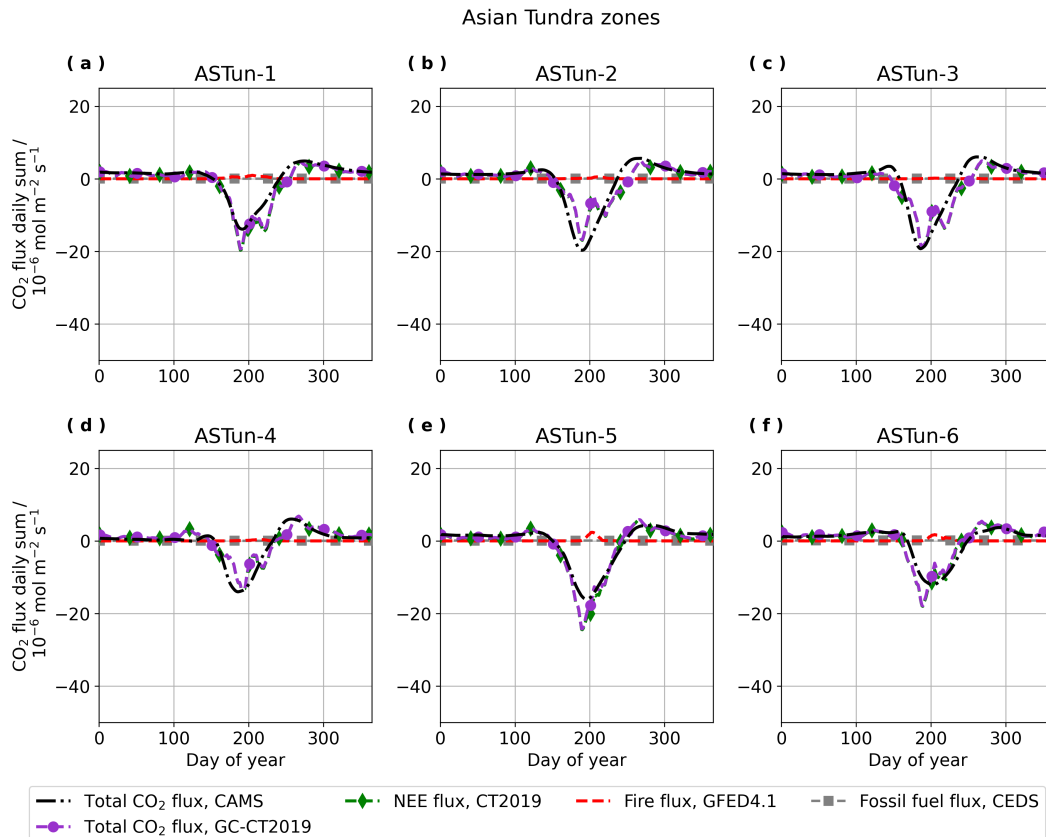
Asian Tundra zones

Figure S54. Time-series of CAMS and GC-CT2019 total daily sum CO_2 flux averaged by day of year (DOY) over 2014-2019 and spatially by 5° latitude by 20° longitude zone in the Asian Tundra region.

References

Chevallier, F.: Validation report for the CO_2 fluxes estimated by atmospheric inversion, v19r1 Version 1.0, https://atmosphere.copernicus.eu/sites/default/files/2020-08/CAMS73_2018SC2_D73.1.4.1-2019-v1_202008_v3-1.pdf, 2020a.

Chevallier, F.: Description of the CO_2 inversion production chain 2020 Version 1.0, https://atmosphere.copernicus.eu/sites/default/files/2020-06/CAMS73_2018SC2_%20D5.2.1-2020_202004_%20CO2%20inversion%20production%20chain_v1.pdf, 2020b.

Deutscher, N. M., Notholt, J., Messerschmidt, J., Weinzierl, C., Warneke, T., Petri, C., and Grupe, P.: TCCON data from Bialystok (PL), Release GGG2014.R2 (Version R2) TCCON data archive, hosted by CaltechDATA, California Institute of Technology, Pasadena, CA, U.S.A., https://doi.org/10.14291/tccon.ggg2014.bialystok01.R2, https://doi.org/10.14291/TCCON.GGG2014.BIALYSTOK01.R2, 2019.

Jacobs, N., Simpson, W. R., Hase, F., Blumenstok, T., Tu, Q., Frey, M., Dubey, M. K., and Parker, H.: https://doi.org/10.3334/ORNLDAAC/1831, 2020a.

Jacobs, N., Simpson, W. R., Wunch, D., O'Dell, C. W., Osterman, G. B., Hase, F., Blumenstock, T., Tu, Q., Frey, M., Dubey, M. K., Parker, H. A., Kivi, R., and Heikkinen, P.: Quality controls, bias, and seasonality of CO2 columns in the boreal forest with Orbiting Carbon Observatory-2, Total Carbon Column Observing Network, and EM27/SUN measurements, Atmos. Meas. Tech., 13, 5033–5063, https://doi.org/10.5194/amt-13-5033-2020, 2020b.

Kivi, R., Heikkinen, P., and Kyrö, E.: TCCON data from Sodankylä (FI), Release GGG2014.R0 (Version GGG2014.R0). TCCON data archive, hosted by CaltechDATA, California Institute of Technology, Pasadena, CA, U.S.A., https://doi.org/10.14291/tccon.ggg2014.sodankyla01.R0, https://doi.org/10.14291/tccon.ggg2014.sodankyla01.R0, 2014.

Lindqvist, H., O'Dell, C. W., Basu, S., Boesch, H., Chevallier, F., Deutscher, N., Feng, L., Fisher, B., Hase, F., Inoue, M., Kivi, R., Morino, I., Palmer, P. I., Parker, R., Schneider, M., Sussmann, R., and Yoshida, Y.: Does GOSAT capture the true seasonal cycle of carbon dioxide?, Atmos. Chem. Phys., 15, 13 023–13 040, https://doi.org/10.5194/acp-15-13023-2015, www.atmos-chem-phys.net/15/13023/2015/, 2015.

Notholt, J., Petri, C., Warneke, T., Deutscher, N. M., Palm, M., Buschmann, M., Weinzierl, C., Macatangay, R. C., and Grupe, P.: TCCON data
5   from Bremen (DE), Release GGG2014.R1 (Version R1) TCCON data archive, hosted by CaltechDATA, California Institute of Technology, Pasadena, CA, U.S.A., https://doi.org/10.14291/tccon.ggg2014.bremen01.R1, https://doi.org/10.14291/TCCON.GGG2014.BREMEN01. R1, 2019.

OCO-2 Science Team/Michael Gunson, Annmarie Eldering: OCO-2 Level 2 bias-corrected XCO2 and other select fields from the full-physics retrieval aggregated as daily files, Retrospective processing V9r, Greenbelt, MD, USA, Goddard Earth Sciences Data and Infor-
10   mation Services Center (GES DISC), https://doi.org/10.5067/W8QGIYNKS3JC, https://disc.gsfc.nasa.gov/datasets/OCO2_L2_Lite_FP_9r/summary, Accessed: [2 December 2019], 2018.

Wunch, D., Mendonca, J., Colebatch, O., Allen, N. T., Blavier, J.-F., Roche, S., Hedelius, J., Neufeld, G., Springett, S., Worthy, D., Kessler, R., and Strong, K.: TCCON data from East Trout Lake, SK (CA), Release GGG2014.R1 (Version R1) TCCON data archive, hosted by CaltechDATA, California Institute of Technology, Pasadena, CA, U.S.A., https://doi.org/10.14291/tccon.ggg2014.easttroutlake01.R1,
15   https://doi.org/10.14291/TCCON.GGG2014.EASTTROUTLAKE01.R1, 2018.